Boundary-Layer Meteorology

A review of Coastal Fog Microphysics during C-FOG

--Manuscript Draft--

Manuscript Number:	BOUN-D-20-00120R2
Full Title:	A review of Coastal Fog Microphysics during C-FOG
Article Type:	Research Article
Keywords:	Fog microphysics; Coastal Fog; visibility; Eddy Dissipation Rate; C-FOG
Corresponding Author:	Ismail Gultepe Environment and Climate Change Canada CANADA
Corresponding Author Secondary Information:	
Corresponding Author's Institution:	Environment and Climate Change Canada
Corresponding Author's Secondary Institution:	
First Author:	Ismail Gultepe
First Author Secondary Information:	
Order of Authors:	Ismail Gultepe
	Andrew J Heymsfield, PhD
	Harindra J Fernando, PhD
	Eric Pardyjak, PhD
	Clive Dorman, PhD
	Qing Wang, PhD
	Edward Creegan, PhD
	Sebastian W Hoch, phd
	David D Flagg
	R. Yamaguchi
	Raghu Krishnamurthy, PhD
	Sasa Gabersek, PhD
	William Perrie, PhD
	Alexei Perelet
	Dhiraj singh
	Rachel Chang, PhD
	Baban Nagare, PhD
	Sandeep Wagh, PhD
	sen wang
Order of Authors Secondary Information:	
Funding Information:	Office of Naval Research (N00014-18-1-2472) — Dr. Harindra J Fernando
Abstract:	Abstract The goal of this paper is to provide an overview the microphysical measurements made during the C-FOG (Toward Improving Coastal Fog Prediction) field project. In addition, we evaluate microphysical parameterizations using the C-FOG

	dataset. C-FOG is designed to advance understanding of liquid fog formation, development, and dissipation in coastal environments to improve fog predictability and monitoring. The project took place along eastern Canada's (Nova Scotia, NS and Newfoundland, NL) coastlines and open water environments from August-October 2018, where environmental conditions play an important role for late-season fog formation. Visibility (Vis), wind speed (U h), and turbulence along coastlines are the most critical weather-related parameters affecting marine transportation and aviation. In the analysis, microphysical observations are summarized first and then they are, together with 3D-wind components, used for fog intensity (visibility) evaluation. Results suggest that detailed microphysical observations collected at the supersites and aboard the Research Vessel (R/V) Hugh R. Sharp are useful for developing microphysical parameterizations. The fog life cycle and turbulence kinetic energy dissipation rate were strongly related to each other. The magnitude of 3D-wind fluctuations was higher during the formation and dissipation stages. An array of cutting-edge instruments used for data collection provided new insight into the variability and intensity of fog (visibility) and microphysics. It is concluded that further modifications in microphysical observations and parameterizations are needed to improve fog predictability of NWP (Numerical Weather Prediction) models.
Response to Reviewers:	Minor corrections suggested by Editor on this microphysical review for CFOG special issue are done in the manuscript and attached.

A review of Coastal Fog Microphysics during C-FOG

I. Gultepe*[,1a,1b,2], A.J. Heymsfield[3], H.J.S Fernando[2], E. Pardyjak[4], C. E. Dorman[5], Q. Wang[6], E. Creegan[7], S. W. Hoch[8], D. D. Flagg[9], R.Yamaguchi[6], R. Krishnamurthy[10], S. Gaberšek[9], W. Perrie[11], A. Perelet[4], D.K. Singh[4], R. Chang[12], B. Nagare[12], S. Wagh[2], and S. Wang[2]

Received: July 02 2020

Abstract The goal of this paper is to provide an overview the microphysical measurements made during the C-FOG (*Toward Improving Coastal Fog Prediction*) field project. In addition, we evaluate microphysical parameterizations using the C-FOG dataset. C-FOG is designed to advance understanding of liquid fog formation, development, and dissipation in coastal environments to improve fog predictability and monitoring. The project took place along eastern Canada's (Nova Scotia, NS and Newfoundland, NL) coastlines and open water environments from August-October 2018, where environmental conditions play an important role for late-season fog formation. Visibility (Vis), wind speed (U_h), and turbulence along coastlines are the most critical weather-related parameters affecting marine transportation and aviation. In the analysis, microphysical observations are summarized first and then they are, together with 3D-wind components, used for fog intensity (visibility) evaluation. Results suggest that detailed microphysical observations collected at the supersites and aboard the Research Vessel (*R/V) Hugh R. Sharp* are useful for developing microphysical parameterizations.

----

*Corresponding Author: Dr. Ismail Gultepe, Ismail.gultepe@uoit.ca
[1a]Environment and Climate Change Canada, MRD, Toronto, ON M3H5T4, Canada
[1b]UOIT, Engineering and Applied Science Department, Oshawa, Ont., Canada
[2]Department of Civil and Environmental Engineering and Earth Sciences, and Department of Aerospace and Mechanical Engineering, University of Notre Dame, Notre Dame, IN 46556, USA
[3]NCAR/MMM, 3450 Mitchell Lane, Boulder, CO 80301, USA
[4]Department of Mechanical Engineering, University of Utah, Salt Lake City, UT 84112, USA
[5]Integrative Ocean. Div., Scripps Ins. of Oceanography, Uni. of California San Diego, La Jolla, CA, USA
[6]Department of Meteorology, Naval Postgraduate School, Monterey, CA 93943, USA.
[7]US Army Research Laboratory, White Sands Missile Range, NM USA
[8]Atmospheric Sciences Department, University of Utah, Salt Lake City, UT, USA
[9] Marine Meteorology Division, U.S. Naval Research Laboratory, Monterey, CA 93943, U.S.A.
[10]Pacific Northwest National Laboratory, Richland, WA, USA
[11]Fisheries and Oceans Canada, Bedford Institute of Oceanography, Dartmouth NS, Canada
[12]Dalhousie University, Department of Physics and Atmospheric Science, Halifax, NS B3H 4R2, Canada

The fog life cycle and turbulence kinetic energy dissipation rate were strongly related to each other. The magnitude of 3D-wind fluctuations was higher during the formation and dissipation stages. An array of cutting-edge instruments used for data collection provided new insight into the variability and intensity of fog (visibility) and microphysics. It is concluded that further modifications in microphysical observations and parameterizations are needed to improve fog predictability of NWP (Numerical Weather Prediction) models.

Keywords: Coastal Fog, Eddy Dissipation Rate, Fog Microphysics NWP parameterization, Visibility.

1 Introduction

Coastal fog plays an important role for weather conditions affecting marine environments that include aviation (Gultepe et al 2020), marine shipping (Fernando et al 2020), sporting and social activities (Pezzoli et al 2010), as well as vegetation (Schemenauer et al 2016; Torregrosa et al 2014). The direct consequence of fog is the impairment of visibility, and hence the 'intensity' of fog is defined in terms of visibility (Vis). Advection supplies moisture for Atlantic-Canadian coastal fog, while the overhead passage of cyclonic or anticyclonic systems fosters its actual formation (Dorman et al. 2020). Other factors such as large-scale subsidence leading to thermal inversions, frontal systems, radiative cooling, topography, tropical cyclones, and turbulence fluxes can also have an impact on the life cycle of coastal fog (Gultepe et al 2007; Toth et al 2011). Intensity of turbulence and turbulence dissipation rate occurred during life cycle of radiation fog were studied by Zhou and Ferrier (2008) and Price (2019) and these suggested that turbulence intensity should be less than a threshold value.

Microphysical measurements were performed using a fog measuring device (FMD, FM100) for the first time by Gultepe et al (2007a) during the FRAM project, followed by others (Niu et al 2010; Spiegel et al 2012; Isaac et al 2020). The FM100 was developed using the principles of a forward scattering probe (FSSP), measurements of which were used in developing Vis parameterization by Gultepe et al (2007b). The FM100 provides droplet spectra, which are used to obtain liquid water content (LWC*),

---

*Definitions are provided in Nomenclature in the end of paper.

mean volume diameter (MVD), effective size (r_{eff}), droplet number concentration (N_d), and the droplet settling rate (LWC•V_f), where V_f is the droplet fall velocity. NWP modeling and evaluation studies of fog have helped to improve forecasting and gain physical insights (e.g. Yang et al. 2009; Gultepe et al. 2007a,b).Warm-fog droplet spectra and its distribution are related to condensation nuclei (CN) and relative humidity with respect to water (RH_w). There have been several studies on this issue, but cloud condensation nuclei (CCN) versus supersaturation with respect to water (S_w) relationships are mostly developed for cloud studies and generally use fixed values of 100 cm^{-3} for marine environments (Thompson et al 2008). In reality, such fixed values may not be valid, and therefore we have seen parametric modifications. Prediction of N_d is obtained using prognostic equations that represent processes related to turbulence, droplet growth, radiative heating/cooling, as well as turbulence flux divergence (Storelvmo et al 2014). Based on assumed modified-gamma distributions, either using Kohler theory (Chen 1994) and/or Twomey parameterization (Twomey 1959), N_d predictions can be performed using single or double moment microphysical schemes (Milbrandt and Yau, 2005a,b; Morrison and Gettelman 2008; Schwenkel and Maronga, 2019). However, these schemes have been developed for clouds and not for fog.

As in Twomey et al (1959), N_d is parameterized based on Kohler theory assuming equilibrium and cooling of an air volume by lifting via the vertical air velocity (w_a). The latter in fog, excluding formation and dissipation conditions, is usually not as strong as in clouds, complicating the application of these parameterizations to fog. Therefore, its usage cannot be verified for all fog types. Another equation for N_d prediction, mainly applicable to climate studies, expresses it as a function of w_a, N_a (aerosol total number concentration) as well as aerosol composition (Abdul-Razzak and Ghan 2000; Ghan et al 1998; 2001). In addition to parameters given in Twomey (1974; 1991), this equation uses aerosol composition as an independent parameter. Clearly, environmental conditions such as air temperature (T_a), dew point temperature (T_d) and RH_w, and w_a as well as aerosol and microphysics parameters (CCN and droplet growth rate) play an important role in N_d prediction, thereby affecting Vis estimation (Schwenkel and Maronga, 2019). In this regard, Gultepe et al (2007b) have suggested that accurate predictions of N_d and LWC are critical for Vis prediction, and Vis cannot be accurate if only LWC is used (Kunkel 1984; Stoelinga and Warner 1999). Vis is usually diagnosed in the post processing stage of forecast model outputs using Stoelinga-Warner's method (Stoelinga and Warner 1999), which includes large uncertainties in fog prediction (Gultepe et al 2006, 2007c).

Lately, field observations from various projects have been used to improve Vis parameterizations (Gultepe et al 2009; 2014; Haeffelin 2010; Price et al 2018; Wang et al 2020) but these are often site dependent because of the nature of N_a spectra and compositional properties (Bergot et al 2005). In this respect, marine fog studies used microphysical parameterizations extensively (Gultepe et al 2009; Gultepe et al 1996). The C-FOG (Toward Improving Coastal Fog Prediction) field project has had better tools to evaluate coastal fog microphysical and dynamical properties, such as droplet and aerosol spectra and turbulence over both the coastal areas and at the ship (Fernando et al 2020).

Vis parameterizations commonly use only RH_w and/or (T_a-T_d) (called dew point depression) to predict fog coverage but they cannot be used for fog intensity (e.g., Vis) because RH_w (as well as T_a-T_d) indicates only the existence of fog (Toth et al., 2011; Gultepe et al 2009; Dimitrova et al 2020). Therefore, fog microphysical parameters such as LWC and N_d are needed for accurate Vis forecasting, but they are not accurately predicted by models (Pu et al 2016, Dimitrova et al 2020, Gultepe and Milbrandt 2010). In single-moment and double moment microphysical schemes used in NWP models, LWC is usually a prognostic variable and N_d is assumed as a fixed value or or obtained either deterministically or prognostically, by making several assumptions on physical terms affecting N_d. If N_d is not fixed, a modified gamma distribution is usually assumed in presenting fog droplet size distribution that is used to obtain N_d.

In this work, C-FOG related studies are briefly summarized; WRF fog simulations using various microphysical and surface boundary layer schemes are performed for Vis predictions at the ship and supersite locations. Another microphysics paper is focused on a case of stratus lowering fog over the coastline based on the *R/V Sharp* observations (Wagh et al 2020). Understanding fog microphysics and its impact on Vis, based on a LES model, is provided by Wainwright and Richter (2020). A study using a Tethered Balloon System (TBS) with aerosol and droplet spectral measurements as well as fog thermodynamics is examined by Singh et al (2020). Detailed coastal fog observations at The Downs, Ferryland (Wang et al. 2020) are studied by providing TBS dynamic and thermodynamic profiles and collecting fog-droplet spectra from a CDP modified to increase and measure the instantaneous flow rate. Perelet et al (2020) present a methodology for using a two-wavelength scintillometer system for measuring fog characteristics on scales of 1 km. Wang et al. (2020) also focused on the impact of the fog layer on optical propagation using contrasting measurements at Ferryland and on the US West Coast. In addition, large-scale synoptic events affecting local fog formation are summarized by Dorman et al (2020). An overview of the C-GOG project is given in Fernando et al. (2020).

The goal of this paper is to provide an overview of coastal fog microphysical measurements and to evaluate microphysical parameterizations based on the C-FOG field project. In addition, the importance of fog Vis predictions is discussed and challenges are noted when turbulence kinetic energy (TKE) dissipation rates are included. The C-FOG field project has provided microphysical observations from several coastal sites and the *R/V Hugh R. Sharp* (hereafter *R/V Sharp*). The paper organization is planned as follows: Section 2 provides information on observations and project design. Section 3 explains the analysis used in Vis and eddy dissipation rate (EDR) parameterizations. Sections 4 and 5 focus on discussions and conclusions, respectively.

2 Field Project and Observations

2.1 Project Location

The C-FOG field campaign took place from 01 September to 07 October 2018. The field campaign took place along the coastlines of Atlantic Canada and the northeastern US. C-FOG is designed to advance our understanding of liquid fog formation, development, and dissipation over coastal environments, and thus improve fog predictability and monitoring. It was designed to capture fog variability in time and space using an array of platforms that included ground, airborne, and shipborne in-situ instruments, remote sensors as well as numerical models. Instruments were located at two supersites (Battery and The Downs sites in Ferryland, NL; Figure 1a,b), four satellite sites, as well as on the *R/V Sharp* (Fernando et al 2020). Figure 1c shows the entire project area overlaid on a satellite SST image for 28 September 2018. A strong SST gradient stands out near the northern region of the project area. In the current study, four cases are presented covering parts of the Intense Operational Periods IOP10 (27–30 Sep 2018) and IOP 12 (03-04 Oct 2018) that mainly represent warm advection fog events (Table 1).

Table 1 Case studies of coastal fog events studied in the present work. T_a is air temperature and SST is sea surface temperature.

Day	Location	Weather
Sep 28 2018	Battery supersite	T_a, SST, warm air advection
Sep 29 2018	Battery supersite	Warm air advection
Sep 28 2018	R/V Sharp	Warm air advection
Oct 04 2018	R/V Sharp	Advection and tropical depression

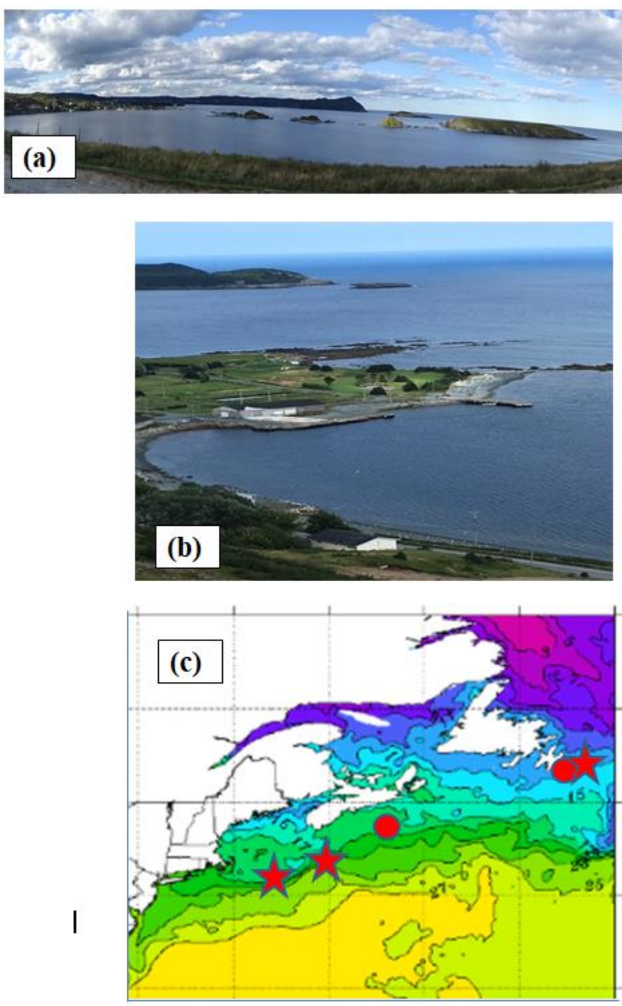

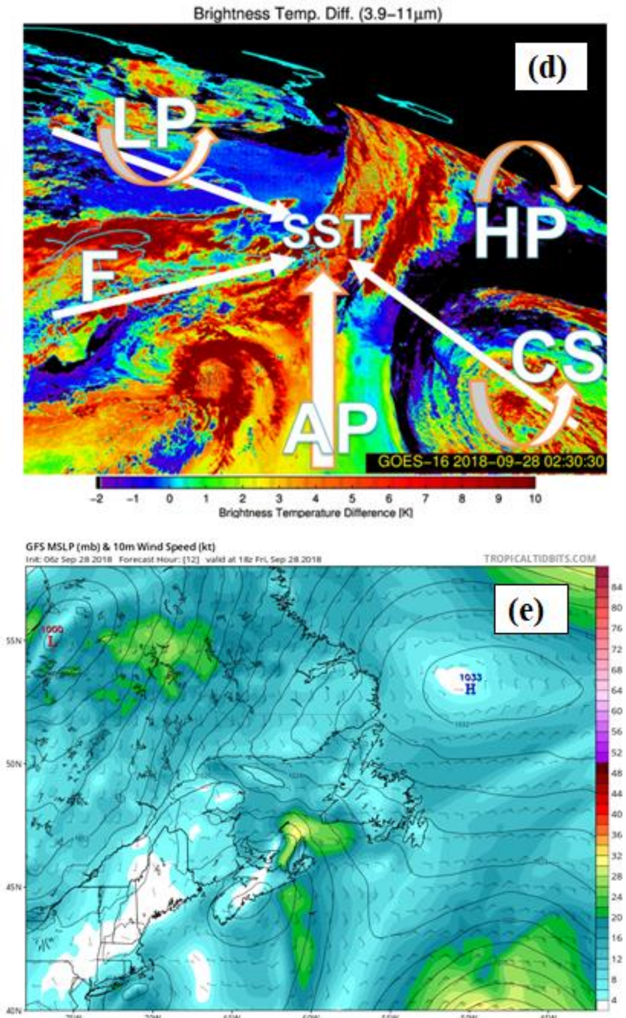

Fig. 1 Ferryland supersite region (a), Battery supersite (b), NOAA NESDIS Geo-Polar blended 5 km SST and entire project area with supersites (red circles) and ship locations (indicated by a red star for foggy days (c), synoptic weather systems affecting project area (d) with LP for "low pressure", F "front", SST "sea surface temperature", AP "advection process", HP "high pressure", and CS "cyclonic system", and US NCEP (National Center for Environmental Prediction) GFS (Global Forecasting System) based surface pressures and wind speed in Knots (e).

2.2 Synoptic Weather Systems

The C-FOG campaign took place at the end of the summer fog season (Gultepe et al 2009). During this time, various weather systems affect coastal-fog conditions. Figure 1d shows the SST for the project area and Fig. 1e is the GFS sea-level pressure and 10 m wind vectors on 28 September 2018. The latter shows major weather systems affecting the project area: a low pressure over Nova Scotia in the NW and associated with a warm frontal system (F) in the east, a high pressure (HP) to the NE, and tropical cyclones to the south east (CS), and warm-air advection processes (AP) resulting from T and q_v gradients along a north-south direction. The tropical cyclones usually became tropical depressions when moved to colder northern latitudes and usually they were about 500 km south and southeast of the main project site. During May 25-Oct 31 2018, 16 tropical depressions occurred over 4-months time period and about 4 of them affected physical conditions somehow at the project site. Their advection of SW quadrant of warm and moist air to N and NW quadrants likely played an important role for fog formation 100s of km away from storm center. . The photos in Figure 2 depict fog cases observed at The Downs supersite, and from the *R/V Sharp*, respectively.

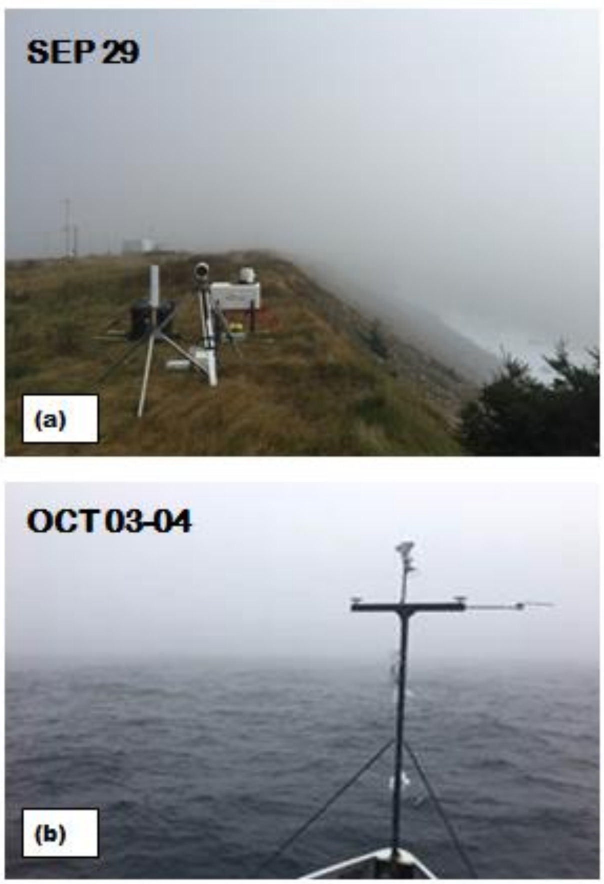

Fig. 2 The pictures of advection process occurring on Sep 28/29 2018 case at the Downs supersite (a) and on Oct 04 2018 (taken from the RV) (b).

2.3 Microphysical Observations

In this subsection, microphysical and meteorological instruments are summarized. All instruments used are summarized in Fernando et al. (2020). These measurements are related to dynamics, microphysics, radiation, aerosol, and thermodynamic properties of the environment. For particle size thresholds, fog droplets usually cover 1-30 µm, cloud droplets 1-100 µm, drizzle drops 100 (or 30)-500 µm , and drizzle and rain drops >100 µm in diameter.

Microphysical instruments used during C-FOG are summarized in Table 2 for the *R/V Sharp* and in Table 3 for all ground-based sites. Special sensors (Table 2) were developed for fog microphysics investigations, including a 'gondola' shaped assembly (located on the *R/V Sharp*) that contained microphysical sensors such as a cloud droplet probe (CDP) and a backscatter cloud probe (BCP) in a gondola unit for measuring droplet sizes ranging from 1-50 and 5-75 µm, respectively A laser precipitation monitor (LPM) for 100 µm to mm sizes and an optical particle counter (OPC) for sizes of 0.3-20 µm using 16 spectral channels allowed fog and drizzle discrimination (Table 2).

Table 2 Microphysical instruments mounted on the *R/V Sharp* during the C-FOG campaign. *Parameters in Column 2:* N_d Droplet number concentration, N_a Aerosol number concentration, SV Sampling Volume, S_w Supersaturation with respect to water, and Vis Visibility. *Parameters in Column 4*: UOIT Ontario Technical University, UU University of Utah, Wood Corporation, DU Dalhousie University, and NDU Notre Dame University.

Instrument Name	Measurements	Height (asl, m)	Owner
CDP, DMT, Gondola	N_d, Droplet spectra (1-50) µm	31.8	UOIT
BCP, DMT, Gondola	N_d, Droplet spectra (5-75) µm	31.8	UOIT
OPC N2, Alphasense	N_a, Aerosol Spectra 0.38-17µm, 16 channels	15	UU
DMT, FM120, near Gondola	N_d, Droplet spectra (1-50) µm	31.6	WOOD
TSI Moudi Impactor 100NR	N_a spectra, 0.18-18 µm, 8 stages, 30 L m^{-1}	37.9	WOOD
Virtual Impactor Inlet	At 20 m, SV=16.7 L min^{-1}	30.1	DU
SMPS 3082, TSI	N_a Spectra, 10-500 nm; SV=1.0 L min^{-1}	30.1	DU
APS 3321, TSI	N_a Spectra, 0.5-20 µm SV=1.0 L min^{-1}	30.1	DU
ACSM, Aerodyne	N_a Composition, <1 µm SV=0.1 L min^{-1}	30.1	DU
CCN-100, DMT	N_a>0.01 µm;S_w=0.2,0.4,0.8,1% SV=0.5 L m^{-1}	30.1	DU
PWD22- Vaisala	Vis <20 km	10	NDU

Also, three Scintillometers (Table 3) with measurements in the NIR (Near Infra-Red) and MW (MicroWave) radiation channels were utilized to allow discrimination of fog from rain (Perelet et al. 2020). Figure 3 shows the microphysical, aerosols, as well as meteorological instruments. Remote-sensing platforms (e.g. microwave radiometer MWR, ceilometer, Lidar), meteorological towers, tethered balloons, and the GOES-R (Geostationary Operational Environmental Satellite-R series) Products (fog coverage and effective droplet size) provided information on horizontal and vertical variability. Observational products are used for fog-visibility parameterization development, with a focus on understanding the influence of dynamical processes such as turbulent mixing and dissipation.

Table 3 Microphysical instruments located at the ground sites during C-FOG field campaign. *The parameters in Column 2*: Vis Visibility, PR Precipitation rate, IR Infrared, SW shortwave, RF radiative fluxes, LWC liquid water content, Z_e radar reflectivity, V_d Doppler velocity, N_a aerosol number concentration, Z_{cb} cloud base height, β backscattering coefficient, λ wavelength, β_n extinction coefficient, CN condensation nuclei, RH relative humidity, T temperature, U_h horizontal wind, and P pressure. *Parameters in Column 7 and 8:* BA Battery Supersite, BH Blackhead site, DO Downs Supersite, UOIT Ontario Technical University, UU University of Utah, UND University of Notre Dame, and NPS (Naval Postgraduate School).

Instrument Name	Measurements	H (agl,m)	Z (agl,m)	Lat [deg]	Lon [deg]	Site	Owner
PWD50-Vaisala	Vis and PR	2	6	47.03443	-52.8782	BA	UOIT
FM100 & FM120	Fog droplet spectra	2	6	47.03443	-52.8782	BA	UOIT
CRN1 Kipp&Zonen	IR&SW up and down RF	2	6	47.03443	-52.8782	BA	UOIT
PMWR MP3017	Profiling, T, RH, LWC	2	6	47.03443	-52.8782	BA	UOIT
MRR, Metek	Z_e & V_d	2	6	47.03443	-52.8782	BA	UOIT
LPM, Metek	Precip. Spectra >100 µm	2	6	47.03443	-52.8782	BA	UOIT
OPC, Alphasense	N_a spectra, >0.3 µm	2	6	47.03443	-52.8782	BA	UU
CL31, Vaisala	Z_{cb} and β	2	6	47.03443	-52.8782	BA	UU
Vaisala PWD 50	Vis (<30 km)	2.9	10	47.52633	-52.6583	BH	UOIT
Vaisala PWD 22	Vis (<30 km)	3	31	47.02181	-52.8731	DO	UND
LPM Metek	Precip. spectra >100 µm	2.74	10	47.52633	-52.6583	BH	UOIT
OPC, Alphasense	Aerosol spect. (0.3-20 µm)	1.37	10	47.52633	-52.6583	BH	UU
DMT CDP	fog droplets (1-50 µm)	3	31	47.02181	-52.8731	DO	NPS
TSI -3563 Nephelometer	3-λ scat& β_n (0.45,0.55,070 µm)	3	31	47.02181	-52.8731	DO	NPS
TSI OPC-310	CN >0.01 µm	3	31	47.02181	-52.8731	DO	NPS
PSAP, Part Soot Abs Photometer	1-λ absorp. at 0.565 µm	3	31	47.02181	-52.8731	DO	NPS
Scintillometer (BLS -900, Scintec AG)	wavelength 0.88 µm extinction	2.9	31	47.02181	-52.8731	DO-BH Tx-Rx	NPS

Scintillometer (BLS 900, Scintec AG)	wavelength 0.88 µm extinction,	2	6	47.03443	-52.8782	BA-DO Tx-Rx	UU
Scint. MWSC 160, Radio.Phy. GmbH	microwave (wavelength 1.860 µm extinction	2	6	47.03443	-52.8782	BA-DO Tx-Rx	UU
Met parameters	RH, T, Uh, P	3	31	47.02181	-52.8731	DO	NPS

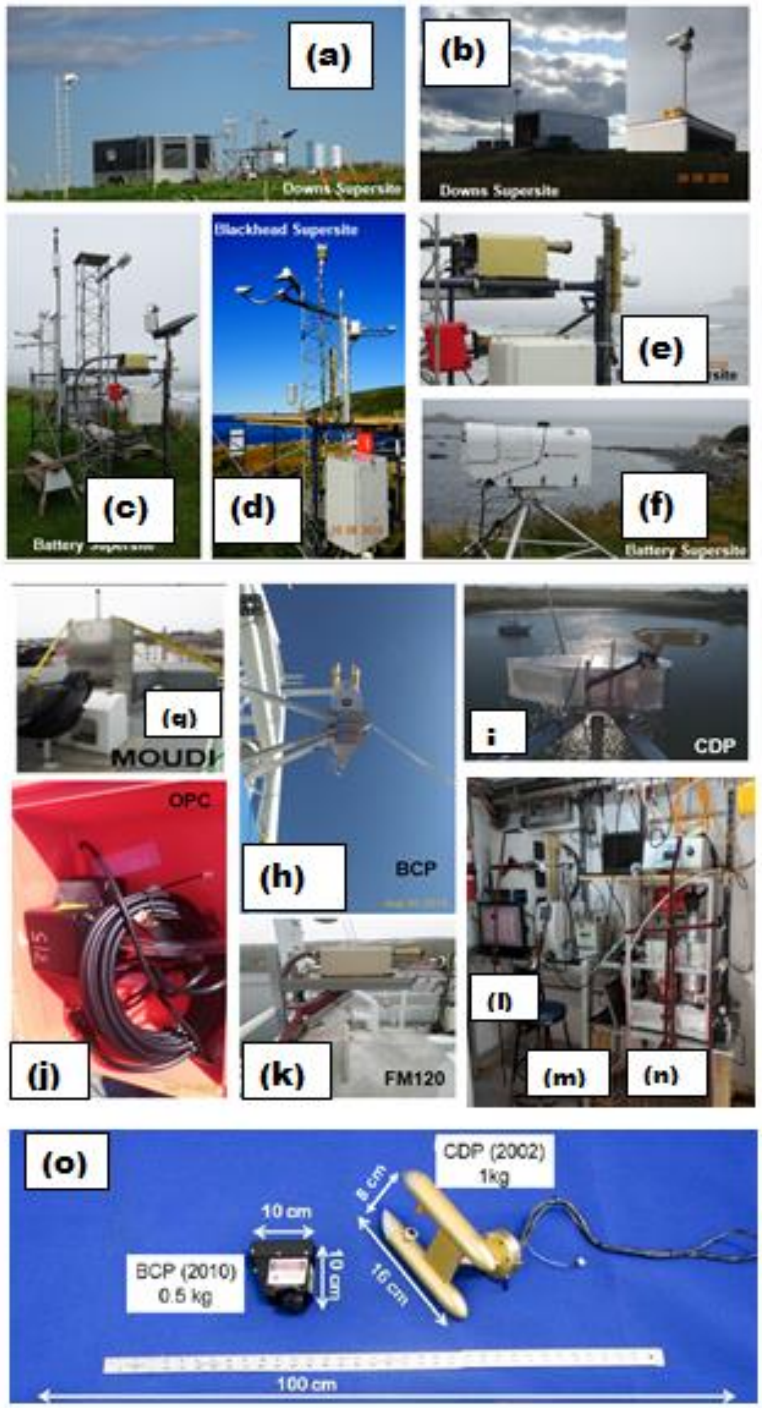

Fig. 3 Project locations with microphysical probes: The battery site (see Table 3) (a), NPS microphysical sensors mounted on a trailer at the Downs site (b) with CDP2 located in a housing at a mast, FM120, PWD,

LPM at Battery (c), PWD, LPM, and OPC at Blackhead (d), a close look of FM120 at Battery (e), PMWR at Battery (f), Wood MOUDI impactor (g), Gondola BCP (h) and CDP2 (i) mounted on Sharp RV, UU OPC (j), Wood Corp FM120 (k), Dalhousie University(DU) CCNC (l), DU SMPS (m), and DU ACSM (n), and Gondola housed CDP and BCP (o) physical characteristics (adapted from Beswick et al. 2014).

2.4 Macro-physical Characteristics

During the installation and campaign period that spanned 7-weeks (Aug 14-Oct 7 2018) various fog conditions existed, as represented by Vis measurements from the Battery site (Fig. 4). This figure shows Vis for 46 days starting from Aug 21 to Oct 7 during which drizzle and light precipitation usually occurred prior to fog. Average fog occurrence during entire campaign was 20-25%.

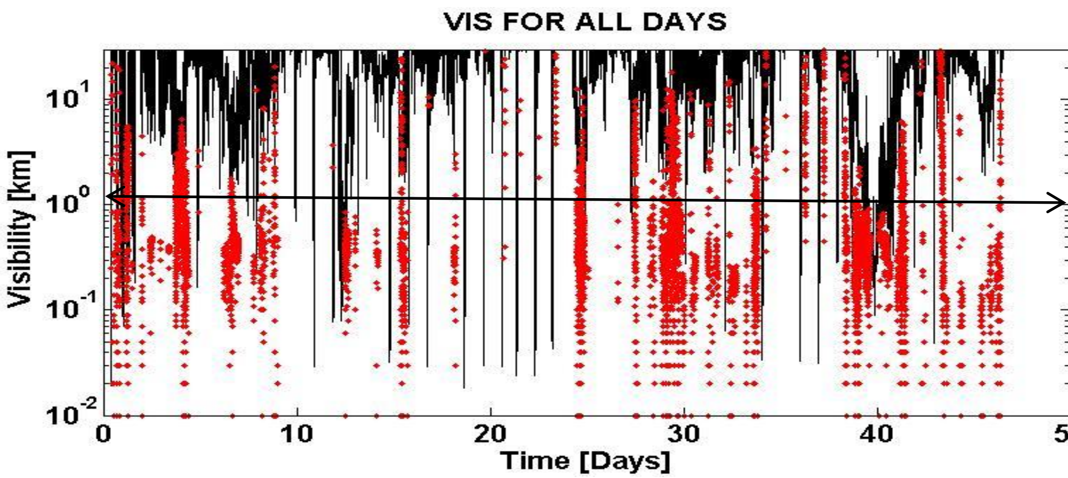

Fig. 4 Time series of Vis obtained from PWD52 present weather sensor for the entire time period from Aug 24 to Oct07 2018. The red dots are for drizzle and black lines are for fog Vis. The line with double arrow indicates Vis level at 1 km.

A CL31 ceilometer measured the backscatter ratio (β) time and height cross sections at the Battery supersite and on the *R/V Sharp* for the 4 cases studied, as shown in Fig. 5. Note that the ceilometer-based fog-top heights are not accurate because of its strong extinction when a large number of smaller fog droplets exist. Figure 5a and 5b are for 28 and 29 September cases, respectively, as observed at the Battery supersite and Fig. 5c and 5d are for 28 September and 04 October cases, respectively, aboard *R/V Sharp*.

The 28 September case at the Battery site, occurred at about 1000 UTC after the stratus layer base lowered from 500 m to the surface over 3 hrs. Some drizzle was observed (indicated by the spiking cloud base in red colour), which disappeared about

1700 UTC. The 29 September case was a continuation of the 28 September case, during which fog briefly lifted at 1600 UTC and then re-formed at 2200 UTC and lasted until almost 1800 UTC, which is not likely related solely to a lowering stratus, but was also likely due to warm-air advection that is verified by using synoptic weather conditions

The *R/V Sharp* data for 28 September (Fig. 5c) show that the cloud base decreased from 500 m at 0000 UTC to almost the surface at 1000 UTC, and then lifted very quickly at 1330 UTC. After this, the stratus base lowered again to form fog at 1400 UTC. At 1600 UTC, the fog base lifted and eventually disappeared. The *R/V Sharp* observations for 04 October show that fog formed again due to stratus lowering around 2000 UTC and lasted until 2300 UTC. Note that the lowering cloud base occurred late on this day and is likely due to IR cooling and/or large-scale subsidence. This might also be related to drizzle that moistened lower layers, eventually led to fog formation (Singh et al 2020; Wagh et al 2020).

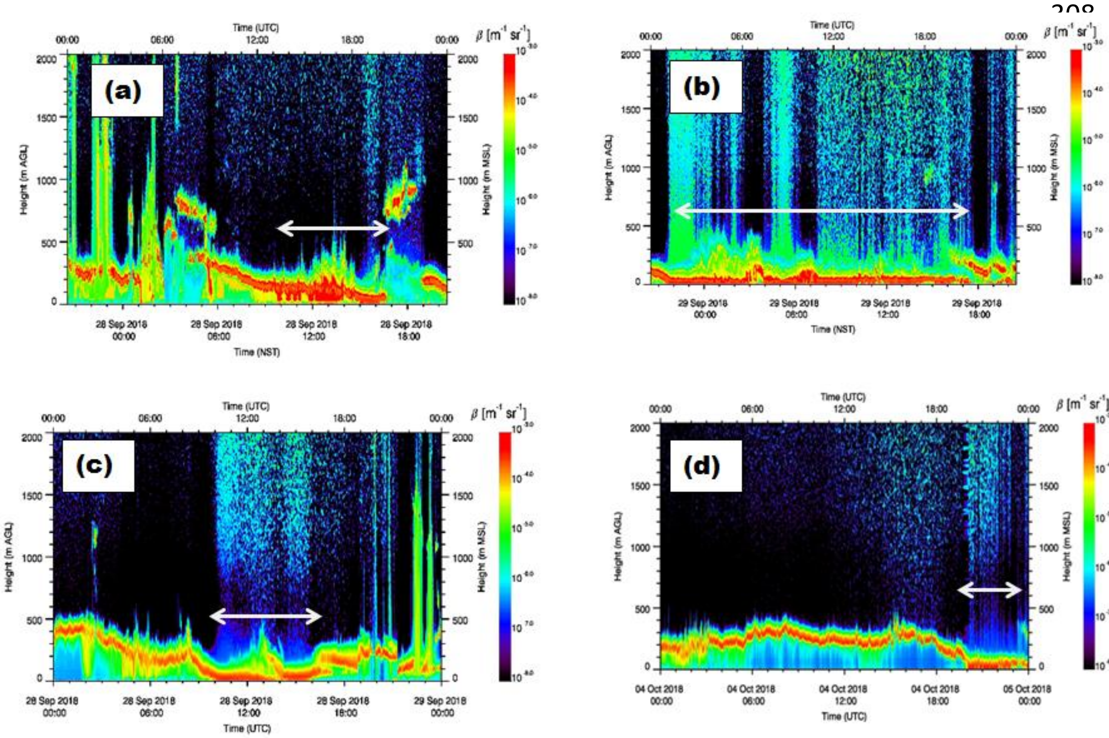

Fig. 5 Time-height cross sections of backscatter coefficient (β) from CL31 ceilometers measurements at the Battery supersite and onboard the Sharp RV for the 4 cases studied; Sep 28 (a) and Sep 29 (b) cases observed at the Battery supersite and Sep 28 (c) and Oct 04 2018 (d) cases at the Sharp RV. The white lines with arrow indicate foggy regions.

The general characteristics of these four fog cases at the Battery supersite and *R/V Sharp* are presented as a backdrop for the development of microphysical parameterizations. Note that ceilometer measurements cannot unequivocally identify fog regions, and ceilometer inferences should be validated using PWD Vis observations.

3. ANALYSIS AND MICROPHYSICAL PARAMETERIZATION

An analysis of the main microphysical and turbulence parameters to be used in the evaluation of fog conditions and for developing parameterizations is provided in this section.

3.1 Time Series of microphysical parameters and Turbulence Dissipation Rate (ε)

Time series were obtained based on various microphysical parameters, including Vis, N_d, LWC, and MVD. Vis was obtained from PWD52 measurements representing various NWS (National Weather Service) codes, droplet spectral measurements of FMD (FM120, in Battery) and CDP and BCP housed in the gondola aboard the *R/V Sharp*. NOAA NWS codes can be found in LPM (2011), based on PR and Vis time series for each hydrometeor type obtained. The FMD was operated at a 1 Hz sampling rate, compared to 1-min Vis measurements from PWD52. All meteorological parameters such as T, RH_w, and wind speed (U_h) and directions were employed as appropriate.

N_d is obtained using the corrected ship heading and apparent wind, which includes both ship speed and wind measurements (Gultepe and Starr 1995). It is corrected by computing the cosine of the angle θ between the heading and the apparent wind measured by an anemometer as

$$N_d = N_c/(SA * TAS * \Delta t), \qquad (1)$$

where the true air speed (TAS) is given by

$$TAS = U_{ha} cos\theta. \qquad (2)$$

In Eq. 1, SA is the sampling area, Δt the sampling interval and N_c the counts of droplets in each bin of the CDP and BCP. N_d is obtained from the FM120 located at the Battery site using a fixed TAS (true air speed) of 5 m s^{-1} for sampling of the environmental air. U_{ha} is the apparent wind speed that includes both ship speed and wind speed. During normal observational conditions, the *R/V Sharp* average speed was about 8 m s^{-1}.

The TKE dissipation rate (ε_{dis}) is usually calculated based on the spectral slope assumption, representing the inertial subrange (Panofsky and Dutton, 1984). In this work, 3D sonic anemometer wind measurements (collected at 20 Hz) at 2 m were used to estimate ε. It should be noted that ε calculation is strongly related to averaging scales and here ε approximately represents scales of 0.3-0.5 km that matches scales of high resolution NWP models. Thus, using a structure function, ε is estimated (Paluch and Baumgardner, 1989; Gultepe and Starr, 1995). Clearly, 1-min averages do not capture inertial subrange scales but a structure function representing 3D scales can be used to calculate ε_{dis} along the mean horizontal wind speed as

$$\varepsilon_{dis} = \frac{1}{2\pi 4.01C}\left[\frac{D_s}{\Delta r^{2/3}}\right]^{3/2}, \quad (3)$$

where C is a constant ~0.18, D_s the structure function and Δr the horizontal distance along main horizontal wind, and these are given, respectively, as

$$D_s = 0.38(\Delta u^2 + \Delta v^2 + \Delta w^2) \text{ and } \Delta r = \Delta t(U_{dx}^2 + U_{dy}^2)^{1/2}. \quad (4)$$

In Eq. 4, Δu, Δv, and Δw represent the change in wind components along x, y, and z axis at unit time interval (Δt), receptively; U_{dx} and U_{dy} are wind speed components along x and y axis, respectively, over Δt. Thus, Eq. 3 can then be used in dissipation rate calculations and evaluation of the fog life cycle. For the NWP models, ε is not always an output parameter; therefore, TKE can be calculated from the following equation (or a transformation equation given in Discussion section) that is used to obtain a threshold for fog formation:

$$TKE = \frac{1}{2}\left(u'^2 + v'^2 + w'^2\right), \quad (5)$$

where $u', v', and\ w'$ are fluctuations of wind x, y, and z components that are calculated over 10 min intervals.

3.2 Visibility Parameterization

The visibility parameterization is calculated diagnostically, which is a function of various moments of DSD (drop size distribution). In this study, N_d and LWC are used in the Vis parameterization; but N_d is replaced with MVD to emphasize that two microphysical parameters are sufficient to calculate Vis (Gultepe et al 2018). It is emphasized that either RH_w or T_a-T_d can be used to indicate the existence of fog, but not intensity (e.g. Vis).

3.2.1 Vis-RH_w Parameterization

The visibility can be parameterized as a function of RH_w, which is measured by a Vaisala HMP 155. RH_w is measured together with T_a from which T_d is estimated. A PWD is used to obtain Vis measurements. The functional relationship between Vis and RH_w is determined by testing various regression fits and selecting the function that 'best' fits the observations. Here, humidity data used for the best fit are first bin averaged in 5% intervals. A derived relationship between Vis and RH_w together with a plot is provided in section 4.1.1 and given in Table 3. Note that we do not use T_a-T_d in the Vis parameterization because RH_w is based on both T_a and T_d (Gultepe and Milbrandt 2011). Therefore, fog coverage is obtained when $RH_w > 95\%$, which is further explained in the results section.

3.2.2 Vis versus Microphysics Parameters

Fog Vis can be obtained in two ways. The *first* is based on an extinction coefficient measured directly by a probe (e.g., PWD) which is then used to retrieve microphysical parameters assuming certain particle size distributions. The *second* is based on droplet spectral measurements from which LWC and N_d (or MVD) can be used to estimate Vis. Usually, direct measurement of Vis cannot be considered in the same way as those obtained from measured particle size spectra, because of measurement issues. Using warm fog microphysical spectral measurements, Gultepe et al (2006) developed a parameterization that is based on the theory of extinction of visible light in a volume of fog droplets as

$$\beta_{ext} = \sum_{r1}^{r2} \pi Q_{eff}(r, \lambda) n(r) r^2 \Delta r \,, \qquad (6)$$

where β_{ext} is the extinction coefficient (cm^{-1}), Q_{eff} the extinction efficiency, r droplet radius (µm), λ the visible light wavelength (µm), n(r) the particle number density (cm^{-3} μm^{-1}), and r^2 the droplet surface area. Q_{eff} is usually assumed to be 2, because size parameters ($k=2\pi r/\lambda$) are within the regions where geometric optics apply. For sizes less than about 5 µm, Q_{eff} can be larger than 2, significantly affecting the extinction of visible light. Equation 5 can be used for calculating β_{ext} if the particle size spectrum is known for each time step, when NWP model simulations exist.

The extinction coefficient (Eq. 6) can be converted into Vis using the Koschmieder (1924) relationship as

$$Vis = \frac{-ln(C)}{\beta_{ext}} . \tag{7}$$

For the meteorological observed range (MOR), C is defined as the threshold value that best fits to conditions whereby the human eye can recognize a target during daytime and is taken as 0.05 (Gultepe et al 2014). Using Eq. 5 and Eq. 6, the Vis can be obtained as

$$Vis = \frac{-(\frac{4}{3})ln(\varepsilon)\rho_w \sum_{r1}^{r2} n(r) r^3 \Delta r}{Q_{ext} LWC \sum_{r1}^{r2} n(r) r^2 \Delta r} . \tag{8}$$

Then, Eq. 7 can be simplified as

$$Vis = 5.216 \frac{\rho_w r_{eff}}{Q_{ext} LWC} , \tag{9}$$

where ρ_w is the liquid water density ≈1000 kg m^{-3}. Vis can be obtained from Eq. 9 if the effective radius (r_{eff}) and LWC are known. Mist conditions (defined as Vis>1 km and RH_w<100%) can also be important for visibility reduction due to swelled aerosols (Fig. 6). A lower limit for mist is usually defined as RH_w~80%. Haze is composed of dry aerosols where RH_w is usally <70%. Lower limit of haze Vis can be down to a few km.

Since N_d is inversely related to particle size (e.g. r_{eff}), as r_{eff} decreases N_d usually increases. Gultepe and Milbrandt (2007) replaced Eq. 9 with the approximate form

$$Vis = \alpha \left[\frac{\rho_w}{Q_{eff} N_d LWC}\right]^{\gamma} , \tag{10}$$

where α and γ are regression constants, and N_d and LWC are obtained from fog DSD, respectively, as

$$N_d = \sum_{r1}^{r2} n(r) \Delta r \tag{11}$$

and

$$LWC = \sum_{r1}^{r2} (\frac{4}{3}) \pi \rho_w n(r) r^3 \Delta r . \tag{12}$$

Assuming that $Q_{eff,}$ and ρ_w are constants, Eq. 10 can be rewritten as

$$Vis = \alpha (N_d LWC)^{-\gamma}, \tag{13}$$

which can be converted to β_{ext} using Eq. 7. For Eq. 13, α and γ are provided in Table 4. In NWP models, Vis is usually diagnosed with post processed model outputs for LWC, which is typically a prognostic output variable. If a numerical forecast model can resolve microphysical processes at small time and space scales, Vis can also be predicted diagnostically. This parameterization does not need droplet spectra at each time step that increases calculation time significantly.

Vis parameterizations may not include effective size (or MVD) because N_d is a function of MVD as follows

$$N_d = \left(\frac{1}{k}\right)\frac{LWC}{MVD^3} \tag{14}$$

where k=(4/3)πρ_w. Moreover, replacing N_d in Eq. 13 with Eq. 14, Vis can be rewritten as follows

$$Vis = \alpha(\left(\frac{1}{k}\right)\ \frac{LWC}{MVD^{3/2}}\ )^{-2\gamma}\ . \tag{15}$$

This suggests that knowing MVD and LWC, Vis can be obtained prognostically from a NWP model simulation without requirement of N_d. Therefore, the 3rd parameter from a DSD may not be required.

4 Results

4.1 The 8 September Case (Battery Site)

4.1.1 Vis-RH_w Parameterization

Vis-RH_w parameterizations are usually derived for fog coverage but not fog intensity, which are obtained based on observations of Vis and RH_w, as well as T_a-T_d differences. RH_w close to 100% indicates the existence of fog layers but does not indicate intensity because of measurement uncertainty in T and T_d measurements and RH_w (Gultepe et al 2019). In fact, RH_w is obtained as a function of T_a and T_d so it is redundant to use both T_a-T_d and RH_w in the same parameterization (Gultepe and Milbrandt 2010; Benjamin et al 2010; Smirnova et al. 2000). Figure 6 shows Vis versus RH_w for 3 sites located in Ferryland, including Battery, Blackhead, and the Downs, for 28 Sep 2018. In this figure, fog (Vis<1 km), mist (2>Vis>1 km), and haze layers (Vis>2 km & RH_w<80%) as well as rain data points are shown. Differences among RH_w values are likely related to location and elevation differences. A best fit for the equation for Vis versus RH_w using 5% RH_w bins is also shown in the figure 6 and given in Table 3.

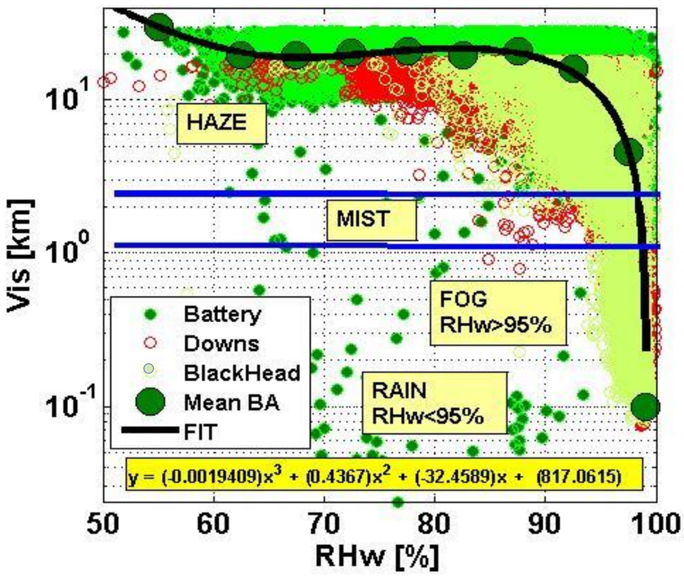

Fig. 6 Vis versus RH_w for NWS hydrometeor classification based on PWD instrument measurements at Battery, Blackhead, and Downs sites on 28 Sep 2018. The fit line is applied to bin averaged RH_w values at 5% intervals. The equation fitted is shown on the plot together with rain data points.

This figure suggests that Vis<1 km corresponds to RH_w>95%, which can be used as a criterion for detecting fog coverage but not intensity. Note that RH_w measurement accuracy is about 10% (Gultepe et al 2019). Haze and mist layers can occur when RH_w > 55% up to RH_w ~ 95% (Vis> 1 km). Rain with Vis <1 km occurs when RH_w < 95%. Evidently there is no clear distinction between mist and haze for Vis (>1 km). Another point is that Blackhead and Downs had a larger RH_w compared to the Battery site, likely due to their higher elevations (30 m versus 2 m).

4.1.2 Time Series of Meteorological Parameters

Time series of Vis, PR, and precipitation types are shown in Fig. 7a based from PWD measurements at 1-min time resolution. Fog and mist are seen mainly in the early morning (segment 1; rectangular box) and later in the day (segment 2). Specifically, a drizzle and light rain event is clearly seen before segment 2, which likely played an important role for BL saturation. During fog events Vis was a few 100s of meters.

Fog formation and dissipation are likely related to the TKE magnitude and dissipation rate, which are related to the fluctuations of 3D wind components. The value for ε is calculated from Eq. 3 using 3D wind components and a 2D structure function (Eq. 4) and utilizing 1-min and 5-min running averages (Fig. 7b). The ε during fog is usually less than for fog free conditions (e.g. 0500 and 2000 UTC). The 3D wind components are shown in Fig. 7c. During fog events (see Vis time series in Fig. 7c), the magnitudes of 3D wind components are found to be significantly lower than for fog free conditions. The vertical air velocity (w_a) fluctuations were significantly smaller compared to u and v components for the entire day, indicating the importance of advection processes in the horizontal direction on the fog life cycle. Figure 7d shows 1-minute averaged local accelerations of u, v, and w_a, indicating that the turbulence intensity levels were almost 50% less compared to fog-free segments.

Results suggest that ε is about $3x10^{-4}$ m^2 s^{-3} in foggy segments compared to >$1x10^{-3}$ m^2 s^{-3} in fog-free conditions, which can be used as a criterion for fog formation and dissipation. These values are found to be comparable to those of Downs site (Grachev et al. 2020) who showed that during foggy conditions ε_{dis} was between $1x10^{-3}$ m^2 s^{-3} and $1x10^{-4}$ m^2 s^{-3}. Some differences between their work and current work is that The Downs site at 30 m likely had stronger wind fluctuations compared to current one at sea level. Another reason may arise due to their use of TKE based on averages done over 15 mins.

4.1.3 Vis parameterization and microphysical parameters

To develop a Vis parameterization, fog microphysical parameters such as N_d, MVD, and LWC are needed because Vis is defined in terms of these parameters. Microphysical parameters are calculated from the FM120 measurements from the Battery site. Figure 8a shows a time series of N_d as a function of LWC, where N_d increases with increasing LWC. N_d time series as a function of log(Vis) is shown in Fig. 8b where log(Vis) ≤ 0 indicates fog conditions. Vis decreases with increasing N_d. These figures suggest that Vis is related to both N_d and LWC (Gultepe et al 2006). Figure 8c shows MVD versus N_d as a function of LWC (colour bar) together with theoretical lines obtained from Eq. 13. The lines ranging from bottom to top in Fig. 8c represent values for LWC = 0.001:0.01:0.1 g

m^{-3} with solid lines, and LWC = 0.1:0.05:0.3 g m^{-3} with dashed lines with theoretical lines calculated using Eq. 13 (c). Clearly MVD is a function of N_d, and decreases with increasing N_d while LWC increases. This suggests that Vis can be obtained as a function of either N_d and LWC or MVD and LWC. Figure 8d shows the fit equation for Vis = f(LWC, N_d) overlaid on observations, where mean values at dx intervals along x axis and percentile values are also shown. This equation is obtained from the measurements at Battery and represents local coastal fog conditions.

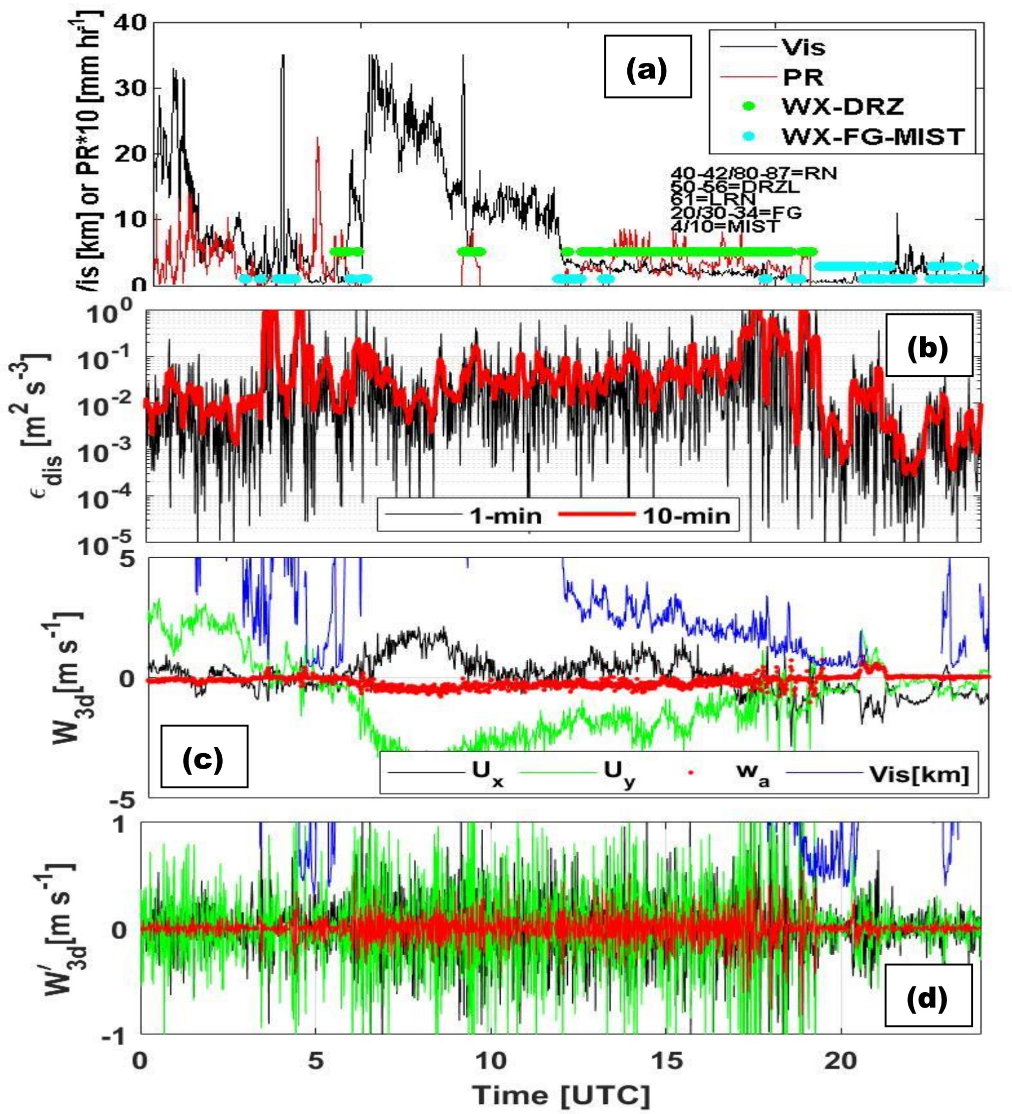

Fig. 7 Vis, PR, and NWS hydrometeor code time series on 28 Sep 2018 for Battery site (a) with fog regions shown with light blue data points, ε_{dis} (TKE dissipation rate) time series for 1-min and 5-min running averages are shown in (b), 1-min averaged 3D wind components of u_x, v_y, and w_a as well as Vis time series

(purple line) are shown in (c) with fog regions indicated as blue coloured horizontal bars, and (c), and acceleration terms du/dt (black line), dv/dt (green line), and dw/dt (red line) with dt=60 s and Vis time series (blue line) are shown in (d). Note that during fog conditions these wind speed changes become comparable low versus fog free conditions.

4.2 The 29 September case (Battery site)

4.2.1 Time Series of Meteorological Parameters

Time series of Vis, PR, and precipitation types are shown in Fig. 9a, similar to the 28 Sep case, representing PWD measurements at 1-min sampling rate. Fog and mist are seen mainly between 0000 UTC and 1200 UTC early morning (segment 1) and mist and drizzle mainly later in the day (segment 2; 1300-0000 UTC). A drizzle event is seen during segment 2. During fog segment 1, Vis is a few hundred meters.

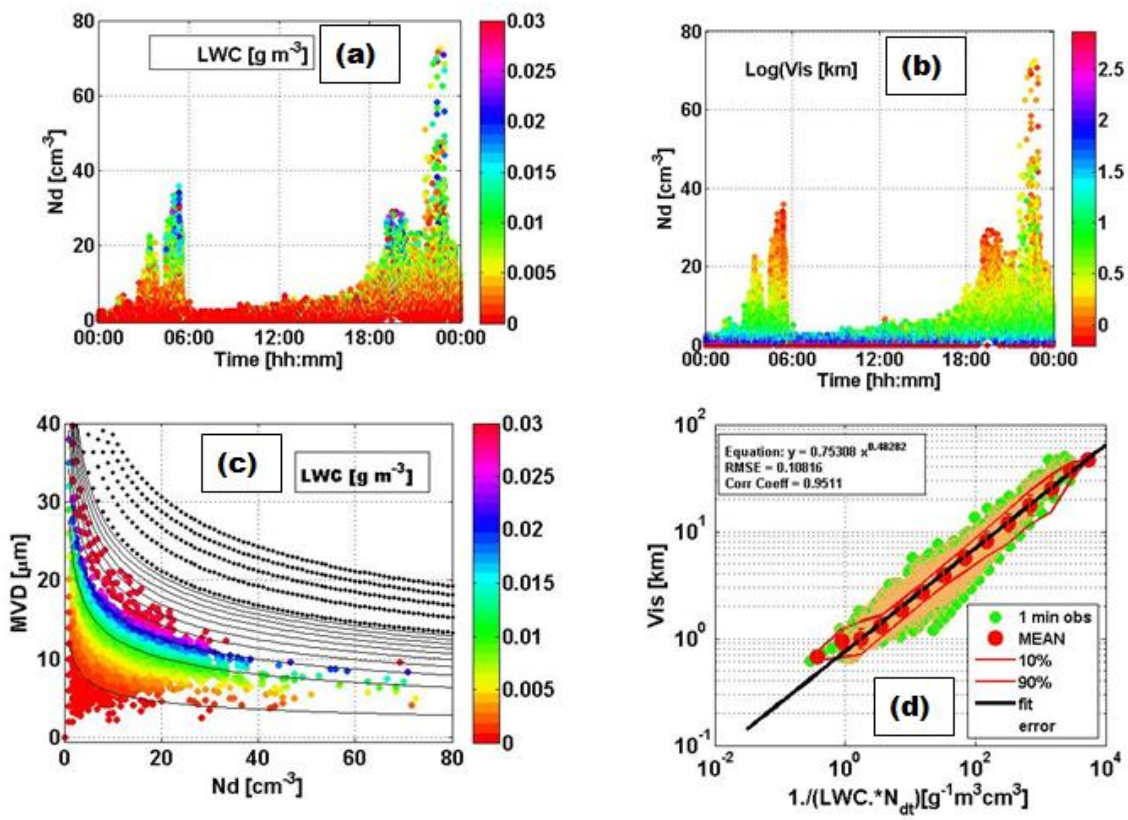

Fig. 8 Time series of N_d coloured by LWC (a), N_d coloured by log(Vis) (b), and MVD versus N_d with points coloured by LWC (LWC=0.001:0.01:0.1 solid lines and LWC=0.1:0.05:0.3 dashed lines) (c) with theoretical lines calculated from Eq. 13. Vis parameterization as a function of fog index (FI along x axis) with statistical parameters and fit equation overlaid on observations are shown in (d) for 28 Sep 2018.

The calculation for ε is similar to the 28 Sep case, utilizing 1-min and 5-min running averages (Fig. 9b). The values for ε are found to fluctuate more during the foggy segment 1 (0000-1000 UTC), than segment 2 (1400-2300 UTC) fog and misty conditions. The values for ε change between $1x10^{-2}$ m^2 s^{-3} and $1x10^{-7}$ m^2 s^{-3} during the foggy segment 1, where u_y is highly variable between +1 and -1 m s^{-1} (Fig. 9c and 9d). Overall, ε_{dis} is less than 10^{-5} m^2 s^{-3} for both fog segments. Figure 9d shows 3D wind components and Vis, where stronger wind fluctuations likely play an important role, leading to increasing Vis values during segment 2 (light fog).

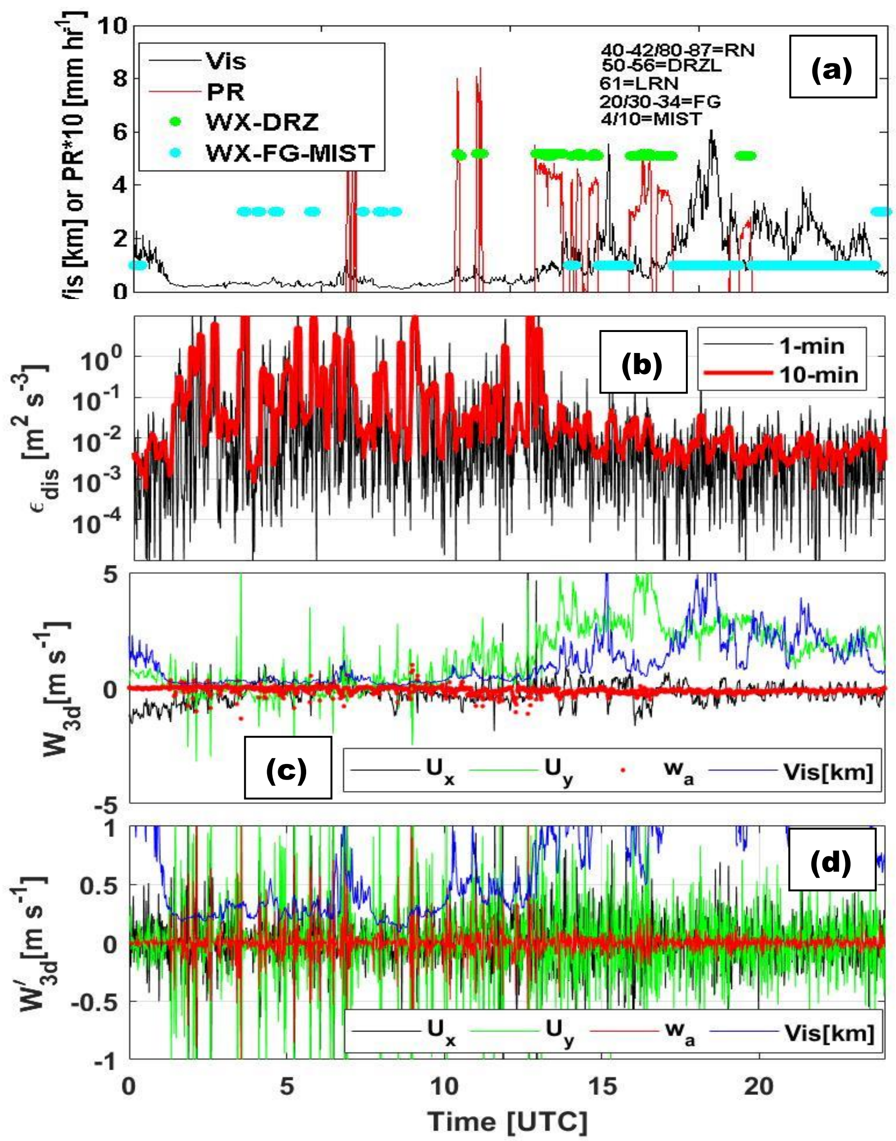

Fig. 9 Vis, PR, and NWS hydrometeor code time series on 29 Sep 2018 for Battery site (a) with fog (drizzle) regions shown with light blue (green) data points, ε_{dis} time series for 1 min and 5 min running

averages are shown in (b), 1-min averaged 3D wind components of u, v, and w_a as well as Vis time series are shown in (c) with fog regions indicated as blue coloured horizontal bars, and (c), and acceleration terms du/dt (black line), dv/dt (green line), and dw/dt (red line) with dt=60 s and Vis time series (blue line) are shown in (d). Note that during fog conditions these wind speed changes become comparable to low versus fog free conditions.

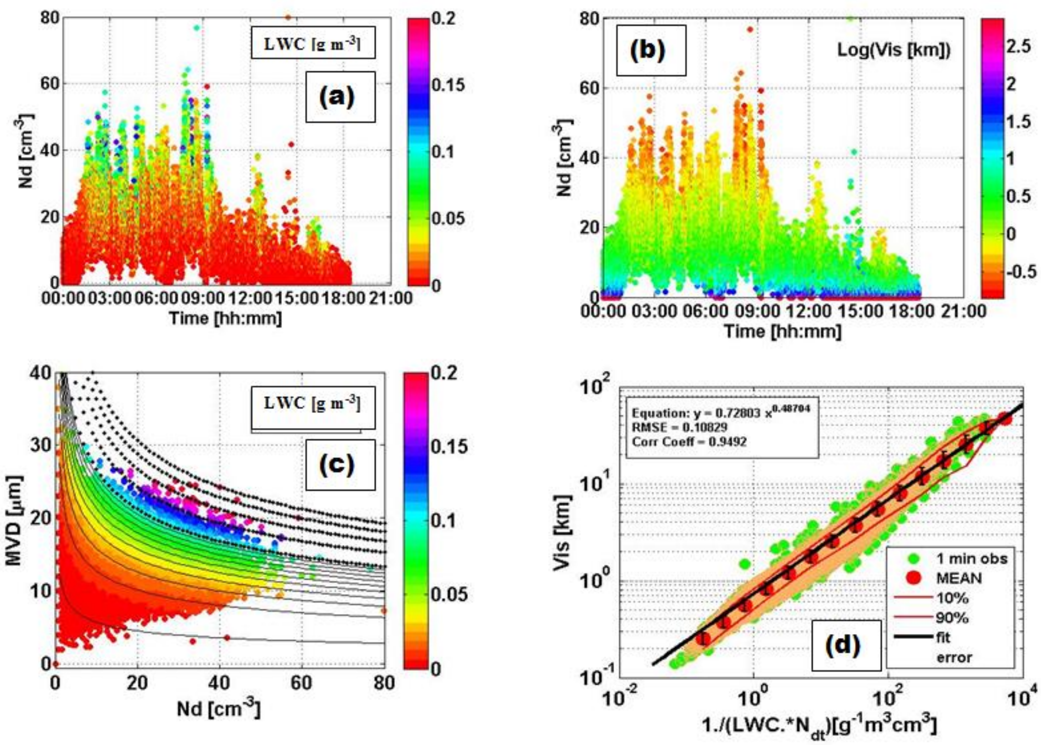

Fig. 10 Time series of microphysical parameters N_d versus LWC (a), N_d versus log(Vis) (b), and MVD versus N_d as a function of LWC (c) with theoretical lines calculated from Eq. 13. Vis parameterization as a function of fog index (FI along x axis) with statistical parameters and fit equation overly on observations are shown in (d) for 04 October 2018.

In summary, most of the ε data points are found below the dissipation rate of $3\text{x}10^{-5}$ m^2 s^{-3} during fog segments. The w_a fluctuations in segment 1 are smaller compared to drizzle and fog conditions seen in segment 2. Note that wetting of the sonic anemometer transmitter/receiver may occasionally cause large fluctuations of wind components during heavy fog conditions. Results suggest that, based on 1-min averages, minimum (max) ε is about $1\text{x}10^{-6}$ m^2 s^{-3} ($3\text{x}10^{-2}$ m^2 s^{-3}) in foggy segment 1, compared to $3\text{x}10^{-5}$ m^2 s^{-3} during mist and drizzle conditions (segment 2). Another point is that southerly wind fluctuations (wind coming from south) are likely responsible for warm and moist advection over the region, leading to fog formation similar to 28 Sep case.

4.2.2 Vis parameterization and microphysical parameters

Results and parameterizations for this case are obtained similar to that of 28 Sep case (Fig. 10). MVD and N_d are found to be comparatively larger on this day (Fig. 10a,b,c). For example, the maximum MVD reaches 40 μm compared to 30 μm on 28 Sep. The maximum N_d is about 60 cm^{-3} compared to a maximum for N_d of 70 cm^{-3} on 28 Sep. Finally, the Vis fit equation is shown in Fig. 10d. Overall, the slope of the best fit line is very similar to the 28 Sep case but with relatively lower values of observed Vis.

4.3 The 28 September Case (RV Sharp)

4.3.1 Time Series of Vis and RV Wind Components

Time series of *R/V Sharp*'s navigation parameters obtained from the VectorNav VN100 IMU and Trimble BX982 Dual GNSS receiver (Fernando et al 2020) are reported here at 1-min intervals (Fig. 11a). This figure shows the *R/V Sharp's* speed with respect to the ground (U_{RV}), true wind speed (U_{hT}), wind speed with respect to ground (U_{hR}) and smoothed values of U_{hR} over 10 mins intervals. During the fog event between 1000 UTC and 1600 UTC, the *R/V Sharp* was heading 250 deg (SW) until 1300 UTC, then changed to 50 deg NE with U_{RV} at about 5-8 m s^{-1}. Low Vis was observed between 1000 UTC and 1600 UTC, during which Vis improved from 1 km to 5 km after *R/V Sharp* changed direction. After 1600 UTC, Vis increased up to 15 km. Low Vis and haze conditions (Fig. 11b) before 1000 UTC likely played an important role later on for drizzle conditions after 1000 UTC. Thereafter, drizzle just before fog formation likely led to moistening of the BL and resulted in fog occurrence at about 1200 UTC.

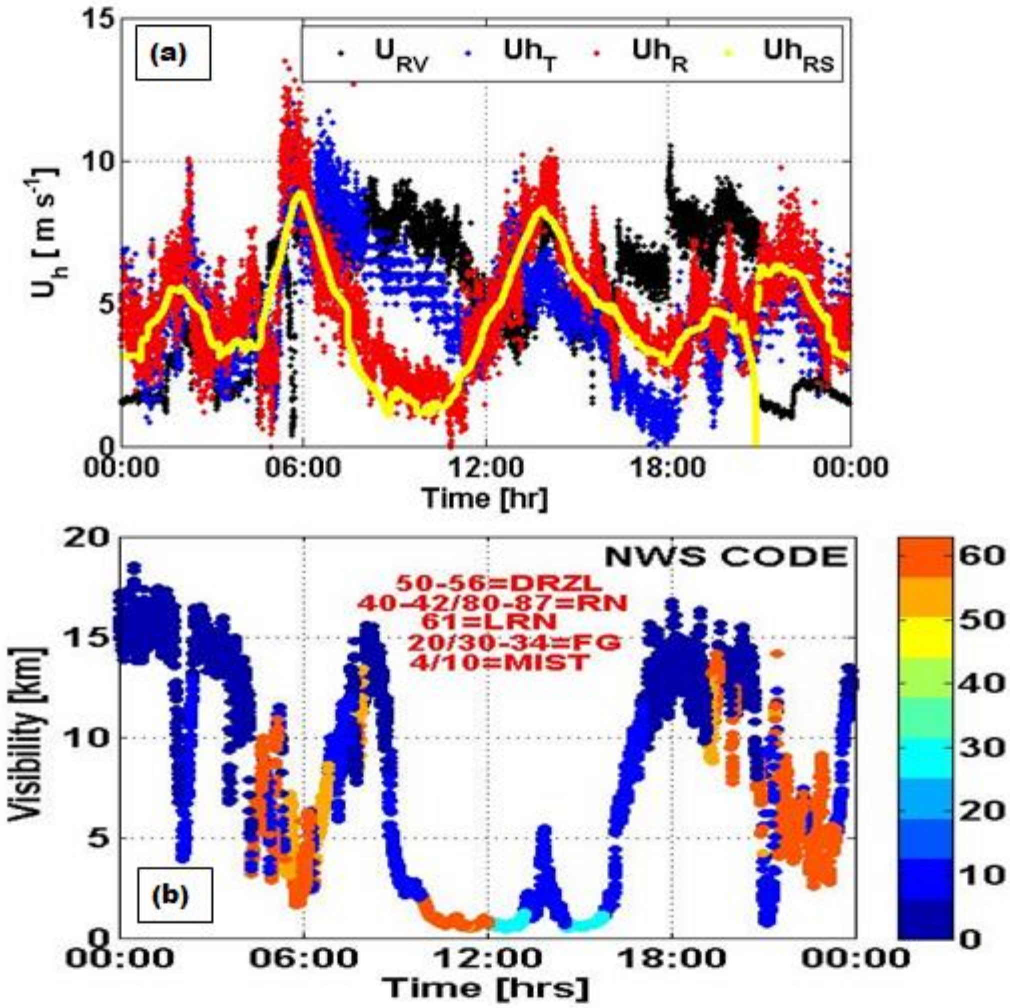

Fig. 11 Time series of U_{RV}, U_{hT}, U_{hR}, and U_{hRS} for 1 min and 10 min running averages are shown in (a) and Vis, PR, and NWS hydrometeor code time series on 28 Sep 2018 (b) with fog regions shown with light blue data points.

4.3.2Vis parameterization and microphysical parameters from the gondola

In this subsection, fog droplet spectral characteristics obtained from the CDP and BCP housed in the gondola (Fig. 2) are investigated. Both CDP and BCP plots were obtained similar to the Battery plots. Note that BCP (Fig. 12) measurement starts at 5 μm compared to CDP at 2 μm (Fig. 13) and had the capability for measurements up to 75 μm. Measurements of N_d, MVD, and LWC are less than 60 cm^{-3}, 40 μm, and 40 g cm^{-3}, respectively. A parameterization is obtained with a power-law form similar to Eq. 12 and is shown in the figure. The best fit line indicates that increasing fog index (FI

=1/(LWC*N_d)) results in increasing Vis, which is found to be similar to the fit line obtained for the Battery site. FI increases with increasing values of either N_d or LWC. Note that N_d can be replaced with MVD using Eq. 14.

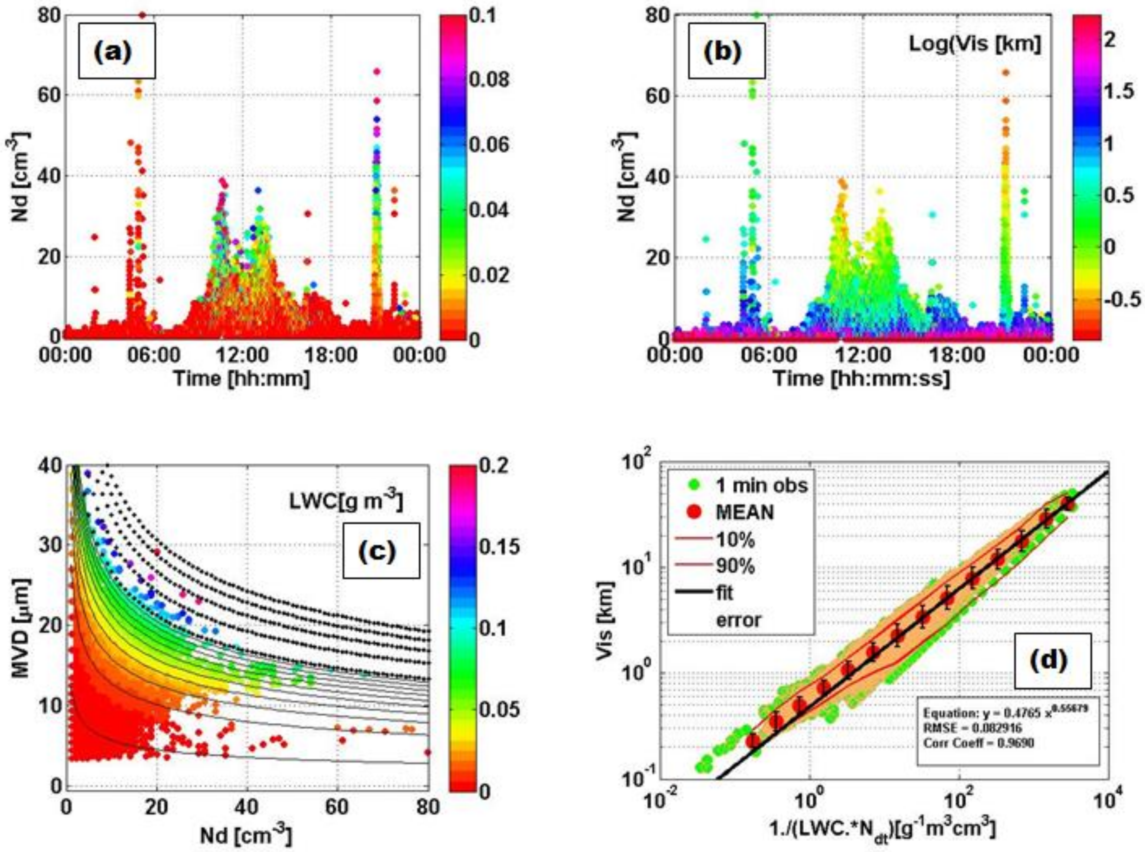

Fig. 12 Time series of microphysical parameters N_d versus LWC (a), N_d versus log(Vis) (b), and MVD versus N_d as a function of LWC (c) with theoretical lines calculated from Eq. 13. Vis parameterization as a function of fog index (FI along x axis) with statistical parameters and fit equation overly on observations are shown in (d) for RV CDP on 28 Sep 2018.

Fog-droplet spectral characteristics obtained from the BCP measurements are shown in Fig. 13. Note that because of missing the first 2 channels in BCP compared to CDP, N_d, LWC, and MVD cannot have the same values for both probes. N_d and LWC are based on BCP measurements and therefore, are expected to be less; but MVD is higher than CDP parameters. Results suggest that max values for N_d are about 15 cm^{-3}, for LWC about 0.07-0.08 g m^{-3}, and for MVD~60 µm.

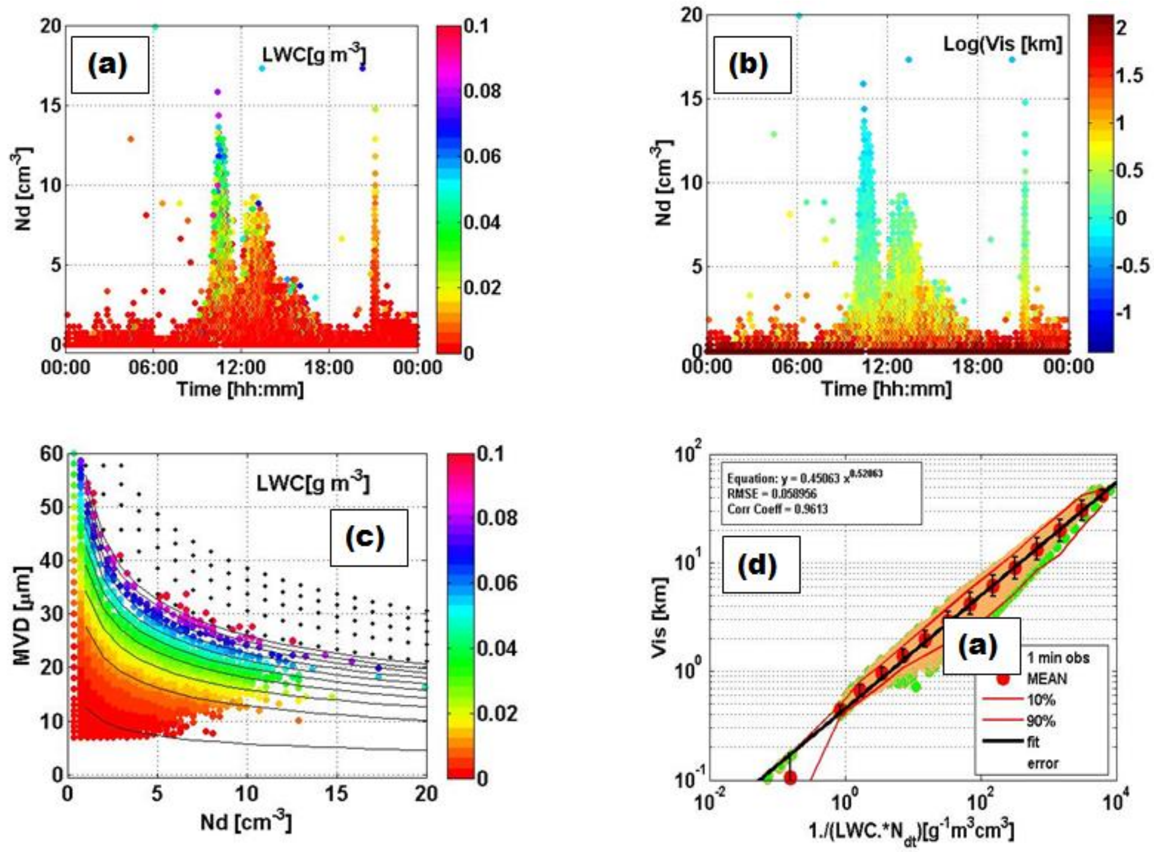

Fig. 13 Time series of microphysical parameters N_d versus LWC (a), N_d versus log(Vis) (b), and MVD versus N_d as a function of LWC (c) with theoretical lines calculated from Eq. 13. Vis parameterization as a function of fog index (FI along x axis) with statistical parameters and fit equation overly on observations are shown in (d) for RV BCP on 28 Sep 2018.

4.4 The 4 October Case (*RV Sharp*)

4.4.1 Time Series of Vis and RV Wind Components

Time series of *R/V Sharp's* navigation parameters are given in Fig. 14a. This figure also shows U_{RV}, U_{hT}, U_{hR}, and smoothed values of U_{hR} over 10-minute intervals. Fog occurred between 1900 and 2300 UTC. Before the fog event at 1900 UTC, the ship was headed 250 deg (SW), and U_{RV} changed from about 4 m s^{-1} to 8 m s^{-1}. U_{hR} was from north during the fog event (not shown). Low Vis (1 km) was observed between 1900 and 2300 UTC and Vis improved to 5 km at 2300 UTC. Before 1900 UTC, Vis increased to 15-20 km. Thereafter, the cloud base lowered to the surface and Vis decreased to <300 m. During low Vis conditions (Fig. 14b) near the end of fog event, drizzle was observed around 2300 UTC. After 1930 UTC, Vis improved significantly.

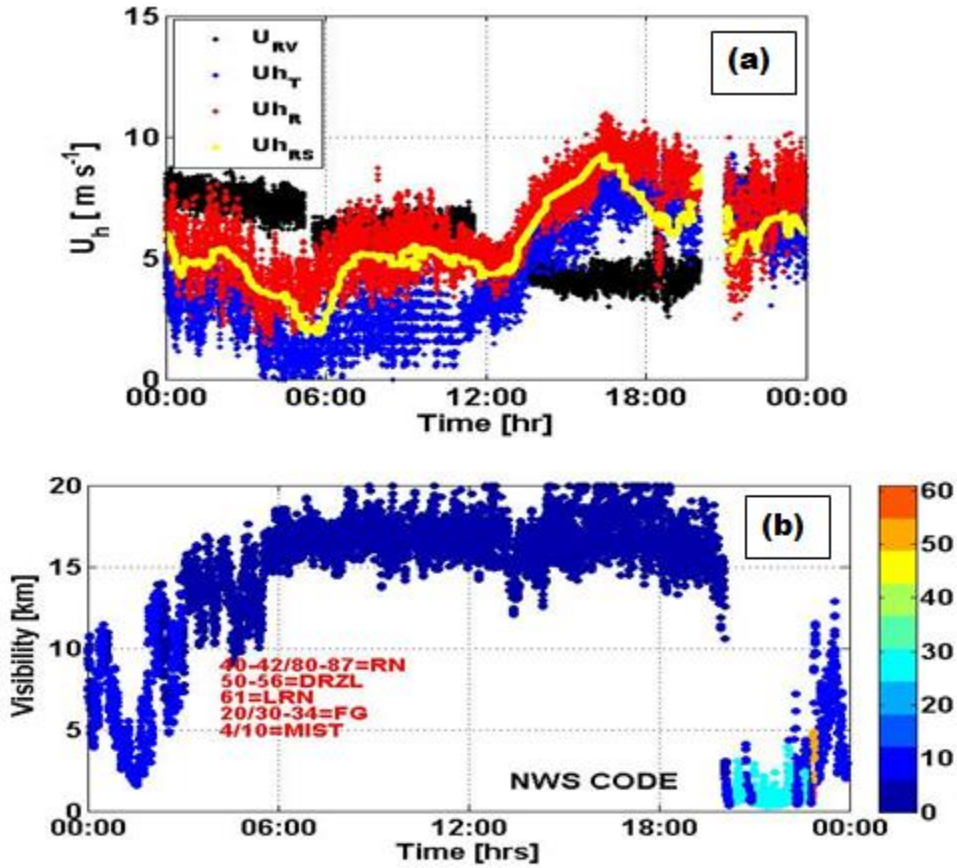

Fig. 14 Time series of U_{RV}, U_{hT}, U_{hR}, and U_{hRS} for 1 min and 10 min running averages are shown in (a) and Vis, PR, and NWS hydrometeor code time series on 28 Sep 2018 (b) with fog regions shown with light blue data points.

4.4.2 Vis Parameterization and Microphysical Parameters from the Gondola

Fog droplet spectral characteristics obtained from the CDP and BCP during the 29 Oct case are shown in Fig. 15 and Fig. 16, respectively. Note that max CDP N_d (Fig. 15a,b) is about 75 cm^{-3} and LWC reaches 0.4 g m^{-3}. Low Vis, representing fog conditions, is found between 2000 and 2200 UTC. MVD (Fig. 16c) ranged from a few μm up to 40 μm at low LWC and N_d but was at about 22 μm when N_d reached a maximum at 70 cm^{-3}. CDP measurements of MVD and LWC were less than 40 μm and 0.45 g m^{-3}, respectively. The parameterization obtained based on CDP measurements are shown in

Fig. 16d. Similar to previous cases, Vis also increases with increasing values of fog index (FI = 1/(LWC*N_d) but decreases with increasing LWC and N_d (with decreasing MVD). The best fit line indicates that increasing FI values result in similar increasing Vis conditions that represent the Battery site.

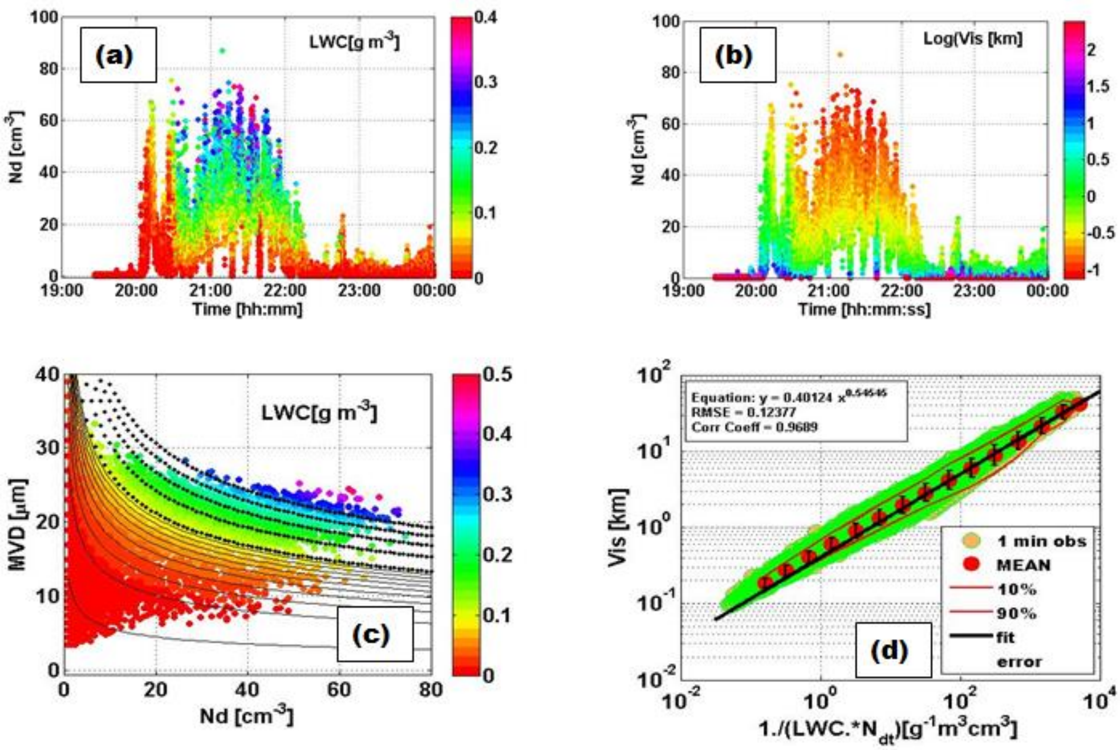

Fig. 15 Time series of microphysical parameters N_d versus LWC (a), N_d versus log(Vis) (b), and MVD versus N_d as a function of LWC (c) with theoretical lines calculated from Eq. 13. Vis parameterization as a function of fog index (FI along x axis) with statistical parameters and fit equation overly on observations are shown in (d) for RV CDP on 04 October 2018.

Fog droplet spectral characteristics based on BCP are shown in Fig. 16. Again, due to missing the first 2 channels of CDP in BCP measurements, CDP, N_d, LWC, and MVD cannot be directly compared to those of CDP measurements. As suggested previously, if there is no drizzle, N_d and LWC based on BCP measurements are expected to be less compared to CDP parameters; but MVD is expected to be higher because of larger droplets. Results suggest that max N_d was about 25 cm^{-3}, LWC about 0.4 g m^{-3}, and MVD~40 μm. The parameterization for this case based on BCP measurements is shown in Fig. 16d. Similar to previous cases, Vis increases with increasing FI.

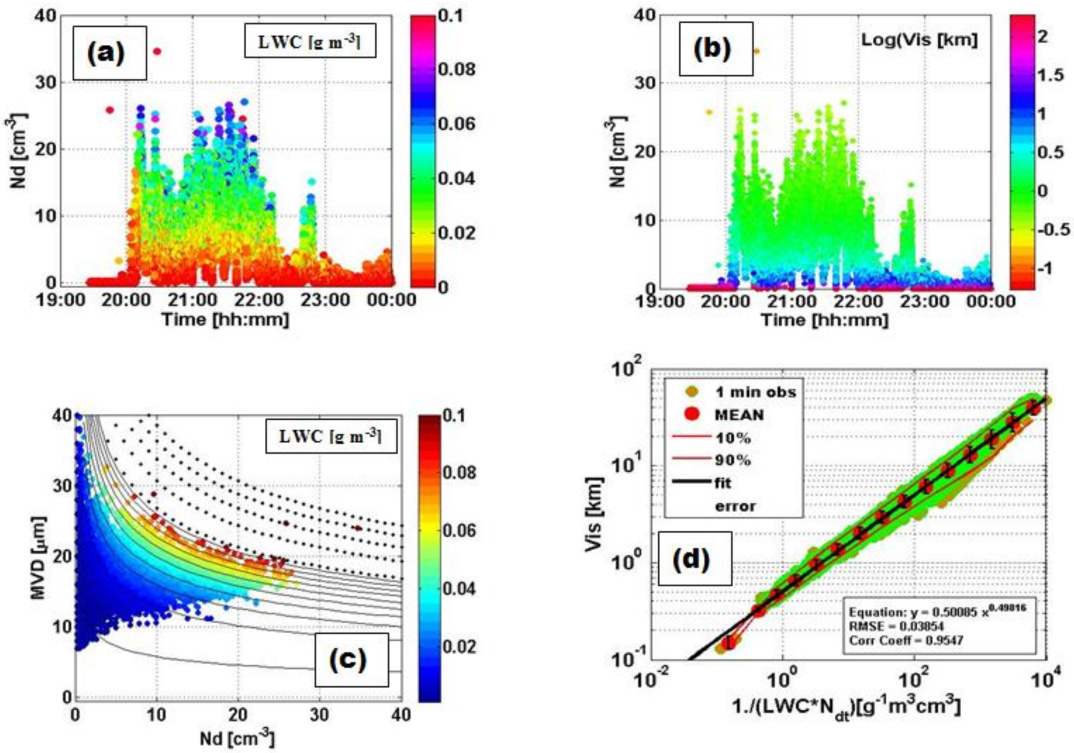

Fig. 16 Time series of microphysical parameters N_d versus LWC (a), N_d versus log(Vis) (b), and MVD versus N_d as a function of LWC (c) with theoretical lines calculated from Eq. 13. Vis parameterization as a function of fog index (FI along x axis) with statistical parameters and fit equation overly on observations are shown in (d) for RV BCP on 04 October 2018.

4.5 Summary of Vis Parameterizations

Vis parameterizations are obtained for each platform (*R/V Sharp* or Battery supersite) using FM100, CDP, and BCP probes and are summarized in Table 4. The Vis-RH_w relationships are also provided to emphasize that they are used only as a threshold for fog formation (e.g. RH_w>95% in Fig. 6). Then, fog intensity (e.g. Vis) can be estimated based on model-predicted values for LWC and N_d (or MVD) (see Eq. 14). Note that the G2007 parameterization (Gultepe et al 2007) was obtained using FSSP measurements based on low-level flying aircraft observations over the Bay of Fundy, NS taken during the RACE (Regional Aerosol and Cloud Experiment) campaign. These parameterizations are discussed in the next section.

Table 4 Summary of C-FOG Vis parameterizations and previous work. The FI (fog index) is defined as 1/(LWC•N_{dt}) with units of [g^{-1} m^3 cm^3].

Case	Parameterization	FMD	Platform location
28 Sep - Battery	Vis=0.7531$(FI)^{0.4828}$	FM100	Ground-C-FOG
29 Sep - Battery	Vis=0.7280$(FI)^{0.4871}$	FM100	Ground-C-FOG
28 Sep -RV	Vis=0.4765$(FI)^{0.5568}$	CDP	Sharp RV-C-FOG
28 Sep -RV	Vis=0.4506$(FI)^{0.5206}$	BCP	Sharp RV-C-FOG
04 Oct -RV	Vis=0.4012$(FI)^{0.5455}$	CDP	Sharp RV-C-FOG
04 Oct -RV	Vis=0.5009$(FI)^{0.4982}$	BCP	Sharp RV-C-FOG
28 Sep - Battery	Vis=-0.009RH^3+0.437RH^2 -2.459RH+817.062	PWD	Ground-C-FOG
Gultepe et al 2007	Vis=1.002$(FI)^{0.6473}$	FSSP	Aircraft Obs. RACE

5 Discussion

5.1 Overview of Fog Forecasting

Fog prediction cannot be done accurately because of rapid changes in its intensity (Vis) over short time and space scales, as well as non-linear relationships between surface and atmospheric conditions. There are several methods for fog prediction. These methods include rule–based techniques (Toth et al. 2007, Zhou and Du 2010), statistical methods (Claxton 2008, Miao et al. 2012), numerical forecast models (Gultepe and Milbrandt 2010; Bott et al. 1990; Muller et al. 2007, 2010; Bott and Trautmann 2002; Clark et al. 2008; Shi et al. 2012) and integrated nowcasting methods (Golding, 1993; Golden, 1998; Wright and Thomas, 1998; Haiden et al. 2014). If no persistence exists and turbulence becomes more dominant, prediction usually fails, unless very short-term data assimilation techniques are performed. More detailed information on fog modeling issues can be found in the works of Gultepe et al. (2007a), Wilfried et al. (2008), Croft et al. (1997) and Fernando et al. (2020).

5.2 NWP and Microphysical Schemes

Prognostic fog forecasting is usually done using model-based prediction of LWC and N_d, and that uses detailed droplet nucleation processes described above. In general, a regional forecast model uses boundary conditions from a global model. As described in Section 1, assuming a gamma size distribution, visibility can be diagnosed from the size distribution parameters such as N_o (intercept parameter), μ (spectral shape parameter), and λ (slope parameter), or either N_{dt} or LWC or both (Gultepe and Milbrandt 2007b, Milbrandt and Yau 2005a,b). If both LWC and N_d are available as prognostic variables, Vis estimation can be obtained using NWP simulations.

Microphysical schemes are used to evaluate fog prediction conditions using NWP models. Cloud-droplet and fog-droplet size distributions are usually represented by a modified-gamma size distribution in NWP models. The parameters used in a modified gamma size distribution are the N_t (total droplet number concentration), and shape and slope parameters. N_t is obtained either from empirical relationships as a function of aerosol number concentrations (N_a) or from a prognostic equation for N_d with assumed size distribution parameters. The microphysical schemes (MPS) such as MY (Milbrandt and Yau 2005a,b), MG (Morrison and Gettelman 2008), and TO (Thompson et al. 2008, 2014) use modified-gamma size distributions and microphysical parameters based on DSD parameters.

The N_d can be obtained directly from N_a diagnostically, as stated, or based on S_w (supersaturation) which is function of vertical air velocity (w_a) and N_a as well as its composition (Twomey 1959; Chen 1994; Kohler 1934). The Kohler curve provides a general equilibrium relationship between an aqueous salt solution droplet size and water vapour. S_w can be calculated as a function of both w_a and N_d and that is directly related to size distribution and the composition and mixing state of aerosols. A similar relationship to Twomey (1959) is also suggested by Ghan et al. (1993, 1997) for large-scale cloud formation. Cohard et al. (1998) extended Twomey's power law expression by using a more realistic four parameter CCN activation spectrum with physiochemical properties of aerosols. The most important parameter to estimate N_d is S_w that is obtained using 3 methods (Schwenkel and Maronga 2019): 1) saturation adjustment scheme, 2) diagnostic scheme where S_w is diagnosed by the prognostic fields of T and q_v, and 3) a prognostic method (Clark 1973; Morrison and Grabowski 2007; Lebo et al. 2012). These methods are not discussed here, but are listed to emphasize the importance of w_a, CCN, and N_d on S_w.

In microphysical schemes, N_d is usually represented with a complete gamma size distribution function as

$$N_d(D) = N_o D^{\mu} e^{-\lambda D}, \tag{16}$$

where D is the diameter, and N_o, μ, and λ_s should also be known to obtain an accurate droplet spectra. The μ parameter is obtained as a function of CCN (Wilkinson et al., 2013) or as $\mu = 1/\eta^2$ *-1* with η the dispersion of radius (sd/mean), which is given by Morrison and Gettelman (2008) as

$$\eta = 0.0005714N_d + 0.2714, \tag{17}$$

where N_d can be obtained as a function of aerosol number concentration (N_a) (Jones et al. 1994; Martin et al. 1994; Gultepe and Isaac, 1999; Gultepe et al. 2015). But N_d versus N_a relationships are not unique, and their variability can be large. In Eq. 15, N_o and λ are usually obtained using a fixed μ and predicted value of total droplet number concentration (N_{dt}) and water vapour mixing ratio (q_w) as

$$\lambda_s = \left[\frac{\pi \rho_w N_{dt} \Gamma(\mu+4)}{6 q_w \Gamma(\mu+1)}\right]^{1/3} \tag{18}$$

and

$$N_{o=} \frac{N_{dt} \lambda^{\mu+1}}{\Gamma(\mu+1)}\,. \tag{19}$$

When models use a single-moment scheme, q_w (e.g. LWC) is predicted but N_{dt} and μ are fixed. In double-moment schemes, usually both q_w and N_{dt} are prognostic variables. N_d prediction is an important step in NWP models for accurate fog Vis estimation.

In the MPS, CCN concentration is assumed to be a function of S_w, and N_a for the ocean (N_{aO}) and land (N_{aL}) air masses set as fixed values. The values for CCN concentration as a function of supersaturation are also given in Fletcher (1966). The CCN parameterization, given as CCN=cS_w^k where c~1000 cm^{-3} and k~1 (a unitless constant), are for continental air masses and ~100 cm^{-3} and ~0.5 for maritime air masses (Feingold et al 1998). Sometimes, N_d is fixed as 100 cm^{-3} over ocean and 300 cm^{-3} over land (Wilkinson et al 2013). In reality, as stated in Cohard et al. (1998), the coefficients c and k change with high S_w. *They suggested that this happens especially in maritime environments*. Therefore, c and k should be matched locally to the activated CN. This suggests that parameterization of S_w and both c and k are critical to improve fog Vis predictions

5.3 Scale Issues

Fog usually happens over small areas and dissipates quickly; therefore, NWP models can have difficulty predicting short lived fog conditions. Although fog models can resolve the smaller scales, most of the physics developed for the NWP model cannot be used for high resolution fog models. Due to cloud coverage over the large scales (1-100 km), some dry air pockets result in lower values of RH_w, LWC, and N_d (Gultepe and Isaac, 1999; 2004) and these need to be extrapolated to fog occurrence scales (usually less than 1 km) (Wilkinson et al 2013). The latter study clearly recognizes the issues for better fog prediction on various grid areas. This suggests that further improvement of fog microphysical parameterizations is required for better fog prediction.

5.4 Variability in Vis

Visibility calculation based on observations and NWP model outputs may include large uncertainties due to fog microphysical and BL processes. Variability in Vis based on measurements of PWD located at Battery, Downs, Blackhead, and Judges Hill sites for 28-29 Sep is shown in Fig. 17. Figure 17a shows mean Vis from all these sites with a standard deviation. Overall, Vis at Judges Hill had the lowest values compared to the other stations, likely due to its elevation of 129 m (Fig. 17b). The second lowest Vis values are found at The Downs site, at 32 m above sea level. Blackhead and Battery Vis follow, with the next highest values. During dense fog conditions, Vis from Blackhead was much higher than others, likely due to the distance between the Blackhead and Ferryland sites. Vis, representing a scale of about 1.5 km, ranged from 0.2 km up to 1 km for any given time (Fig. 17); therefore, NWPs should be capable of simulating fog conditions at 1 min time intervals and 100 m spatial scales.

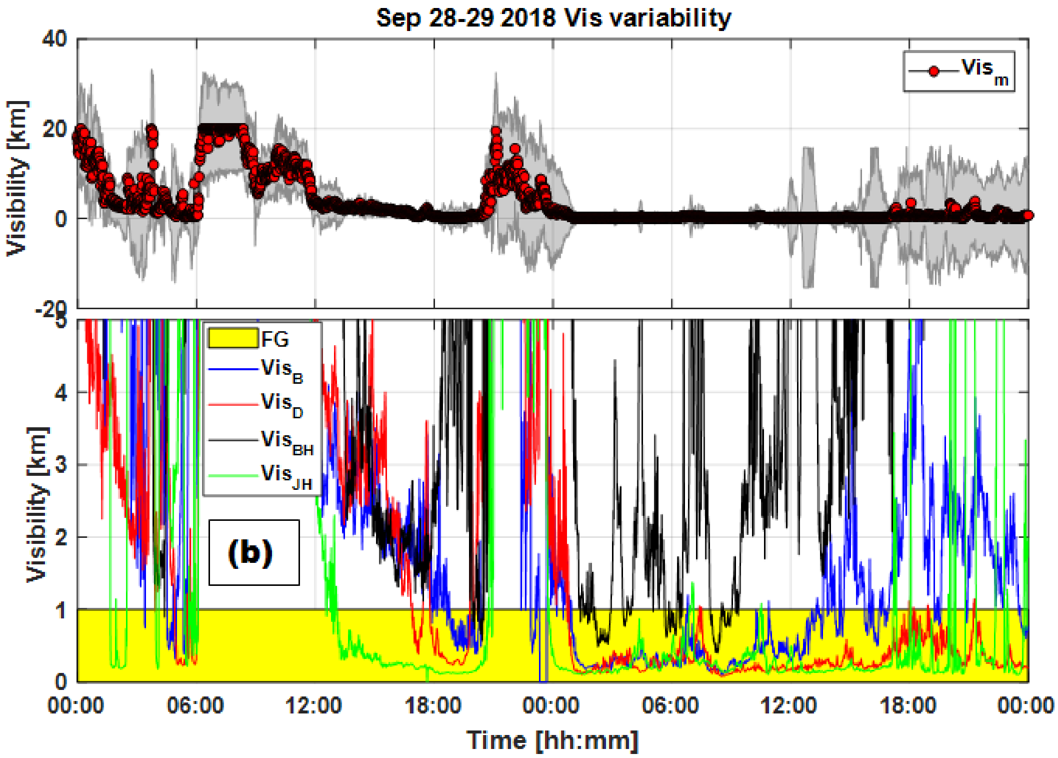

Fig. 17 Time series of mean (red filled circles) and sd (gray coloured regions) of Vis based on measurements of PWDs (indicated in (b)) are shown in (a). Time series of Vis representing Battery (Vis_B), Downs (Vis_D), Blackhead (Vis_{BH}), and Judges Hill (Vis_{JH}) for 28-29 Sep 2018 are shown in (b). Fog regions are shown for Vis<1 km (yellow coloured area).

5.5 Variability in sonic anemometer wind components

The 3-D wind component time series of mean and sd obtained from the (20Hz) measurements of sonic anemometers located at 1, 2, 5, 8, and 15 m levels of the Battery supersite tower are shown in Fig. 18a for 28-29 Sep cases. Figure 18b shows 3D wind components and Vis from each of the 5 levels. The U_{3d} values (3-D wind speed) between 0600-1200 UTC indicate some noise in the data and should be ignored because of heavy condensation on the prongs of the sonic anemometers. The largest U_{3d} fluctuations are seen at 5, 8, and 15 m levels but these were reduced to lower values during fog events on May 28 (Fig. 18b). Vertical air velocities (w_a) in Fig. 18c are obtained at the same levels as in Fig. 18b. Figure 18c shows the mean and standard deviation of w_a obtained from measurements, representing all levels from 1 m up to 15 m. Clearly, w_a fluctuations were higher in the fog-free layers compared to foggy layers, indicating greater turbulent heat, moisture and momentum fluxes in the vertical direction. Note that large fluctuations of

w_a at 15 m from 0600 to 1200 UTC in Fig. 18d were likely noise, as noted previously. The w_a fluctuations within the fog layers were found generally between +0.3 and -0.3 m s^{-1}, but were more than -0.7 m s^{-1} and +0.7 m s^{-1} in fog-free layers. These suggest that without estimating wind fluctuations at 3 axis accurately, NWP models cannot properly handle the fog life cycle.

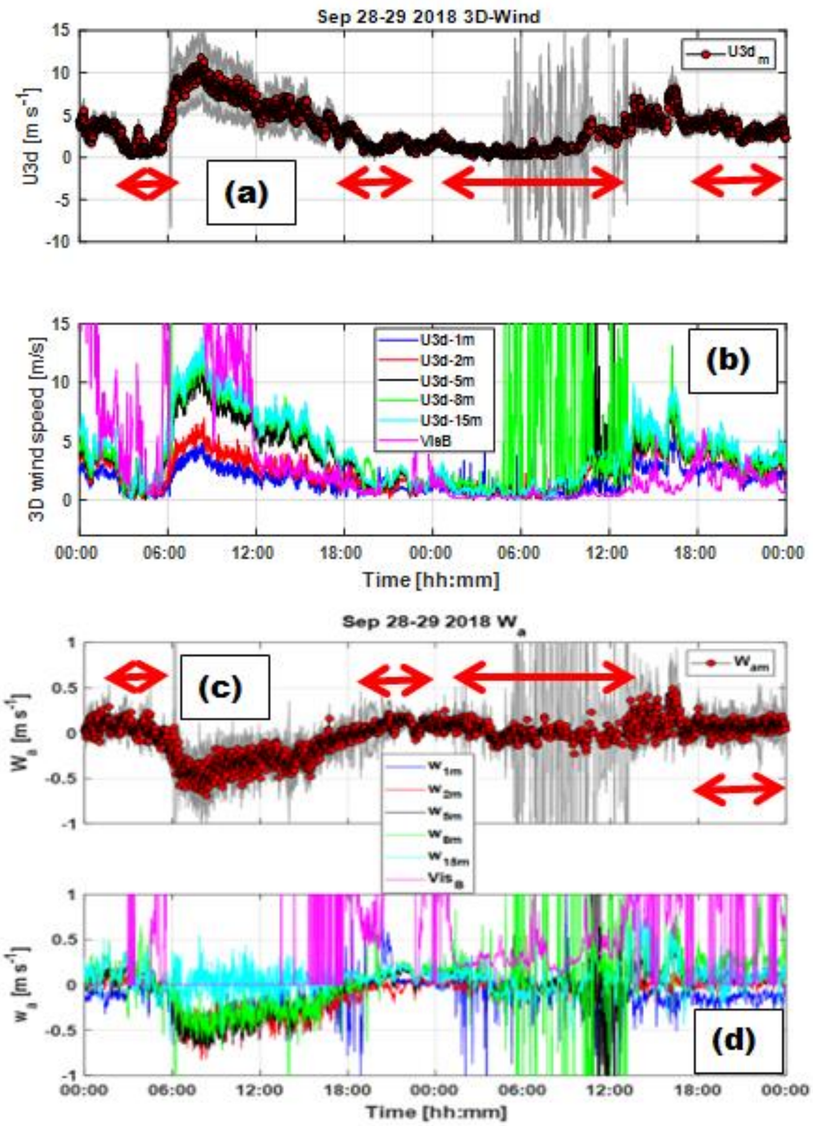

Fig. 18 Wind components obtained from the sonic anemometers located at 1, 2, 5, 8, and 15 meters levels of a tower and Vis at 2 m (purple line) are shown in (a) for mean and sd of U_{3d} (3D wind component) and in (b) for U_{3d} for each level, representing 28-29 Sep cases at the Battery supersite. Mean (red filled circles) and sd (gray lines) of vertical air velocity (w_a) are shown in (c) and w_a measurements at each level are shown in (d). Fog layers indicated by red double arrow are obtained from PWD Vis shown in (d) and previous plots.

5.5 N_d Uncertainty and Droplet Spectra

Droplet spectra from CDP, BCP, and FM120 probes include uncertainties related to the calculations of TAS, turbulence, wind speed and ship direction. The aspirator used in FM100 pulls in air at about 5 m s^{-1} but winds coming directly into the inlet can increase (or decrease) the aspirator wind speed. Usually, using a higher TAS compared to a fixed TAS at 5 m s^{-1} set up in FM120 results in a significant decrease (~50-100%) in N_d. For ship measurements, these errors can be much larger. For example, a ship heading north (0 degrees) at 8 m s^{-1} plus a wind from NE can result in

$$TAS = U_{RV} + U_h cos\theta. \quad (20)$$

Therefore, the error in TAS estimation, applying a derivative of TAS with respect to time, can be written as

$$\varepsilon_{TAS} = \frac{dTAS}{dt} = \frac{dU_{RV}}{dt} + U_h \frac{dcos\theta}{dt} + cos\theta \frac{dU_h}{dt}. \quad (21)$$

The l.h.s of Eq. 20, ε_{TAS} represents an error in TAS per unit time [(m s^{-1})/s]. Assuming that error in the first term of the r.h.s of Eq. 20 is approximately 1 m s^{-1} per unit time (e.g., dt=1 s) at U_{RV}=8 m s^{-1}, and U_h has an error of 10% say at 0.5 m s^{-1} and wind directional error is about 10 degrees (second term on the rhs), then using U_h=10 m s^{-1}, ε_{TAS}=1 m s^{-1}+ 10 m s^{-1}* (cos30-cos40) +cos(30)*0.5 m s^{-1}=1.0+1.0+0.43=2.43 m s^{-1}. Absolute error in TAS~18 m s^{-1} can then be calculated at about 15%. This means that N_d uncertainty is also about 15%, but likely increases with decreasing TAS. Following works can be suggested for further statistical evaluation of the analysis uncertainty; Moffat (1982) and Kline and McClintock (1953).

Figure 19 shows fog droplet spectra obtained from the CDP and BCP probes for Sep 28 (a and b) and Oct 04 (c and d) cases. The mean (black line) and standard deviation (red line) of each bin during fog events of Sep 28 and Oct 4 are shown. Each coloured line represents 1 s spectra. Clearly, Sep 28 droplet spectrum is much different from the Oct 04 droplet spectra, based on both probes. Multi-modes in DSD indicate the various fog regimes that were likely related to droplet fall velocities (V_f) and w_a. For both cases, DSD did not indicate drizzle droplet sizes > 50 µm. MVD for the Oct 04 was much larger than for the Sep 28 case. Note that the mean DSD can shift upward if a lower threshold of N_d is chosen to have a higher value (e.g. 1 # cm^{-3} instead of 0.1 # $cm^{-3)}$. In BCP measurements, having a large value for N_d at about 25 μm, may indicate cooling processes leading to increasing values for N_d.

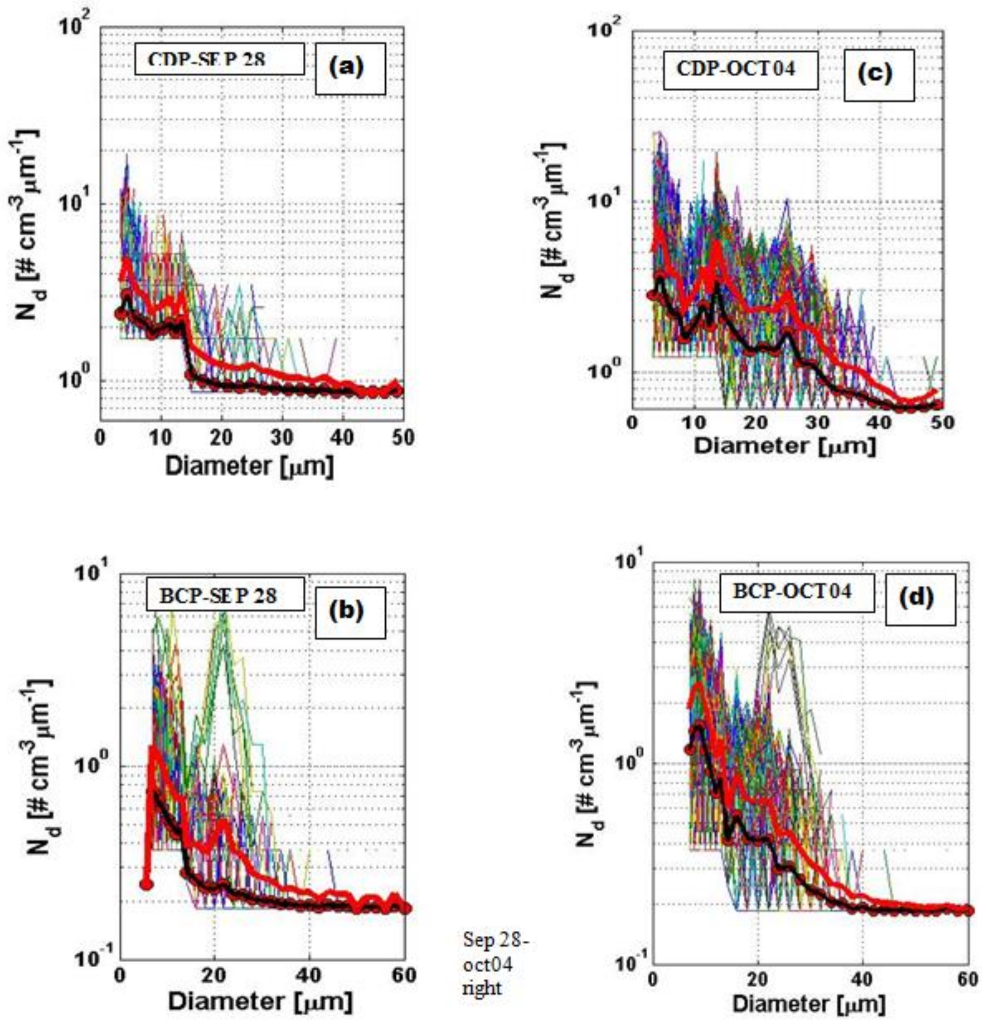

Fig. 19 Fog droplet spectra vs diameter obtained from CDP and BCP probes for 28 Sep (a and b) and Oct 04 (c and d) cases. The mean (black line) and sd (red line) values of each bin during time periods representing fog events of 28 Sep and 4 Oct 2018 are also shown on the plots. Each line with a colour represents 1 s spectra.

Sea spray particles can also affect N_d spectra (at 10m) significantly because of breaking waves, especially at small size ranges because of their low settling rates. In the marine environment, droplets can be generated by wave breaking processes, which can then be counted as fog droplets. Entrainment of air at breaking wave crests leads to the formation of a large number of bubbles, which emerge at the ocean surface because of their positive buoyancy and then burst into droplets at the water surface (Troitskaya et al 2018). The spray production due to the bursting of bubbles with sizes smaller than <10 μm has been studied by Blanchard (1963) and Spiel (1995, 1997, 1998). All of these studies suggest that bursting bubbles are the main source of the ocean spray process, generating droplets with radii less than 50 μm (Wu, 1981).

5.6 Impact of TKE Dissipation Rate on Vis

Fog occurs usually at the end of a dynamically unstable environment along coastlines and marine environments and is augmented sometimes by thermal inversions, keeping moisture trapped below a stable layer. Thereafter, when the mature fog stage has developed under dynamically stable conditions, fog dissipates as a result of droplet growth, increasing turbulence, entrainment, and solar heating. All these factors play an important role for fog dissipation without considering direct impact of a larger scale event such as pressure systems and associated fronts. In this work, calculated dissipation rates suggest that higher ε_{dis} values result in improved Vis conditions. Accuracy of ε_{dis} will not be discussed here, except in its usage in a fog prediction scheme. TKE dissipation rate is calculated in NWP models using TKE based on various turbulence prediction schemes (Mellor and Yamada 1982; Castelli et al 2005; Duynkerke 1988); therefore, it can be used to improve fog prediction.

Table 5. Mean and std of TKE dissipation rate calculated using Eq. 3 and Eq. 23, representing 1 hr time segments based on a 10-min filtering method for Sep 28 and Sep 29 2018 cases. Sep 29 case did not have wind measurements during heavy fog conditions. Reddish coloured area indicates missing data due to increased precipitation on the sonic anemometer located at the Battery.

Method	*Sep 28 Mean ε_{dis} [$m^2 s^{-3}$]*	*Sep 28 Std ε_{dis} [$m^2 s^{-3}$]*	*Sep 29 Mean ε_{dis} [$m^2 s^{-3}$]*	*Sep 29 Std ε_{dis} [$m^2 s^{-3}$]*
Using Eq. 3 Foggy	1.23×10^{-2}	1.73×10^{-2}	1.65×10^{-2}	1.19×10^{-2}
Using Eq. 26 Foggy	8.73×10^{-2}	24.94×10^{-2}	7.53×10^{-2}	9.21×10^{-2}
Using Eq. 3 Clear	7.76×10^{-2}	10.3×10^{-2}	-	-
Using Eq. 26 Clear	20.00×10^{-2}	25.59×10^{-2}	-	-

Table 5 is prepared using Eq. 3 and Eq. 26 for mean and std of ε_{dis} during foggy and fog free conditions, representing means of 1 hr time intervals. It shows that for both Sep 28 and 29, foggy conditions had much smaller ε_{dis} than fog free conditions (excluding Sep 29 case). For fog free conditions on Sep 29,ε_{dis} was corrupted due to precipitation on the 3D sonic anemometer optics. It is shown based on Table 5 that fog occurs usually when ε_{dis}<1x10^{-2} m^2 s^{-3} and dissipates for ε_{dis}>10x10^{-2} m^2 s^{-3}. Between these two limits, intermediate fog intensity can likely occur. A conversion equation between ε_{dis} and TKE (Scully et al 2011) can be obtained using,

$$L = C_\mu^3 \frac{TKE^{3/2}}{\varepsilon_{dis}}, \quad (22)$$

where L and C_μ are turbulent length scale (kz=0.41*2) where k is the Von Karman constant and z is the height (m) above sea level, and the non-dimensional stability function, respectively, that is assumed as a constant (0.447). Then, Eq. 22 can be rewritten for eddy dissipation rate as

$$\varepsilon_{dis} = C_\mu^3 \frac{TKE^{3/2}}{kz} \quad (23a)$$

Note that ε_{dis} and TKE are function of scales that need to be further evaluated and developed to improve NWP models based fog Vis predictions. After using the values of parameters given above, Eq. 23a becomes

$$\varepsilon_{dis} = 0.8199\sqrt[2]{TKE^3} \quad (23b)$$

Based on ε time series (Figs. 7 and 9) and equations given in Table 4, we can suggest the following parameterizations for fog (Vis<1 km & RH_w>95%), mist (Vis>1 km & RH_w>80%), and light fog (Vis>1 km & RH_w>95%) conditions, respectively, as

for $RH_w > 95\%$ & $\varepsilon_{dis} < 10^{-2} m^2 s^{-3}$;

$$Vis = 0.412(LWC \cdot N_d)^{-0.5455} \quad (24)$$

for $80\% < RH_w < 95\%$ & $\varepsilon_{dis} < 10^{-2} m^2 s^{-3}$;

$$Vis = -0.0094RH_w^3 + 0.437RH_w^2 - 32.459RH_w + 817.062 \quad (25)$$

and

for $RH_w > 95\%$ & $\varepsilon_{dis} > 10x10^{-2} m^2 s^{-3}$;

$$Vis = 1.002(LWCN_d)^{-0.6473}. \qquad (26)$$

The thresholds for TKE corresponding ε_{dis} thresholds for fog and clear air segments are estimated as <4.06x10^{-2} m^2 s^{-2} and >18.9x10^{-2} m^2 s^{-2}, respectively. Between them, fog to light fog/mist conditions may occur but this needs further analysis.

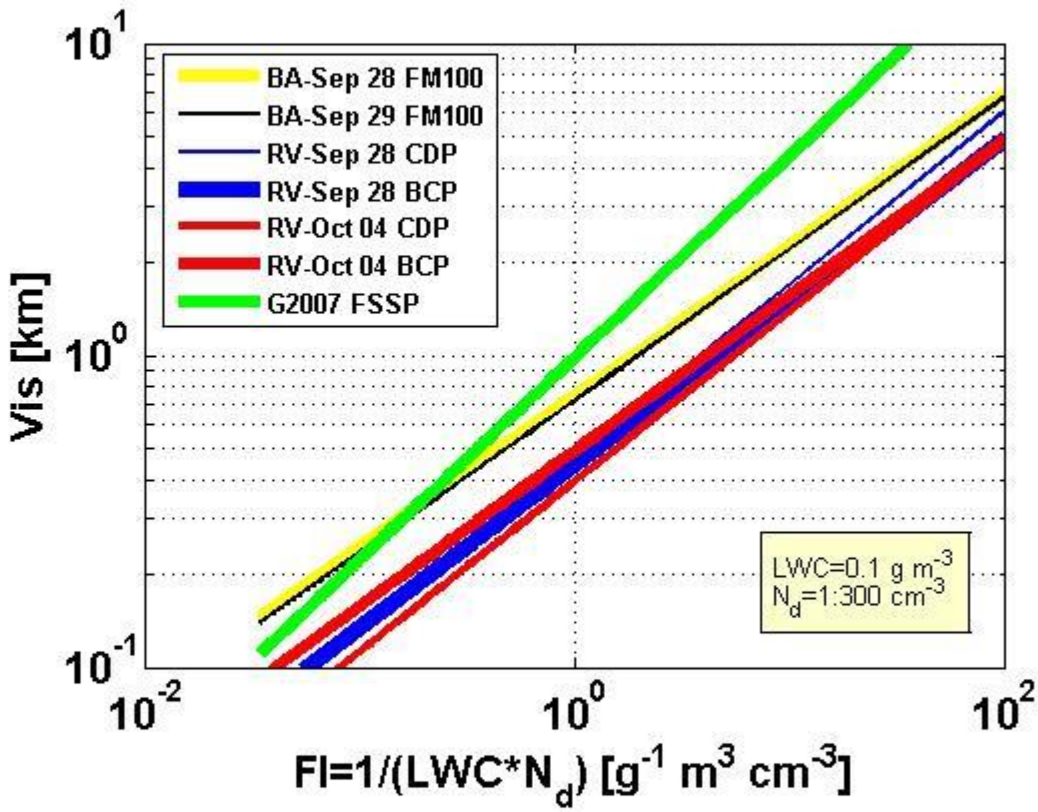

Fig. 20 Vis parameterizations obtained for all the cases based on Table 4. LWC was fixed at 0.1 g m^{-3} while N_d changed from 1 to 300 cm^{-3}. RV represents research vessel, BA Battery, G2007 Gultepe et al (2007) and FI fog index. FM100, CDP, BCP, and FSSP probes are used for droplet spectral measurements.

6 Conclusions

In this paper, Vis associated with fog environmental parameters such as RH_w, 3D wind components, and microphysical parameters, including LWC, N_d, and MVD were studied for four cases. Results representing two IOPs from the Battery supersite and two IOPs from the *R/V Sharp* are used in Vis parameterization development and to verify the previous parameterizations. Based on the results of this work, the following points can be drawn:

1. Synoptic weather conditions and ocean-atmosphere interactions are the larger-scale factors that affect coastal fog microphysics and visibility. The cold ocean surface off the coast of Ferryland was usually a major reason for fog formation observed there.
2. The main synoptic weather systems that affected fog were usually related to a high-pressure system located to the NE, a low-pressure system along W-NW, and a chain of tropical cyclonic motions. This may not be valid early in the fog season and usually can be valid during the Fall transition period
3. Vis is found to be less than 1 km when RH_w is greater than 95%, and this suggests that the T_a-T_d difference is an important variable indicating fog regions, but not intensity.
4. By decreasing dynamic activity, indicated by smaller 3D wind fluctuations and lifting, the eddy dissipation rate decreases during mature fog conditions that can be used for a threshold for prediction of mature fog conditions. Wind components; u, v, and w_a are relatively smaller in fog-developed regions than in fog-free regions.
5. The w_a fluctuations were 0.1 m s^{-1} during mature fog conditions compared to >0.3 m s^{-1} for fog-free regions. Note that these values can be much larger at the time scale of 16Hz or 32Hz.
6. The TKE dissipation rate was usually $<10^{-2}$ m^2 s^{-3} during mature fog events compared to $>10^{-1}$ m^2 s^{-3} for fog–free regions and can be used for fog prediction criteria based on NWP models.
7. Vis parameterizations that we constructed suggest that the slopes of the Vis versus fog index (FI) relationships are consistent with each other; but found to be comparably smaller in magnitude. This can be related to the nature of the measurement platform, fog season, as well as cloud versus fog measurements.
8. Vis is expected to be function of LWC and N_d and this can be replaced with LWC and MVD without involvement of a 3rd parameter; this can be more generally applicable for NWP models.

9. Vis<1 km observations showed a large variability, covering an area of a few km^2 (1.5 km^2) up to 20 km^2, and the difference was very high between a station at height 129 m (Judges' Hill) compared to one at the sea level, 2 m, (Battery station) although the horizontal separation distance was only about 1.0 km.
10. BCP droplet number concentration is found to be at least half of the CDP N_d and this is likely due to BCP's higher threshold of 5 μm; there were no droplets larger than 50 μm.
11. There were double and triple peaks for fog DSDs and this can affect the NWP's fog prediction algorithms and needs to be further researched.

Based on these points, it is suggested that Vis parameterizations can be obtained using both dynamical and microphysical parameters, but fog droplet spectra representation for various fog conditions need to be further investigated. Specifically, the turbulence impact on droplet spectra and the nucleation processes are very critical for the fog life cycle in low vertical air velocity situations. Moreover, this is the most important parameter affecting the auto-conversion of fog droplets to drizzle formation.

Acknowledgments: This research was funded by the Office of Naval Research Award # N00014-18-1-2472 entitled: Toward Improving Coastal Fog Prediction (C-FOG).During project, Dr. R Krishnamurthy is partially funded by the Pacific Northwest National Laboratory (PNNL) which is operated for the DOE by Battelle Memorial Institute under Contract DE-AC05-76RLO1830.

Nomenclature

BCP: Backscattering Cloud Probe	RF: radiative fluxes
C: A constant ~0.18 in Eq. 3	SA: Sample Area
C: Visibility threshold constant as 0.05	SV: sampling volume
CN: Condensation nuclei	T_a: Air temperature
CCN: Cloud Condensation Nuclei	T_d: Td: dew point temperature
CDP: Cloud Droplet Probe	TKE: Turbulent Kinetic Energy
D_s: The structure function	u, v, w_a: Measured wind components along x,y, z
DSD: Droplet Size Distribution	u',v', w': Wind fluctuations
FI: Fog Index	U_{ha}: The apparent wind speed
FSSP: Forward Spectral Scattering Probe	U_{dx} and U_{dy}: wind speed along x and y axis at dt t
FM100: DMT fog measuring device (FMD)	U_{RV}: *RV Sharp's* speed with respect to the ground
IR and SW: Infrared and shortwave rad.fluxes	U_{hT} : True wind speed over 10 mins intervals
k: The Von Karman constant as 0.41	U_{hR}: Wind speed with respect to ground
L: Turbulent length scale	U_{3D}: 3D wind component

L: The turbulent length scale	Vis: Visibility
LES: large eddy simulation	V_f: Droplet fall velocity
LWC: liquid water content	V_d: Doppler velocity
MVD: Mean Volume Diameter	Vis_B: Vis at Battery site
n(r): Droplet number spectra	Vis_D: Vis at Downs site
N_a: Aerosol number concentration	Vis_{BH}: Vis at Blackhead site
N_{aO}: Aerosol number conc. over ocean	Vis_{JH}: Vis at Judges Hill site
N_{aL}: Aerosol number concentration over land	Z_e: Radar reflectivity factor
N_c: Droplet counts	z: The height (m)
N_d: Droplet number concentration	α and γ: empirical constants in Eq. 13
N_{dt}: total droplet number concentration	μ: spectral shape parameter
N_o: intercept parameter	λ: slope parameter
NWP: Numerical Weather Prediction	β_{ext}: Extinction coefficient
PR: Precipitation Rate	β: Lidar backscatter coefficient
Q_{eff}: Extinction efficiency	η: the dispersion of radius (sd/mean),
r: droplet radius	$\rho_{w:}$ water density
r_{eff}: Effective radius	θ: Angle between the ship heading and U_{ha}
Δr: The horizontal distance in Eq. 3.	ε: Eddy dissipation rate
Δt: Time interval	ε_{TAS}: Error in TAS
RH_w: relative humidity with respect water	

References

Abdul-Razzak, H., and S. Ghan (2000) A parameterization of aerosol activation: 2. Multiple aerosol type, *J. Geophys. Res*., 105, 6837–6844.

Benjamin, S.G., B.D. Jamison, W.R. Moninger, S.R. Sahm, B.E. Schwartz, and T.W. Schlatter (2010) Relative Short-Range Forecast Impact from Aircraft, Profiler, Radiosonde, VAD, GPS-PW, METAR, and Mesonet Observations via the RUC Hourly Assimilation Cycle. *Mon. Wea. Rev.*, 138, 1319–1343, https://doi.org/10.1175/2009MWR3097.1

Blanchard, D. C. (1963) The electrification of the atmosphere by particles from bubbles in the sea. *Prog. Oceanogr.*, 1, 73–202, https://doi.org/10.1016/0079-6611(63)90004-1

Bergot, T., D. Carrer, J. Noilhan, and P. Bougeault (2005) Improved Site-Specific Numerical Prediction of Fog and Low Clouds: A Feasibility Study. *Wea. Forecasting*, 20, 627–646, https://doi.org/10.1175/WAF873.1

Beswick, K., D. Baumgardner, M. Gallagher, A. Volz-Thomas, P. Nedelec4, K.-Y. Wang, and S. Lance (2014) The backscatter cloud probe – a compact low-profile autonomous optical spectrometer *Atmos. Meas. Tech*., 7, 1443–1457. www.atmos-meas-tech.net/7/1443/2014/doi:10.5194/amt-7-1443-2014

Bott A., U. Sievers, and W. Zdunkowski (1990) A Radiation Fog Model with a Detailed Treatment of the Interaction between Radiative Transfer and Fog Microphysics. *J. Atmos. Sci.*, 47, 2153–2166.

Bott A, and T. Trautmann (2002) PAFOG – A new efficient forecast model of radiation fog and low-level stratiform clouds. *Atmos. Res*. 64, 191–203.

Bott A, and T. Trautmann (2002) PAFOG – A new efficient forecast model of radiation fog and low-level stratiform clouds. *Atmos. Res*. 64, 191–203.

Burrows, W. R. and G. Toth (2011) Automated fog and stratus forecasts from the Canadian RDPS operational NWP model. *Extended Abstracts, 24th Conference on Weather and Forecasting*, 23-27 January, 2011, Seattle, WA, USA, 33pp, Amer. Meteor. Soc. DOI: 10.13140/2.1.4852.0648.

Castelli, S.T., E. Ferrero, D. Anfossi and R. Ohba (2005) Turbulence Closure Models and their Application in RAMS *Environmental Fluid Mechanics*, 5, 169–192

Chen, J. P. (1994) Theory of Deliquescence and Modified Kohler Curves, J. Atmos. Sci., 51, 3505-3516.

Clark, T. L. (1973) Numerical modeling of the dynamics and microphysics of warm cumulus convection, J. Atmos. Sci., 30, 857–878.

Claxton, B.M. (2008) using a neural network to benchmark a diagnostic parameterization: The Met Office’s visibility scheme. *Q. J. R. Meteorol. Soc.*, 134, 1527-1537

Cohard, JM, Jean-Pierre Pinty, and Carole Bedos (1998) Extending Twomey's Analytical Estimate of Nucleated Cloud Droplet Concentrations from CCN Spectra. *J. Atmos. Sci.*, 55, 3348–3357.

Croft, P.J., Pfost, R.L., Medlin, J.M., and Johnson, G.A. (1997) Fog forecasting for the southern region: A conceptual model approach. *Weather Forecast. 12*, 545–556.

Dimitrova, R., A. Sharma • H. J. S. Fernando, I. Gultepe, V. Danchovski, S. Wagh, S. Bardoel, S. Wang (2020) WRF model simulations for coastal fog prediction. *Boundary-Layer Meteorol.* In Press.

Dorman, C.E., Hoch, S.W., Gultepe, I., Fernando, H.J.S., Krishnamurthy, R. (2020) Large scale synoptic weather systems and fog during the C-FOG field experiment. *Boundary-Layer Meteorol. In Press.*

Duynkerke, P.G.: 1988, Application of the E-ε turbulence closure model to the neutral and stable atmospheric boundary layer, *J. Atmos. Sci.* **45**, 865–880

Fernando, H.J.S., I. Gultepe, C. Dorman, E. Pardyjak, Q. Wang, S. Hoch, D. Richter, E. Creegan, S. Gaberšek, T. Bullock, C. Hocut, R. Chang, D. Alappattu, R. Dimitrova, D. Flagg, A. Grachev, R. Krishnamurthy, D.J. Singh, I. Lozovatsky, B. Nagare, A. Sharma, S. Wagh, C. Wainwright, M. Wroblewski, R. Yamaguchi, S. Bardoel, R.S. Coppersmith, N. Chisholm, E. Gonzales, N. Gunawardena, O. Hyde, T. Morrison, A. Olson, A. Perelet, W. Perrie, S. Wang, B. Wauer (2020) C-FOG: Life of Coastal Fog, *Bull of AMS*, DOI: https://doi.org/10.1175/BAMS-D-19-0070.1 1880-3. V. 176, No. 5, 1977-2017.

Fletcher, N.H. (1966) *The physics of rainclouds*. Cambridge University Press, 390 pp.

Feingold, G., S. Yang, R. M. Hardesty, and W. R. Cotton (1998) Feasibility of Retrieving Cloud Condensation Nucleus Properties from Doppler Cloud Radar, Microwave Radiometer, and Lidar. *J. Atmos. Oceanic Technol*., 15, 1188–1195.

Ghan, S. J., G. Guzman, and H. Abdul-Razzak (1998) Competition between sea salt and sulfate particles as cloud condensation nuclei, *J. Atmos. Sci*., 55, 3340– 3347.

Ghan, S. J., N. S. Laulainen, R. C. Easter, R. Wagener, S. Nemesure, E. G. Chapman, Y. Zhang, and L. R. Leung (2001) Evaluation of aerosol direct radiative forcing in MIRAGE, *J. Geophys. Res*., 106, 5295–5316.

Ghan, S. J., C. C. Chuang, and J. E. Penner (1993) A Parameterization of Cloud Droplet Nucleation, Part I: Single Aerosol Type. *Atmos. Res*. 30:197-221.

Ghan, S. J., Leung, L. R., Easter, R. C., and Abdul-Razzak, H. (1997) Prediction of cloud droplet number in a general circulation model, *J. Geophys. Res*., 102, 777–794.

Golding B. W. (1998) Nimrod: A system for generating automated very short range forecasts. *Meteorol. Appl*. 5, 1–16.

Golding, B. W. (1993) A study of the influence of terrain on fog development. *Mon. Weather Rev.*, 121, 2529-2541.

Grachev A.A., Krishnamurthy R., Fernando H.J.S., Fairall C.W., Bardoel S.L., Wang S. (2020) Atmospheric turbulence measurements in coastal zone with and without fog. *Boundary-Layer Meteorol.*, current issue (submitted).

Gultepe, I., Pardyjak, S. W. Hoch, H.J.S Fernando, C. Dorman, D.D. Flagg, R. Krishnamurthy, Q. Wang, S. Gaberšek, E. Creegan, N. Scantland, S. Desjardins, A. Heidinger, M. Pavolonis, A.J. Heymsfield (2020) Coastal Fog Microphysics Using In-Situ Observations and GOES-R Retrievals. *Boundary-Layer Meteorol. In Press.*.

Gultepe, I., and Milbrandt, J. (2007a) Microphysical observations and mesoscale model simulation of a warm fog case during FRAM project. *Pure Appl. Geophys.* 2007, *164*, 1161–1178.

Gultepe, I., M. D. Müller, and Z. Boybeyi (2006) A new warm fog parameterization scheme for numerical weather prediction models. *J. Appl. Meteor*., 45, 1469-1480.

Gultepe, I., and Starr, D. O'C. (1995) Dynamical structure and turbulence in cirrus clouds: Aircraft observations during FIRE. *J. Atmos. Sci*., 52, 4659-4182.

Gultepe I, and G.A. Isaac (1996) The relationship between cloud droplet and aerosol number concentrations for climate models. *Inter. J. of Clim*. 16, 941-946.

Gultepe, I., Isaac, G. A., Leaitch, W. R., and Banic, C. M. (1996) Parameterization of marine stratus microphysics based on in-situ observations: Implications for GCMs. *J. Climate,* 9, 345-357.

Gultepe, I., and G. A. Isaac (1999) Scale effects on averaging of cloud droplet and aerosol number concentrations: observations and models. *J. Climate,* 12, 1268-1279.

Gultepe, I., R. Tardif, S.C. Michaelides, J. Cermak, A. Bott, J. Bendix, M. Müller, M. Pagowski, B. Hansen, G. Ellrod, W. Jacobs, G. Toth, S.G. Cober (2007c) Fog research: a review of past achievements and future perspectives. *J. of Pure and Applied Geophy.*, Special issue on fog, edited by I. Gultepe. 164, 1121-1159.

Gultepe, I., M. Pagowski, and J. Reid (2007b) Using surface data to validate a satellite based fog detection scheme. *J. of Weather and Forecasting*, 22, 444-456.

Gultepe, I., G. Pearson J. A. Milbrandt, B. Hansen, S. Platnick, P. Taylor, M. Gordon, J. P. Oakley, and S.G. Cober (2009) The fog remote sensing and modeling (FRAM) field project. *Bull. Of Amer. Meteor. Soc*., 90, 341-359.

Gultepe, I., and J. A. Milbrandt (2010) Probabilistic Parameterizations of Visibility Using Observations of Rain Precipitation Rate, Relative Humidity, and Visibility. *J. Appl. Meteor. Climatology*. 49, 36–46.

Gultepe, I., T. Kuhn, M. Pavolonis, C. Calvert, J. Gurka, G.A. Isaac, A. J. Heymsfield, P.S.K. Liu, B. Zhou, R. Ware, B. Ferrier, J. Milbrandt, B. Hansen, and B. Bernstein (2014) Ice fog in Arctic during FRAM-IF project: Aviation and nowcasting applications. *Bulletin of Amer. Met. Soc.*, 95, 211–226.

Gultepe, I., B. Zhou, J. Milbrandt, A. Bott, Y. Li, A. J. Heymsfield, B. Ferrier, R. Ware, M. Pavolonis, T. Kuhn, J. Gurka, P. Liu, and J. Cermak (2015) A review on Ice Fog: Observations and Modeling. *Atmospheric Research*. DOI: 10.1016/j.atmosres. 2014.04.014.

Gultepe, I. (2019) Low level ice clouds-ice fog. *Encylopedia of Water: Science, Technology, and Society*, edited by Patricia A. Maurice. ISBN: 9781119300755 John Wilesy & Sons Inc., DOI: 10.1002/9781119300762.wsts0140. 19 pp.

Gultepe, I., Pardyjak, E., Hoch, S.W., Fernando, H.J.S., Dorman, C., Flagg, D.D., Krishnamurthy, R., Wang, Q., Gaberšek, S., Creegan, E., Scantland, N., Desjardins, S., Heidinger, A., Pavolonis, M., Heymsfield, A.J., Coastal Fog Microphysics Using In-Situ Observations and GOES-R Retrievals, *Boundary Layer Meteorology*, accepted.

Haeffelin, M., T. Bergot, T. Elias, R. Tardif, D. Carrer, P. Chazette, M. Colomb, P. Drobinski, E. Dupont, J. Dupont, L. Gomes, L. Musson-Genon, C. Pietras, A. Plana-Fattori, A. Protat, J. Rangognio, J. Raut, S. Rémy, D. Richard, J. Sciare, and X. Zhang (2010) Parisfog. *Bull. Amer. Meteor. Soc.*, 91, 767–783, https://doi.org/10.1175/2009BAMS2671.1

Haiden, T., A. Kann, and G. Pistotnik (2014) Nowcastiong with INCA during SNOW-V10. J. *Pure and App. Geophy*. 171, No: 5-6, 231-242.

Isaac, G.A., T. Bullock, J. Beale, and S. Beale (2020) Characterizing and Predicting Marine Fog Offshore Newfoundland and Labrador. *Wea. Forecasting,* **35**, 347–365, https://doi.org/10.1175/WAF-D-19-0085.1

Jones, A., DL Roberts, and A. Slingo (1994) A climate model study of indirect radiative forcing by anthropogenic sulfate aerosols. *Nature*, 370, 450-453.

Kline, S. J., and F. A. McClintock (1953) Analysis of uncertainty in single-sample experiments. *Mechanical Engineering* 75, 3-9.

Koschmieder, H. (1924) Theorie der horizontalen sichewite, *Beitr. Phys. Atmos*., 12, 33-53.

Köhler, H. (1936) The nucleus in and the growth of hygroscopic droplets. *Trans. Faraday Soc.*, 32, 1152–1161, https://doi.org/10.1039/TF9363201152.

Kunkel, B.A. 1984 Parameterization of droplet terminal velocity and extinction coefficient in fog models. *J. Clim. Appl. Meteorol.* 1984, *23*, 34–41.

Lebo, Z. J., Morrison, H., and Seinfeld, J. H. (2012) Are simulated aerosol induced effects on deep convective clouds strongly dependent on saturation adjustment?, *Atmos. Chem. Phys*., 12, 9941–9964, https://doi.org/10.5194/acp-12-9941-2012.

LPM (2011) *Laser Precipitation Monitor*. 5.4110.xx.x00, V2.5x STDNWS. Adolf Thies GmbH&Co. KG. Document # 000904. 66 pp.

Martin, G. M., D. W. Johnson, and A. Spice (1994) The measurement and parameterization of effective radius of droplets in warm stratocumulus clouds. *J. Atmos. Sci*., 51, 1823–1842.

Mellor, G., and T. Yamada (1982) Development of a turbulence closure model for geophysical fluid problems. *Rev. Geophys. Space Phys*., 26, 851–875.

Miao, Y., R. Potts, X. Huang, G. Elliott, and R. Rivett (2012) A Fuzzy Logic Fog Forecasting Model for Perth Airport *J. Pure and App. Geophy.* 169, No: 5-6 , 1107-1119.

Milbrandt, J.A. and M.K. Yau (2005a) A Multimoment Bulk Microphysics Parameterization. Part I: Analysis of the Role of the Spectral Shape Parameter. *J. Atmos. Sci*., 62, 3051–3064, https://doi.org/10.1175/JAS3534.1

Milbrandt, J.A. and M.K. Yau (2005b) A Multimoment Bulk Microphysics Parameterization. Part II: A Proposed Three-Moment Closure and Scheme Description. *J. Atmos. Sci*., 62, 3065–3081, https://doi.org/10.1175/JAS3535.1

Moffat, R. J. (1982) Contributions to the theory of single-sample uncertainty analysis. 250-258 pp.

Morrison, H. and Grabowski, W. W. (2007) Comparison of bulk and bin warm-rain microphysics models using a kinematic framework, *J. Atmos. Sci.,* 64, 2839–2861.

Morrison, H., and A. Gettelman (2008) A New Two-Moment Bulk Stratiform Cloud Microphysics Scheme in the Community Atmosphere Model, Version 3 (CAM3). Part I: Description and Numerical Tests. *J. Climate*, 21, 3642–3659.

Muller M. D., M. Masbou, and A. Bott (2010) Three-dimensional fog forecasting in complex terrain. *Quart. J. Roy. Meteor. Soc.*, 136, 2189-2202.

Muller, M. D., C. Schmutz, and E. Parlow (2007) A one dimensional ensemble forecast and assimilation system for fog prediction. *J. Pure Appl. Geophys*., 164, 1241–1264.

Niu, S.J., Lu, C.S., Zhao, L.J., Lu, J.J., and Yang, J. (2010) Analysis of the microphysical structure of heavy fog using a droplet spectrometer: a case study, *Adv. Atmos. Sci.* 27(6), 1259-1275, doi:10.1007/s00376-010-8192-6.

Paluch, I.R. and D.G. Baumgardner (1989) Entrainment and Fine-Scale Mixing in a Continental Convective Cloud. *J. Atmos. Sci.*, 46, 261–278, https://doi.org/10.1175/1520-0469(1989)046<0261:EAFSMI>2.0.CO;2

Panofsky, H. A., and J. A. Dutton (1984) *The atmosphere Turbulence*. John Wiley and Sons, 397 pp.

Perelet, A., I. Gultepe, S. W. Hoch, and E. Pardyjak (2020) Response of infrared and microwave scintillometer to hydrometeors. *Boundary-Layer Meteorol. In Press.*.

Pezzoli, A., Moncalero, M., Boscolo, A., Cristofori, E., Giacometto, F., Gastaldi, S., Vercelli, G. (2010) The meteo-hydrological analysis and the sport performance: which are the connections? The case of the XXI Winter Olympic Games, Vancouver 2010. *Journal of Sports Medicine and Physical Fitness*, **50**:19-20.

Price, J.D., S. Lane, I.A. Boutle, D.K. Smith, T. Bergot, C. Lac, L. Duconge, J. McGregor, A. Kerr-Munslow, M. Pickering, and R. Clark (2018) LANFEX: A Field and Modeling Study to Improve Our Understanding and Forecasting of Radiation Fog. *Bull. Amer. Meteor. Soc.*, 99, 2061–2077, https://doi.org/10.1175/BAMS-D-16-0299.1

Price, J. D. (2019) On the formation and development of radiation: An observational study. Bound. Layer Meteor. 172, 167–197.

Pu, Z., Chachere, C., Hoch, S., Pardyjak, E., & Gultepe, I. (2016). Numerical prediction of cold season fog events over complex terrain: The performance of the WRF model during MATERHORN-Fog and early evaluation. *Pure and Applied Geophysics*. https://doi.org/10.1007/s00024-016-1375-z.

Schemenauer, R.S., I. Gultepe, Witiw, M. (2016) Fog Studies. *Meteorological Technology International*. April Issue, 52-54.

Schwenkel, J., and B. Maronga (2019) Large-eddy simulation of radiation fog with comprehensive two-moment bulk microphysics: impact of different aerosol activation and condensation parameterizations *Atmos. Chem. Phys*., 19, 7165–7181, 2019. https://doi.org/10.5194/acp-19-7165-2019

Scully, M. E., W.R. Geyer, J. H. Trowbridge (2011) The Influence of Stratification and Nonlocal Turbulent Production on Estuarine Turbulence: An Assessment of Turbulence Closure with Field Observations. *J. of Phys. Ocean*., 41, 166-185. DOI: 10.1175/2010JPO4470.1

Shi, C., L. Wang, H. Zhang, X. Deng, Y. Li, and M. Qiu (2012) Fog Simulations Based on Multi-Model System: A Feasibility Study. *Pure Appl. Geophys*. 169, 941–960.

Singh, D.K., Sebastian W. Hoch, Ismail Gultepe, and Eric R. Pardyjak (2020) A case study of the life cycle of a stratus-lowering coastal fog event in Newfoundland, CA. *Boundary-Layer Meteorology*, Submitted.

Smirnova, T.G., S.G. Benjamin, J.M. Brown (2000) Case study verification of RUC/MAPS fog and visibility forecasts. Preprints, *9th Conf. on ARAM, AMS*, Orlando, FL, 31-36.

Spiegel, J. K., Zieger, P., Bukowiecki, N., Hammer, E., Weingartner, E., and Eugster, W. (2012) Evaluating the capabilities and uncertainties of droplet measurements for the fog droplet spectrometer (FM-100), *Atmos. Meas. Tech*., 5, 2237–2260, https://doi.org/10.5194/amt-5-2237-2012.

Spiel, D. E. (1995) On the births of jet drops from bubbles bursting on water surfaces. *J. Geophys. Res*., 100, 4995–5006, https://doi.org/10.1029/94JC03055.

Spiel, D. E. (1997) More on the births of jet drops from bubbles bursting on seawater surfaces. *J. Geophys. Res.*, 102, 5815–5821, https://doi.org/10.1029/96JC03582.

Spiel, D. E. (1998) On the births of film drops from bubbles bursting on seawater surfaces. *J. Geophys. Res.*, 103, 24 907–24 918, https://doi.org/10.1029/98JC02233.

Stoelinga, T. G. and T. T. Warner (1999) Non-hydrostatic, mesobeta-scale model simulations of cloud ceiling and visibility for an east coast winter precipitation event. *J. Appl. Meteor*., 38, 385-404.

Storelvmo, T., J. E. Kristjansson, Steven J. Ghan, Alf Kirkevag, Ø. Seland, and Trond Iversen (2006) Predicting cloud droplet number concentration in Community Atmosphere Model (CAM)-Oslo, *JGR*, 111, D24208, doi:10.1029/2005JD006300

Thompson, G., and T. Eidhammer (2014) A study of aerosol impacts on clouds and precipitation development in a large winter cyclone. *J. Atmos. Sci.*, 71, 3636–3658, doi:10.1175/ JAS-D-13-0305.1.

Thompson G., P. R. Field, R. M. Rasmussen, and W. D. Hall (2008) Explicit forecasts of winter precipitation using an improved bulk microphysics scheme. Part II: Implementation of a new snow parameterization. *Mon. Wea. Rev.*, 136, 5095–5115, doi:10.1175/2008MWR2387.1.

Torregrosa, A., T. A. O'Brien, and I.C. Faloona (2014), Coastal fog, climate change, and the environment. *Eos*, 95 (50), 473; DOI: 10.1002/2014EO500001.

Toth, G., I. Gultepe, J. Milbrandt, B. Hansen, G. Pearson, C. Fogarty, and W. Burrows (2011) *The Environment Canada Handbook on Fog and Fog Forecasting. Environment Canada.* Tech. Manual. ISBN # 978-1-100-52518-1. Available from Environment Canada, Toronto, Canada. 93 pp.

Troitskaya, Y., A. Kandaurov, O. Ermakova, D. Kozlov, and D. Sergeev, and S, Zilitinkevich (2018) The ''Bag Breakup'' Spume Droplet Generation Mechanism at High Winds. Part I: Spray Generation Function. *J. of Physical Ocean*., 48, 2167-2188.

Twomey, S. (1959) The nuclei of natural cloud formation. Part II: The supersaturation in natural clouds and the variation of cloud droplet concentration. *Geophys. Pure Appl.*, 43, 243–249.

Twomey, S. (1974) Pollution and planetary albedo, *Atmos. Environ*., 8, 1251–1256.

Twomey, S. (1991) Aerosols, Clouds and Radiation, *Atmos Environ*., 25, 2435–2442.

Wagh, S., R. Krishnamurthy , C. Wainwright, S. Wang and H. J. S. Fernando, and I. Gultepe (2020) Microphysics of Marine Fog during Stratus cloud lowering. *Boundary-Layer Meteorol. In Press.*.

Wainwright, C., and D. Richter (2020) Investigating the sensitivity of marine fog to physical and microphysical processes using large-eddy simulation. *Boundary-Layer Meteorol*., In Press.

Wang, S., Li Yi, S. Zhang , X. Shi, and X. Chen (2020) The Microphysical Properties of a Sea-Fog Event along the West Coast of the Yellow Sea in Spring, *MDPI Atmosphere*, *11*, 413; doi:10.3390/atmos11040413

Wang, Q., et al. (2020) Coastal fog microphysics and dynamic at Downs Supersite during C-FOG, *BLM*, submitted.

Wilfried, J., V. Nietosvaara, A. Bott, J. Bendix, J. Cermak, M. Silas, I. Gultepe (2008) *Short range forecasting methods of fog visibility and low clouds.* COST Action 722, Earth System Science and Environmental Management Final report on COST-722 Action. ISBN # 978-92-898-0038-9Available from COST Office, Avenue Louise 149, B-1050 Brussel, Belgium. 489 pp.

Wilkinson JM, A. N.F. Porson, F. J. Bornemann, M. Weeks, P.R. Field, and A. P. Lock (2013) Improved microphysical parametrization of drizzle and fog for operational forecasting using the Met Office Unified Model, *Q. J. Roy. Meteorol. Soc*., 139, 488-500.

Wright B. J., and Thomas N. (1998) An objective visibility analysis and very short- range forecasting system. *Meteorol. Appl.* 5. 157–181.

Wu, J. (1981) Evidence of sea spray produced by bursting bubbles. *Science,* 212, 324–326, https://doi.org/10.1126/science.212.4492.324.

Yang, D., H. Ritchie, S. Desjardins, G. Pearson, A. MacAfee, and I. Gultepe (2009) High Resolution GEM-LAM application in marine fog prediction: Evaluation and diagnosis. *Weather and Forecasting*. 25, 727-748.

Zhou, B. and J. Du (2010) Fog prediction from a multi-model mesoscale ensemble prediction system. *Wea. Forecasting*, 25, 303-322.

Zhou, B. and B. S. Ferrier (2008) Asymptotic analysis of equilibrium radiation fog. *J. App. Met. And Clim.*, 47, 1704-1722. https://doi.org/10.1175/2007JAMC1685.1.

REVIEWER 1

Responses are given in red colored text

Thanks for your constructive points and comments on the importance of this work. We improved the manuscript based on your suggestions. We also improved the text further for clarity.

1. The TKE dissipation rate was found under certain level for C-fog events. This is an important finding of this study. Some other studies, (e.g. Zhou and Ferrier 2008, "Asymptotic analysis of equilibrium in radiation fog" on JAMC, Price2019, "On the Formation and Development of Radiation Fog: An Observational Study" on BLM), also found turbulence intensity must be smaller than a threshold for radiation fog. So turbulence has similar role in C-fog and radiation fog?

Please add these 2 references and some discussion.

1. We included these two papers in the introduction section now. Somehow missed these in introduction. Thanks for the point.

We now discussed this in Discussion section, and stated that this needs to be further researched because rad fog occurs usually in calm conditions. This means that EDR criteria can be still valid for rad fog prediction conditions but lower than this of marine environments.

2. Suggesting TKE dissipation rate in rule-based fog prediction is a good idea. But in regular NWP model, TKE dissipation rate is not output field. Most of NWP models have TKE output. So please also prove a threshold for TKE in the rule.

2. This is provided now in the equation/text. Thanks for the point.

3. Line 114: "LWC and Nd are needed for accurate Vis forecasting, but they are not accurately predicted by models".

Please provide reference(s) for this statement

3. A couple refs is provided now; Gultepe and Milbrandt ; Pu et al

4. Line 174 for the project area and Fig. 1e is the GFS, which model for GFS, is from Canadian or US NCEP's GFS?

4. This is from US NCEP's GFS and text is midified.

5. Line 1154 Wilkinson JM, A. N.F. Porson, F. J. Bornemann, M. Weeks, P.R. Field, and A. P. Lock (2013) Q. J. Roy. 1155, Meteorol. Soc., 139, 488-500. The tile is missing

5. This is added now, was a mistake.

Reviewer #2 Comments on BOUN-D-20-00120

Responses are given in red colored text

Reviewer Recommendation Term: 'Minor Revisions'

Comments to Author:

General comments:

This work studies coastal fog microphysics and its visibility that affect visibility parameterizations. It uses detail in-situ observations representing coastal fog based on a vessel and supersites. Their results suggested that environmental conditions play an important role for late-season fog formation. Visibility (Vis), wind speed (Uh), and turbulence along coastlines are the most critical weather-related parameters affecting marine transportation and aviation. In the analysis, microphysical observations are summarized together with 3D wind components and used for fog intensity (visibility) evaluation.Overall their conclusions stated that EDR is a critical parameter affecting microphysics and that should be part of NWP developments. In addition, they summarized microphysical parameterizations for coastal/marine fog research and clearly provided issues for microphysical measurement biases. In the summary, my comments are usually minor and believe this work will be very useful for coastal/marine fog research related to observations and prediction of fog.

Thank you very much for the points you made, we considered all your points in the text coherently and equally important. We also improved the paper for eqs and figures for clarity.

Major points

* Please prepare a nomenclature for parameters used in the paper because there are many of them and not easy to follow up.

This is prepared now in the end of text.

* In a paper in this C-FOG special issue on coastal fog; this needs to be rewritten to and modified as "In this work, CFOG related studies are briefly summarized; …"

This is corrected.

* LN 142; Move this after first sentence in parag. In addition, the importance fog Vis predictions is discussed and challenges are noted when turbulence kinetic energy (TKE) dissipation rates are included.

Modified now.

*** 3.1 Time Series of Nd and Turbulence Dissipation Rate (ε)-change this to "3.1 Time series of microphysics and turbulence….."**

It is modified.

Minor points

LN76- ……may not be valid {, and therefore we have seen parametric modifications} take out the part in brackets

This is done now.

LN84: take out "or specifically coastal fog"

This is done.

LN87: latter in fog is usually not as strong as in clouds; you should say except during formation and dissipation conditions.

This is modified now.

LN105: In this respect, marine fog and cloud studies- change it to "marine fog and BL stratiform clouds"

Corrected.

LN110: take out "Although" and modified sentence, and put "but" before "they"

This is done.

LN116; LWC is a prognostic variable, but not Nd (assumed as fixed). Change this to "LWC is a prognostic variable and Nd is assumed as a fixed value

Modified.

LN138; please take out this sentence "C-FOG is designed to advance our understanding of liquid fog formation, development, and dissipation over coastal environments, and thus improve fog predictability and monitoring"

Taken out.

LN186; In this subsection, microphysical instruments as well as other available sensors-change to "microphysical and meteorological instruments are summarized" Table 2 : col 4, add ASL.

This is improved now.

LN231; Aug 14Oct 7 2018; needs a "-"

Modified.

LN299; normal to stable

Corrected.

LN288; "Uha is the apparent wind speed that includes both ship speed and wind speed", this should go to above.

It is modified now.

LN324; take out "only"

Done.

Results:

These are nice results with comparisons and derivations. Novel work here is that EDR used as criteria for Vis evaluation and this helps advancement of research on fog studies.

Yes it is correct that this can improve the Vis predictions using models.

Discussions: it is a good summary of issues related to coastal fog and its monitoring/predictions.

Conclusions:

Item 5; please explain 1 min versus 20 Hz values, and scale dependency

Improved now.

-References: Please check for refs in case of missing ones/citations.

This is checked and corrected.

Thanks for your improvements on the paper.

REVIEWER 3

Responses are given in red colored text

Reviewer #3 Comments on BOUN-D-20-00120

Reviewer Recommendation Term: 'Minor Revisions'

Comments to Author:

This study summarizes the microphysical observations carried out during C-FOG field campaign. Using the microphysical measurements along with the 3D wind components, authors have shown the magnitude of 3D-wind fluctuations was higher during the formation and dissipation stages of FOG life cycle. The observations reported in the present study strengthen our current understanding of life cycle of coastal fog and helps in improving the existing microphysical parameterization schemes for accurate fog forecast of NWP models. Overall the study is very good and manuscript is well written. The following minor comments need to be addressed before considering it for publication.

Specific comments:

Lines 56-58: What are anticyclonic storms? Reference has been submitted and hence cannot be checked. I thought fog formed in quiescent conditions. Need clarification.

It is corrected as anticyclonic system, was a mistake. These systems can transport moisture and heat over colder regions of ocean, corrected. Various corrections are also done for the manuscript to improve the quality. Thanks for your points improve the paper.

Line 138: "(Toward Improving Coastal Fog Prediction)" should go to line 119 where C-FOG is first introduced

It is done.

Line 142:"the importance fog Vis predictions" should be "the importance of fog Vis predictions"

Corrected.

Figure 1: color bars too small; parenthesis missing after "days"; vectors in panel (e) cannot be seen; what is the meaning of the two stars in panel (c) and the acronyms in panel (b)? It should be made clear in the caption.

This is improved now.

Line 176: cold front or warm front?

Improved as warm front.

Line 177: how many tropical cyclones? How strong were they and how far away did they get from the measuring sites? This information is needed to gauge their potential impact on the weather conditions at the site.

Over 6 week time period we located at least 4 tropical systems, and they were usually 500 km south or south east of the project location. This is now clarified.

Line 194: the acronym CDP was already defined in line 129, no need to do it again Lines 190-197: for readers that may not be familiar with this, can you please provide the typical radius of droplets in clouds and in fog and drizzle events?

Second definition is taken out, and improved. Droplet sizes are provided as 1-30 micron for fog, 30-100 micron as drizzles, and 1-100 micron for cloud droplets because usually clouds are more active dynamically compared to fog events. This is improved now.

Lines 205-209: define the acronyms NIR, MW, LIDAR and GOES-R

These are defined now.

Table 2: Not sure it is a good idea to have Table 2aand 2b, better to have Table 2 and Table 3. In Table 2b, is Z the height above mean sea-level and H the height aboveground level?

We separate them as 2a and 2b because we cant fit them into 1-page.

Now tables are given as T2 and T3, and text is modified accordingly.

Z and H are defined now.

Figure 3 and others: No need to add "Shows" at the beginning of the caption Line 231: spacing is missing at the end Line

Corrected for all figures and

LN231: It is modified for spacing.

234: "prior to fog, and average" should be "prior to fog. The average"

Corrected now.

Figure 4: Fog is defined as horizontal visibility impaired by water droplets dropping below 1 km. Perhaps a horizontal line corresponding to Vis = 1km can be drawn to better highlight the fog events, or shade as you do in Figure 17.

This is improved now as suggested. Vis=1 km is shown with a line now.

Figure 5: again, very hard to see color bar and labels, please improve the quality of the figure

This is corrected, and we have original figs that will be provided to printing office.

Lines 252-253 and 259-262: can you prove these hypothesisis with the available measurements?

Yes, we can, and modified the first sentence but second one is already shown by the given reference.

Section 3: I suggest using a better title as you are describing the theory here. An equation can be provided for Vis-RHw parameterization in section 3.2.1 or at least refer to section 4.1.1 for more details.

Title is modified and Eq. is provided now/refer to section 4.1.1

Line 365: Mist refers to visibility between 1 and 2 km and haze between 2 and 4 km even though different thresholds are used. Stating mist as having a visibility >1 km is incorrect as there is an upper-limit.

These values are not firm unfortunately and need to be further discussed; mist Vis>1 km but <5 km with RH>80%, and haze is usually Vis>5 km with RH<80%, and this is clarified now.

Lines 880-883: TCs do not occur that often in the region, but it is still nice to report on their impacts

Agree and this is slightly modified now.

Thanks for your constructive points.

****

A review of Coastal Fog Microphysics during C-FOG

I. Gultepe,[1a,1b,2], A.J. Heymsfield[3], H.J.S Fernando[2], E. Pardyjak[4], C. E. Dorman[5], Q. Wang[6], E. Creegan[7], S. W. Hoch[8], D. D. Flagg[9], R.Yamaguchi[6], R. Krishnamurthy[10], S. Gaberšek[9], W. Perrie[11], A. Perelet[4], D.K. Singh[4], R. Chang[12], B. Nagare[12], S. Wagh[2], and S. Wang[2]*

Received: July 02 2020

Abstract The goal of this paper is to provide an overview the microphysical measurements made during the C-FOG (*Toward Improving Coastal Fog Prediction*) field project. In addition, we evaluate microphysical parameterizations using the C-FOG dataset. C-FOG is designed to advance understanding of liquid fog formation, development, and dissipation in coastal environments to improve fog predictability and monitoring. The project took place along eastern Canada's (Nova Scotia, NS and Newfoundland, NL) coastlines and open water environments from August-October 2018, where environmental conditions play an important role for late-season fog formation. Visibility (Vis), wind speed (U_h), and turbulence along coastlines are the most critical weather-related parameters affecting marine transportation and aviation. In the analysis, microphysical observations are summarized first and then they are, together with 3D-wind components, used for fog intensity (visibility) evaluation. Results suggest that detailed microphysical observations collected at the supersites and aboard the Research Vessel (*R/V*) *Hugh R. Sharp* are useful for developing microphysical parameterizations. The fog life cycle and turbulence kinetic energy dissipation rate were strongly related to each other. The magnitude of 3D-wind fluctuations was higher during the formation and

----

*Corresponding Author: Dr. Ismail Gultepe, Ismail.gultepe@uoit.ca
[1a]Environment and Climate Change Canada, MRD, Toronto, ON M3H5T4, Canada
[1b]UOIT, Engineering and Applied Science Department, Oshawa, Ont., Canada
[2]Department of Civil and Environmental Engineering and Earth Sciences, and Department of Aerospace and Mechanical Engineering, University of Notre Dame, Notre Dame, IN 46556, USA
[3]NCAR/MMM, 3450 Mitchell Lane, Boulder, CO 80301, USA
[4]Department of Mechanical Engineering, University of Utah, Salt Lake City, UT 84112, USA
[5]Integrative Ocean. Div., Scripps Ins. of Oceanography, Uni. of California San Diego, La Jolla, CA, USA
[6]Department of Meteorology, Naval Postgraduate School, Monterey, CA 93943, USA.
[7]US Army Research Laboratory, White Sands Missile Range, NM USA
[8]Atmospheric Sciences Department, University of Utah, Salt Lake City, UT, USA
[9] Marine Meteorology Division, U.S. Naval Research Laboratory, Monterey, CA 93943, U.S.A.
[10]Pacific Northwest National Laboratory, Richland, WA, USA
[11]Fisheries and Oceans Canada, Bedford Institute of Oceanography, Dartmouth NS, Canada
[12]Dalhousie University, Department of Physics and Atmospheric Science, Halifax, NS B3H 4R2, Canada

dissipation stages. An array of cutting-edge instruments used for data collection provided new insight into the variability and intensity of fog (visibility) and microphysics. It is concluded that further modifications in microphysical observations and parameterizations are needed to improve fog predictability of NWP (Numerical Weather Prediction) models.

Keywords: Fog Microphysics. Coastal Fog. Visibility. Eddy Dissipation Rate

1 Introduction

Coastal fog plays an important role for weather conditions affecting marine environments that include aviation (Gultepe et al 2020), marine shipping (Fernando et al 2020), sporting and social activities (Pezzoli et al 2010), as well as vegetation (Schemenauer et al 2016; Torregrosa et al 2014). The direct consequence of fog is the impairment of visibility, and hence the 'intensity' of fog is defined in terms of visibility (Vis). Advection supplies moisture for Atlantic-Canadian coastal fog, while the overhead passage of cyclonic or anticyclonic systems~~storms~~ fosters its actual formation (Dorman et al. 2020). Other factors such as large-scale subsidence leading to thermal inversions, frontal systems, radiative cooling, topography, tropical cyclones, and turbulence fluxes can also have an impact on the life cycle of coastal fog (Gultepe et al 2007; Toth et al 2011). Intensity of turbulence and turbulence dissipation rate occurred during life cycle of radiation fog were studied by Zhou and Ferrier (2008) and Price (2019) and these suggested that turbulence intensity should be less than a threshold value.

Microphysical measurements were performed using a fog measuring device (FMD, FM100) for the first time by Gultepe et al (2007a) during the FRAM project, followed by others (Niu et al 2010; Spiegel et al 2012; Isaac et al 2020). The FM100 was developed using the principles of a forward scattering probe (FSSP), measurements of which were used in developing Vis parameterization by Gultepe et al (2007b). The FM100 provides droplet spectra, which are used to obtain liquid water content (LWC*),

---

*Definitions are provided in Nomenclature in the end of paper.

Formatted: Indent: First line: 0"

mean volume diameter (MVD), effective size (rR_{eff}), droplet number concentration (N_d), and the droplet settling rate ($LWC \bullet V_f$), where V_f is the droplet fall velocity. NWP modeling and evaluation studies of fog have helped to improve forecasting and gain physical insights (e.g. Yang et al. 2009; Gultepe et al. 2007a,b).Warm-fog droplet spectra and its distribution are related to condensation nuclei (CN) and relative humidity with respect to water (RH_w). There have been several studies on this issue, but cloud condensation nuclei (CCN) versus supersaturation with respect to water (S_w) relationships are mostly developed for cloud studies and generally use fixed values of 100 cm^{-3} for marine environments (Thompson et al 2008). In reality, such fixed values may not be valid, and therefore we have seen parametric modifications. (Thompson et al 2014). Prediction of N_d is obtained using prognostic equations that represent processes related to turbulence, droplet growth, radiative heating/cooling, as well as turbulence flux divergence (Storelvmo et al 2014). Based on assumed modified-gamma distributions, either using Kohler theory (Chen 1994) and/or Twomey parameterization (Twomey 1959), N_d predictions can be performed using single or double moment microphysical schemes (Milbrandt and Yau, 2005a,b; Morrison and Gettelman 2008; Schwenkel and Maronga, 2019). However, these schemes have been developed for clouds and not for fog. or specifically coastal fog.

As in Twomey et al (1959), N_d is parameterized based on Kohler theory assuming equilibrium and cooling of an air volume by lifting via the vertical air velocity (w_a). The latter in fog, excluding formation and dissipation conditions, is usually not as strong as in clouds, complicating the application of these parameterizations to fog. Therefore, its usage cannot be verified for all fog types. Another equation for N_d prediction, mainly applicable to climate studies, expresses it as a function of w_a, N_a (aerosol total number concentration) as well as aerosol composition (Abdul-Razzak and Ghan 2000; Ghan et al 1998; 2001). In addition to parameters given in Twomey (1974; 1991), this equation uses aerosol composition as an independent parameter. Clearly, environmental conditions such as air temperature (T_a), dew point temperature (T_d) and RH_w, and w_a as well as aerosol and microphysics parameters (CCN and droplet growth rate) play an important role in N_d prediction, thereby affecting Vis estimation (Schwenkel and Maronga, 2019). In this regard, Gultepe et al (2007b) have suggested that accurate predictions of N_d and LWC are critical for Vis prediction, and Vis cannot be accurate if only LWC is used (Kunkel 1984; Stoelinga and Warner 1999). Vis is usually diagnosed in the post processing stage of forecast model outputs using Stoelinga-Warner's method (Stoelinga and Warner 1999), which includes large uncertainties in fog prediction (Gultepe et al 2006, 2007c).

Lately, field observations from various projects have been used to improve Vis parameterizations (Gultepe et al 2009; 2014; Haeffelin 2010; Price et al 2018; Wang et al 2020) but these are often site dependent because of the nature of N_a spectra and compositional properties (Bergot et al 2005). In this respect, marine fog ~~and cloud~~ studies ~~have been used to develop m~~ used microphysical parameterizations extensively (Gultepe et al 2009; Gultepe et al 1996). The C-FOG (Toward Improving Coastal Fog Prediction) field project has had better tools to evaluate coastal fog microphysical and dynamical properties, such as droplet and aerosol spectra and turbulence over both the coastal areas and at the ship (Fernando et al 2020).

~~Although~~ Vis parameterizations commonly use only RH_w and/or (T_a-T_d) (called dew point depression) to predict fog coverage but ~~,~~ they cannot be used for fog intensity (~~drop of~~e.g., Vis) because RH_w (as well as T_a-T_d) indicates only the existence of fog (Toth et al., 2011; Gultepe et al 2009; Renata et al 2020). Therefore, fog microphysical parameters such as LWC and N_d are needed for accurate Vis forecasting, but they are not accurately predicted by models (Pu et al 2016, Renata et al 2020, Gultepe and Milbrandt 2010). In single-moment and double moment microphysical schemes used in NWP models, LWC is usually a prognostic variable~~,~~ and ~~but not~~ N_d is ~~(~~assumed as a fixed value or~~). In double moment schemes, N_d can be~~ or obtained either deterministically or prognostically, by making several assumptions on physical terms affecting N_d. If N_d is not fixed, a modified gamma distribution is usually assumed in presenting fog droplet size distribution that is used to obtain N_d.

Formatted: Subscript

Formatted: Subscript

~~In a paper in this C-FOG special issue on coastal fog~~ In this work, C-FOG related studies are briefly summarized; ~~(Dimitrova et al 2020),~~ WRF fog simulations ~~predictions~~ using~~with~~ various microphysical and surface boundary layer schemes are performed~~tested~~ for Vis predictions at the ship and supersite locations. Another microphysics paper is focused on a case of stratus lowering fog over the coastline based on the *R/V Sharp* observations (Wagh et al 2020). Understanding fog microphysics and its impact on Vis, based on a LES model, is provided by Wainwright and Richter (2020). A study using a Tethered Balloon System (TBS) with aerosol and droplet spectral measurements as well as fog thermodynamics is examined by Singh et al (2020). Detailed coastal fog observations at The Downs, Ferryland (Wang et al. 2020) are studied by providing TBS dynamic and thermodynamic profiles and collecting fog-droplet spectra ~~and aerosol extinction parameters~~ from a ~~cloud droplet probe (CDP)~~ fog measuring device ~~in a housing unit~~. Perelet et al (2020) present a methodology for using a two-wavelength scintillometry system for measuring fog characteristics on scales of 1 km. Wang et al. (2020) also focused on the impact of the fog layer on optical propagation using contrasting measurements at Ferryland and on the US West Coast. In addition, large-scale synoptic events affecting local fog formation are summarized by Dorman et al (2020). An overview of the C-GOG project is given in Fernando et al. (2020).

The goal of this paper is to provide an overview of coastal fog microphysical measurements and to evaluate microphysical parameterizations based on the C-FOG ~~(*Toward Improving Coastal Fog Prediction*)~~ field project. In addition, the importance of fog Vis predictions is discussed and challenges are noted when turbulence kinetic energy (TKE) dissipation rates are included. ~~C-FOG is designed to advance our understanding of liquid fog formation, development, and dissipation over coastal environments, and thus improve fog predictability and monitoring.~~ The C-FOG field project has provided microphysical observations from several coastal ~~land~~ sites and the *R/V Hugh R. Sharp* (hereafter *R/V Sharp*). ~~In addition, the importance fog Vis predictions is discussed and challenges are noted when turbulence kinetic energy (TKE) dissipation rates are included.~~ The paper organization is planned as follow: Section 2 provides information on observations and project design. Section 3 explains the analysis used in Vis and eddy dissipation rate (EDR) parameterizations. Sections 4 and 5 focus on discussions and conclusions, respectively.

2 Field Project and Observations

2.1 Project Location

The C-FOG field campaign took place from 01 September to 07 October 2018. The field campaign took place along the coastlines of Atlantic Canada and the northeastern US. C-

FOG is designed to advance our understanding of liquid fog formation, development, and dissipation over coastal environments, and thus improve fog predictability and monitoring. It was designed to capture fog variability in time and space using an array of platforms that included ground, airborne, and shipborne in-situ instruments, remote sensors as well as numerical models. ~~The field campaign took place along the coastlines of Atlantic Canada and the northeastern US.~~ Instruments were located at two supersites (Battery and The Downs sites in Ferryland, NL; Figure 1a,b), four satellite sites, as well as on the *R/V Sharp* (Fernando et al 2020). Figure 1c shows the entire project area overlaid on a satellite SST image for 28 September 2018. A strong SST gradient stands out near the northern region of the project area. In the current study, four cases are presented covering parts of the Intense Operational Periods IOP10 (27–30 Sep 2018) and IOP 12 (03-04 Oct 2018) that mainly represent warm advection fog events (Table 1).

Table 1 Case studies of coastal fog events studied in the present work. T_a is air temperature and SST is sea surface temperature.

Day	Location	Weather
Sep 28 2018	Battery supersite	T_a, SST, warm air advection
Sep 29 2018	Battery supersite	Warm air advection
Sep 28 2018	R/V Sharp	Warm air advection
Oct 04 2018	R/V Sharp	Advection and tropical depression~~cyclone~~

~~**Fig. 1** Ferryland supersite region (a), Battery supersite (b), SST and entire project location with ship locations (indicated by a red star for foggy days (c), synoptic weather systems affecting project area (d), and GFS (Global Forecasting System) surface pressures and wind speed in Knots (e).~~

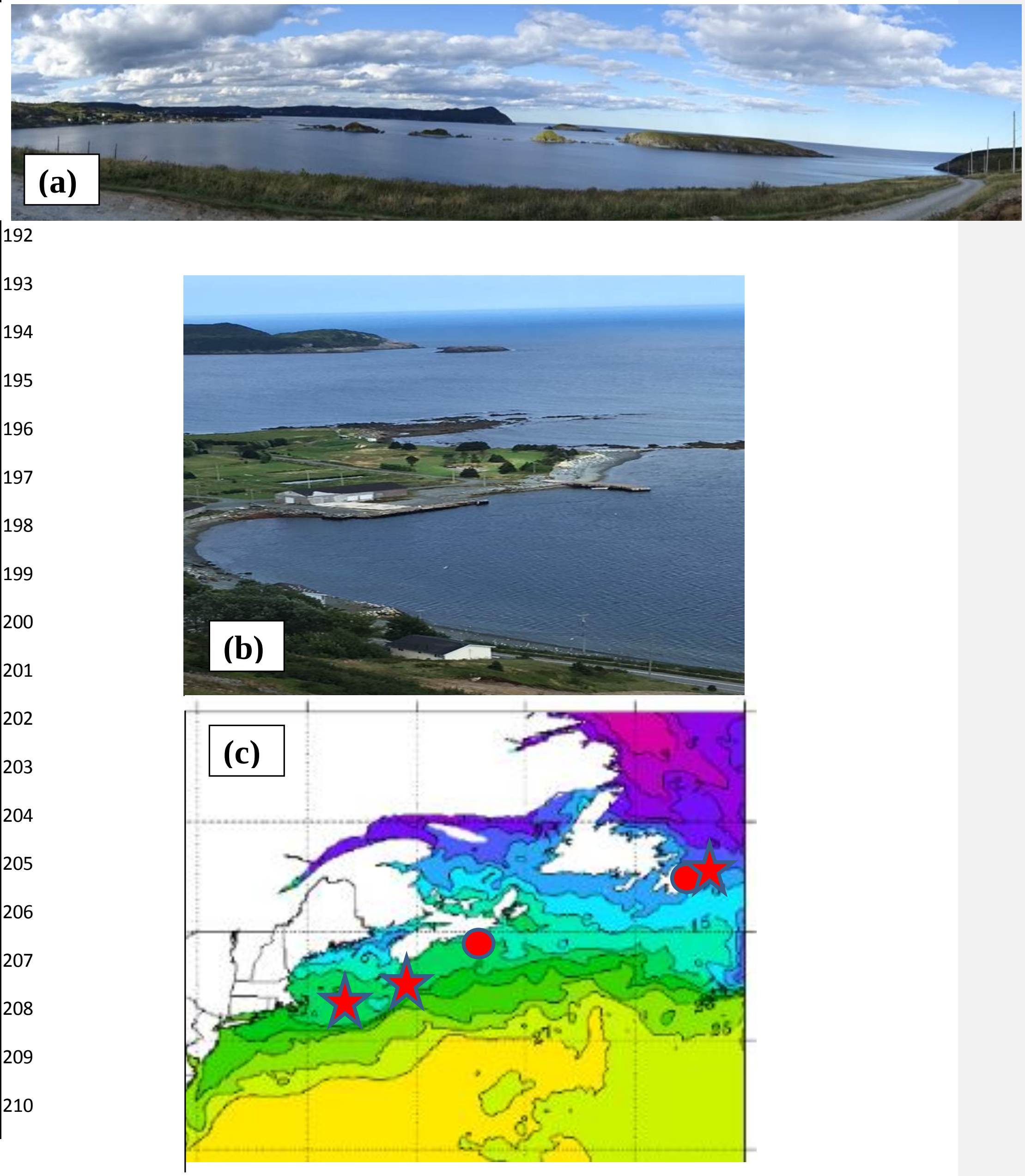
(a)
(b)
(c)

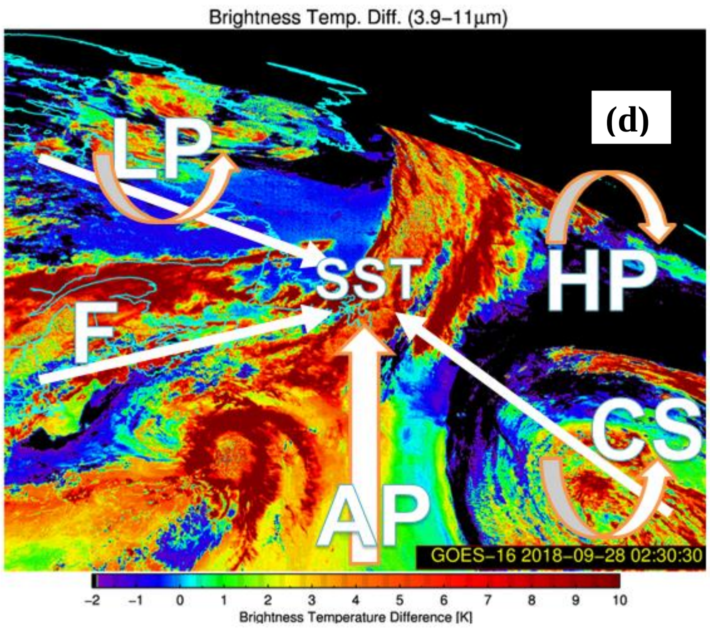

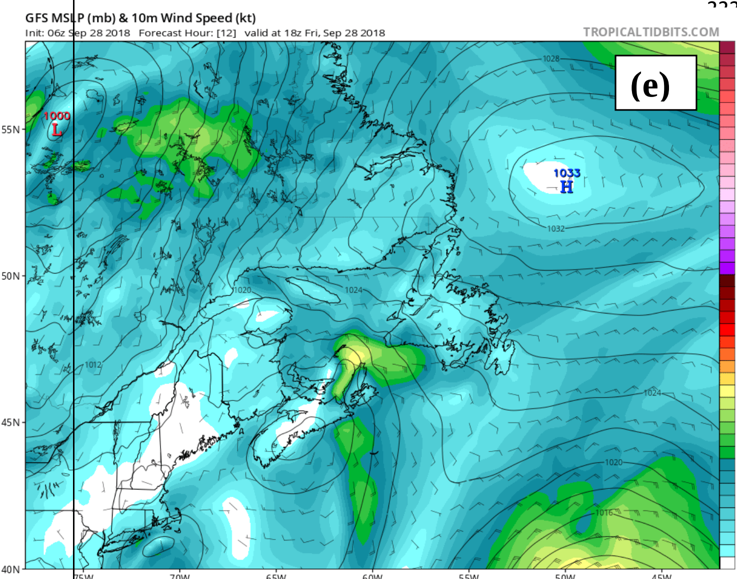

Fig. 1 Ferryland supersite region (a), Battery supersite (b), NOAA NESDIS Geo-Polar blended 5 km SST and entire project area with supersites (red circles) and ship locations (indicated by a red star for foggy days (c), synoptic weather systems affecting project area (d) with LP for "low pressure", F "front", SST "sea surface temperature", AP "advection process", HP "high pressure", and CS "cyclonic system", and US

NCEP (National Center for Environmental Prediction) GFS (Global Forecasting System) based surface pressures and wind speed in Knots (e).

2.2 Synoptic Weather Systems

The C-FOG campaign took place at the end of the summer fog season (Gultepe et al 2009). During this time, various weather systems affect coastal-fog conditions. Figure 1d shows the SST for the project area and Fig. 1e is the GFS sea-level pressure and 10 m wind vectors on 28 September 2018. The latter shows- major weather systems affecting the project area: a low pressure over Nova Scotia in the NW and associated with a warm frontal system (F) in the east, a high pressure (HP) to the NE, and tropical cyclones- to the south east (CS), and warm-air advection processes (AP) resulting from T and q_v gradients along a north-south direction. The tropical cyclones usually became tropical depressions when moved to colder northern latitudes and usually they were about 500 km south and southeast of the main project site. During May 25-Oct 31 2018, 16 tropical depressions occurred over 4-months time period and about 4 of them affected physical conditions somehow at the project site. Their advection of SW quadrant of warm and moist air to N and NW quadrants likely played an important role for fog formation 100s of km away from storm center. Figure 1e is an example (Sep 28 case) illustrating the placements of the above mentioned weather systems. The photos in Figure 2 depict fog cases observed at The Downs supersite, and from the *R/V Sharp*, respectively.

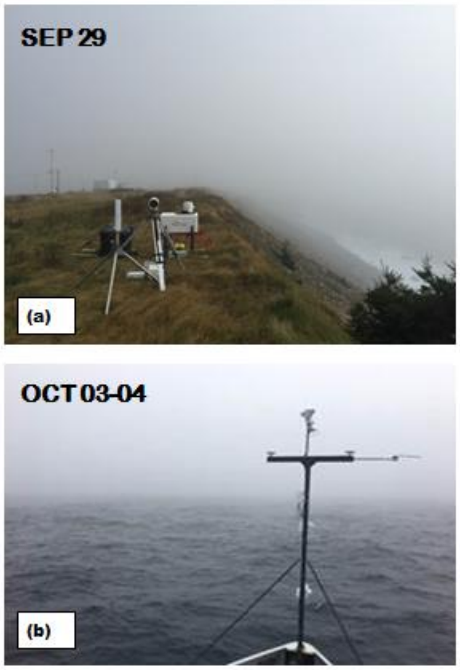

Fig. 2 ~~shows t~~The pictures of advection process occurring on Sep 28/29 2018 case at the Downs supersite (a) and on Oct 04 2018 (taken from the RV) (b).

2.3 Microphysical Observations

In this subsection, microphysical and meteorological instruments ~~as well as other available sensors~~ are summarized. All instruments used are summarized in Fernando et al. (2020). These measurements are related to dynamics, microphysics, radiation, aerosol, and thermodynamic properties of the environment. For particle size thresholds, fog droplets usually cover 1-30 µm, cloud droplets 1-100 µm, drizzle drops 100 (or 30)-500 µm , and drizzle and rain drops >100 µm in diameter.

Microphysical instruments used during C-FOG are summarized in Table 2~~a~~ for the *R/V Sharp* and in Table ~~2b~~ 3 for all ground-based sites. Special sensors (Table 2~~a~~) were developed for fog microphysics investigations, including a 'gondola' shaped assembly (located on the *R/V Sharp*) that contained microphysical sensors such as a cloud droplet probe (CDP) and a backscatter cloud probe (BCP) in a gondola unit for measuring droplet sizes ranging from 1-50 and 5-75 µm, respectively~~.~~ A laser precipitation monitor (LPM) for 100 µm to mm sizes and an optical particle counter (OPC) for sizes of 0.3-20 µm using 16~~20~~ spectral channels allowed fog and drizzle discrimination (Table 2).

Table 2~~a~~ Microphysical instruments mounted on the *R/V Sharp* during the C-FOG campaign. *Parameters in Column 2:* N_d Droplet number concentration, N_a Aerosol number concentration, SV Sampling Volume, S_w Supersaturation with respect to water, and Vis Visibility. *Parameters in Column 4*: UOIT Ontario Technical University, UU University of Utah, Wood Corporation, DU Dalhousie University, and NDU Notre Dame University.

Instrument Name	Measurements	Height (asl, m)	Owner
CDP, DMT, Gondola	N_d, Droplet spectra (1-50) µm	31.8	UOIT
BCP, DMT, Gondola	N_d, Droplet spectra (5-75) µm	31.8	UOIT
OPC N2, Alphasense	N_a, Aerosol Spectra 0.38-17µm, 16 channels	15	UU
DMT, FM120, near Gondola	N_d, Droplet spectra (1-50) µm	31.6	WOOD
TSI Moudi Impactor 100NR	N_a spectra, 0.18-18 µm, 8 stages, 30 L m^{-1}	37.9	WOOD
Virtual Impactor Inlet	At 20 m, SV=16.7 L min^{-1}	30.1	DU
SMPS 3082, TSI	N_a Spectra, 10-500 nm; SV=1.0 L min^{-1}	30.1	DU
APS 3321, TSI	N_a Spectra, 0.5-20 µm SV=1.0 L min^{-1}	30.1	DU
ACSM, Aerodyne	N_a Composition, <1 µm SV=0.1 L min^{-1}	30.1	DU
CCN-100, DMT	N_a>0.01 µm;S_w=0.2,0.4,0.8,1% SV=0.5 L m^{-1}	30.1	DU
PWD22- Vaisala	Vis <20 km	10	NDU

Also, three Scintillometers (Table 3~~2b~~) with measurements in the NIR (Near Infra-Red) and MW (MicroWave) radiation channels were utilized to allow discrimination of fog from rain (Perelet et al 2020). Figure 3 shows the microphysical, aerosols, as well as meteorological instruments. Remote-sensing platforms (e.g. microwave radiometer MWR, ceilometer, Lidar), meteorological towers, tethered balloons, and the GOES-R (Geostationary Operational Environmental Satellite-R series) Products (fog coverage and effective droplet size) provided information on horizontal and vertical variability. Observational products are used for fog-visibility parameterization development, with a focus on understanding the influence of dynamical processes such as turbulent mixing and dissipation.

Table 3~~2b~~ Microphysical instruments located at the ground sites during C-FOG field campaign. *The parameters in Column 2*: Vis Visibility, PR Precipitation rate, IR Infrared, SW shortwave, RF radiative fluxes, LWC liquid water content, Z_e radar reflectivity, V_d Doppler velocity, N_a aerosol number concentration, Z_{cb} cloud base height, β backscattering coefficient, λ wavelength, β_n extinction coefficient, CN condensation nuclei, RH relative humidity, T temperature, U_h horizontal wind, and P pressure. *Parameters in Column 7 and 8:* BA Battery Supersite, BH Blackhead site, DO Downs Supersite, UOIT Ontario Technical University, UU University of Utah, UND University of Notre Dame, and NPS Navy Postgraduate School.

Instrument Name	Measurements	H (agl,m~~m~~) ~~AGL~~	Z (agl,m)	Lat [deg]	Lon [deg]	Site	Owner
PWD50-Vaisala	Vis and PR	2	6	47.03443	-52.8782	BA	UOIT
FM100 & FM120	Fog droplet spectra	2	6	47.03443	-52.8782	BA	UOIT
CRN1 Kipp&Zonen	IR&SW up and down RF	2	6	47.03443	-52.8782	BA	UOIT
PMWR MP3017	Profiling, T, RH, LWC	2	6	47.03443	-52.8782	BA	UOIT
MRR, Metek	Z_e & V_d	2	6	47.03443	-52.8782	BA	UOIT
LPM, Metek	Precip. Spectra >100 µm	2	6	47.03443	-52.8782	BA	UOIT
OPC, Alphasense	N_a spectra, >0.3 µm	2	6	47.03443	-52.8782	BA	UU
CL31, Vaisala	Z_{cb} and β	2	6	47.03443	-52.8782	BA	UU
Vaisala PWD 50	Vis (<30 km)	2.9	10	47.52633	-52.6583	BH	UOIT
Vaisala PWD 22	Vis (<30 km)	3	31	47.02181	-52.8731	DO	UND
LPM Metek	Precip. spectra >100 µm	2.74	10	47.52633	-52.6583	BH	UOIT
OPC, Alphasense	Aerosol spect. (0.3-20 µm)	1.37	10	47.52633	-52.6583	BH	UU
DMT CDP	fog droplets (1-50 µm)	3	31	47.02181	-52.8731	DO	NPS
TSI -3563 Nephelometer	3-λ scat& β_n (0.45,0.55,070 µm)	3	31	47.02181	-52.8731	DO	NPS
TSI OPC-310	CN >0.01 µm	3	31	47.02181	-52.8731	DO	NPS
PSAP, Part Soot Abs Photometer	1-λ absorp. at 0.565 µm	3	31	47.02181	-52.8731	DO	NPS
Scintillometer (BLS -900, Scintec AG)	wavelength 0.88 µm extinction	2.9	31	47.02181	-52.8731	DO-BH Tx-Rx	NPS
Scintillometer (BLS 900, Scintec AG)	wavelength 0.88 µm extinction,	2	6	47.03443	-52.8782	BA-DO Tx-Rx	UU
Scint. MWSC 160, Radio.Phy. GmbH	microwave (wavelength 1.860 µm extinction	2	6	47.03443	-52.8782	BA-DO Tx-Rx	UU
Met parameters	RH, T, Uh, P	3	31	47.02181	-52.8731	DO	NPS

Formatted Table

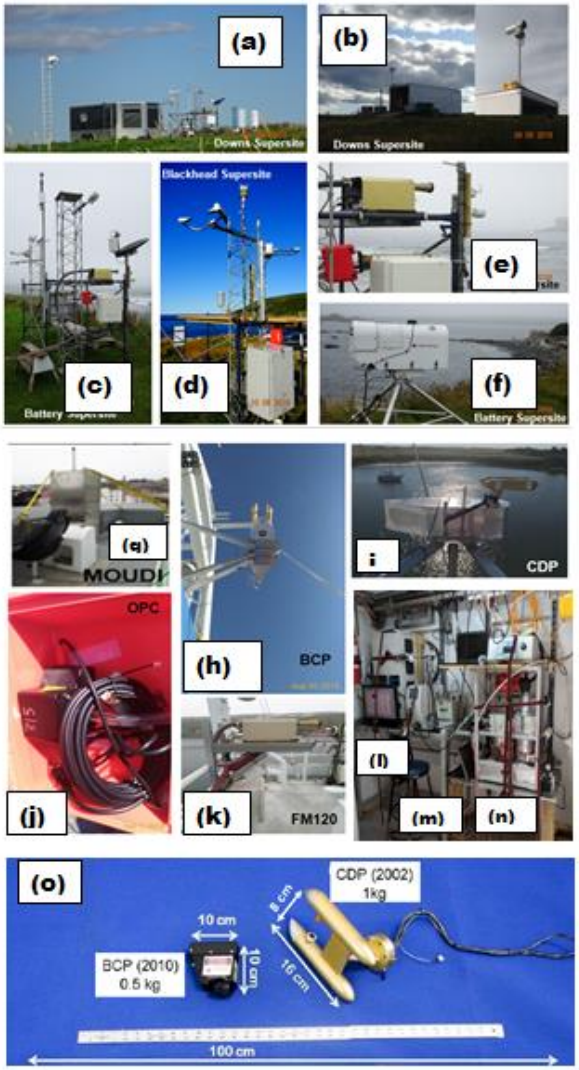

Fig. 3 P~~Shows p~~roject locations with microphysical probes: NPS microphysical sensors mounted on a trailer at the Downs site (a), CDP2 located in a housing shown in (b), FM120, PWD, LPM at Battery (c), PWD, LPM, and OPC at Blackhead (d), a close look of FM120 at Battery (e), PMWR at Battery (f), Wood MOUDI impactor (g), Gondola BCP (h) and CDP2 (i) mounted on Sharp RV, UU OPC (j), Wood Corp FM120 (k), Dalhousie University(DU) CCNC (l), DU SMPS (m), and DU ACSM (n), and Gondola housed CDP and BCP (o) physical characteristics (adapted from Beswick et al 2014).

2.4 Macro-physical Characteristics

During the installation and campaign period that spanned 7-weeks (Aug 14~~-~~Oct 7 2018) various fog conditions existed, as represented by Vis measurements from the Battery site (Fig. 4). This figure shows Vis for 46 days starting from Aug 21 to Oct 7 during which drizzle and light precipitation usually occurred prior to fog.~~, and a~~ Average fog occurrence during entire campaign was about 20-25%.

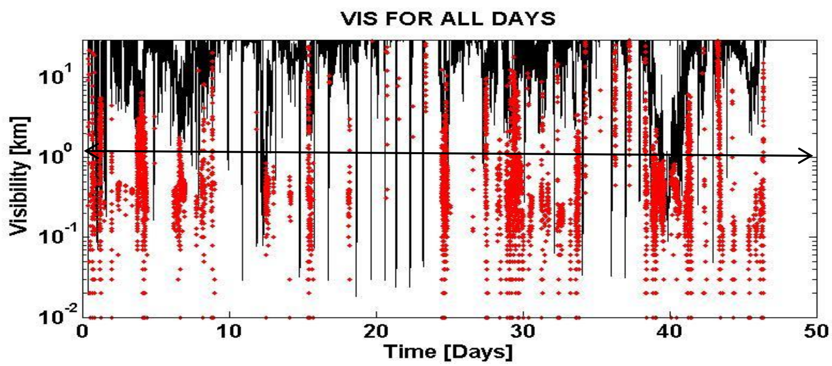

Fig. 4 ~~Shows~~ T~~t~~ime series of Vis obtained from PWD52 present weather sensor for the entire time period from Aug 24 to Oct07 2018. The red dots are for drizzle and black lines are for fog Vis. Transition from fog to drizzle cannot be exactly defined. The line with double arrow indicates Vis level at 1 km.

A CL31 ceilometer measured the backscatter ratio (β) time and height cross sections at the Battery supersite and on the *R/V Sharp* for the 4 cases studied, as shown in Fig. 5. Note that the ceilometer-based fog-top heights are not accurate because of its strong extinction when a large number of smaller fog droplets exist. Figure 5a and 5b are for 28 and 29 September cases, respectively, as observed at the Battery supersite and Fig. 5c and 5d are for 28 September and 04 October cases, respectively, aboard *R/V Sharp*.

The 28 September case at the Battery site, occurred at about 1000 UTC after the stratus layer base lowered from 500 m to the surface over 3 hrs. Some drizzle was observed (indicated by the spiking cloud base in red color), which disappeared about 1700 UTC. The 29 September case was a continuation of the 28 September case, during which fog briefly lifted at 1600 UTC and then re-formed at 2200 UTC and lasted until almost 1800 UTC, which is not likely related solely to a lowering stratus, but was also likely due to warm-air advection that is verified by using synoptic weather conditions~~.~~

The *R/V Sharp* data for 28 September (Fig. 5c) show that the cloud base decreased from 500 m at 0000 UTC to almost the surface at 1000 UTC, and then lifted very quickly at 1330 UTC. After this, the stratus base lowered again to form fog at 1400 UTC. At 1600 UTC, the fog base lifted and eventually disappeared. The *R/V Sharp* observations for 04 October show that fog formed again due to stratus lowering around 2000 UTC and lasted until 2300 UTC. Note that the lowering cloud base occurred late on this day and is likely due to IR cooling and/or large-scale subsidence. This might also be related to drizzle that moistened lower layers, eventually led to fog formation (Singh et al 2020; Wagh et al 2020).

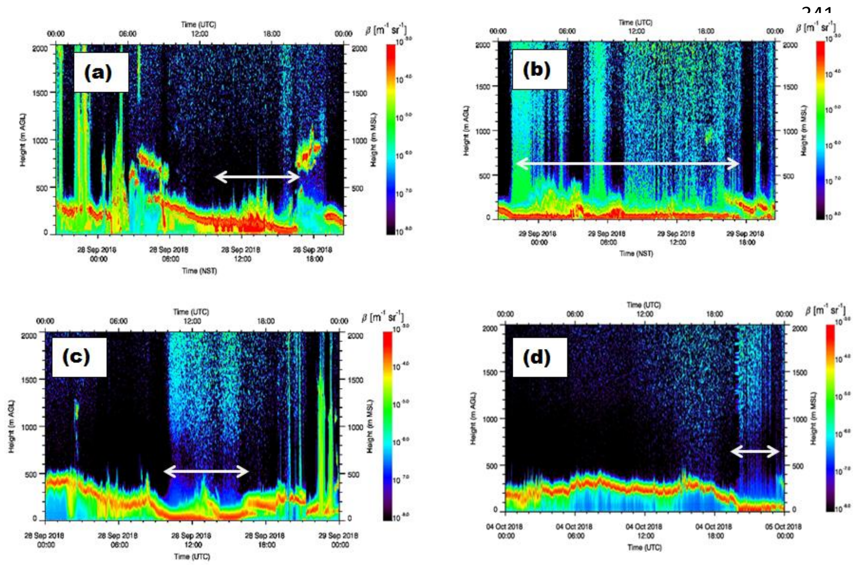

Fig. 5 Time-height cross sections of backscatter coefficient (β) from CL31 ceilometers measurements at the Battery supersite and onboard the Sharp RV for the 4 cases studied; Sep 28 (a) and Sep 29 (b) cases observed at the Battery supersite and Sep 28 (c) and Oct 04 2018 (d) cases at the Sharp RV. The white lines with arrow indicate foggy regions.

The general characteristics of these four fog cases at the Battery supersite and *R/V Sharp* are presented as a backdrop for the development of microphysical parameterizations. Note that ceilometer measurements cannot unequivocally identify fog regions, and ceilometer inferences should be validated using PWD Vis observations.

3. ANALYSIS AND MICROPHYSICAL PARAMETERIZATION

An analysis of the main microphysical and turbulence parameters to be used in the evaluation of fog conditions and for developing parameterizations is provided in this section.

3.1 Time Series of microphysical parameters~~of N_d~~ and Turbulence Dissipation Rate (ε)

Time series were obtained based on various microphysical parameters, including Vis, N_d, LWC, and MVD. Vis was obtained from PWD52 measurements representing various NWS (National Weather Service) codes, droplet spectral measurements of FMD (FM120, in Battery) and CDP and BCP housed in the gondola aboard the *R/V Sharp*. NOAA NWS codes can be found in LPM (2011), based on PR and Vis time series for each hydrometeor type obtained. The FMD was operated at a 1 Hz sampling rate, compared to 1-min Vis measurements from PWD52. All meteorological parameters such as T, RH_w, and wind speed (U_h) and directions were employed as appropriate.

N_d is obtained using the corrected ship heading and apparent wind, which includes both ship speed and wind measurements (Gultepe and Starr 1995). It is corrected by computing the cosine of the angle θ between the heading and the apparent wind measured by an anemometer as

$$N_d = N_c \sout{C}/(SA * TAS * \Delta t), \quad (1)$$

where the true air speed (TAS) is given by

$$TAS = U_{ha} cos\theta. \quad (2)$$

In Eq. 1, SA is the sampling area, Δt the sampling interval and N_c~~C~~ the counts of droplets in each bin of the CDP and BCP. N_d is obtained from the FM120 located at the Battery site ~~was obtained~~ using a fixed TAS (true air speed) of 5 m s^{-1} for sampling of the environmental air. U_{ha} is the apparent wind speed that includes both ship speed and wind speed. During ~~normal~~ normal observational conditions, the *R/V Sharp* average speed was about 8 m s^{-1}.

The TKE dissipation rate (ε_{dis}) is usually calculated based on the spectral slope assumption, representing the inertial subrange (Panofsky and Dutton, 1984). In our work, 1-minute averaged data from 3D sonic anemometer wind measurements (collected at 20 Hz) at 2 m were used to estimate ε. This calculation uses an assumption that turbulence fluctuations do not change over 1 min intervals. It should be noted that ε calculation is strongly related to averaging scales and here ε approximately represents scales of 0.3-0.5 km that matches scales of high resolution NWP models Thus, using a structure function, ε is estimated (Paluch and Baumgardner, 1989; Gultepe and Starr, 1995). Clearly, 1-min averages do not capture inertial subrange scales but a structure function representing 3D scales can be used to calculate ε_{dis} along the mean horizontal wind speed as

$$\varepsilon\varepsilon_{dis} = \frac{1}{2\pi 4.01C}\left|\frac{D_s}{\Delta r^{2/3}}\right|^{3/2}, \quad (3)$$

where C is a constant ~0.18, D_s the structure function and Δr the horizontal distance along main horizontal wind, and these are given, respectively, as

$$D_s = 0.38(\Delta u^2 + \Delta v^2 + \Delta w^2) \text{ and } \Delta r = d\Delta t(U_{dx}^2 + U_{dy}^2)^{1/2}. \quad (4)$$

In Eq. 4, Δu, Δv, and Δw represent the change in wind components along x, y, and z axis at unit time interval (Δt), receptively; U_{dx} and U_{dy} are wind speed components along x and y axis, respectively, over Δt. ~~in Cartesian system~~ over ~~dt (sampling time period).~~ Thus, Eq. 3 can then be used in dissipation rate calculations and evaluation of the fog life cycle. For the NWP models, ε is not always an output parameter; therefore, TKE can be calculated from the following equation (or a transformation equation given in Discussion section) that is used to obtain a threshold for fog formation:

$$TKE = \frac{1}{2}\left(u'^2 + v'^2 + w'^2\right), \quad (5)$$

where $u', v', and\ w'$ are fluctuations of wind x, y, and z components that are calculated over 10 min intervals.

3.2 Visibility Parameterization

The visibility parameterization is calculated diagnostically, which is a function of various moments of DSD (drop size distribution). In this study, N_d and LWC are used in the Vis parameterization; but N_d is replaced with MVD to emphasize that two microphysical parameters are sufficient to calculate Vis (Gultepe et al 2018). It is emphasized that either RH_w or T_a-T_d can ~~only~~ be used to indicate the existence of fog, but not intensity (e.g. Vis).

3.2.1 Vis-RH_w Parameterization

The visibility can be parameterized as a function of RH_w, which is measured by a Vaisala HMP 155. RH_w is measured together with T_a from which T_d is estimated. A PWD is used to obtain Vis measurements. The functional relationship between Vis and RH_w is determined by testing various regression fits and selecting the function that 'best' fits the observations. Here, humidity data used for the best fit are first bin averaged in 5% intervals. A derived relationship between Vis and RH_w together with a plot is provided in section 4.1.1 and given in Table 3. Note that we do not use T_a-T_d in the Vis parameterization because RH_w is based on both T_a and T_d (Gultepe and Milbrandt 2011). Therefore, fog coverage is obtained when $RH_w > 95\%$, which is further explained in the results section.

Formatted: Subscript

3.2.2 Vis versus Microphysics Parameters

Fog Vis can be obtained in two ways. The *first* is based on an extinction coefficient measured directly by a probe (e.g., PWD) which is then used to retrieve microphysical parameters assuming certain particle size distributions. The *second* is based on droplet spectral measurements from which LWC and N_d (or MVD) can be used to estimate Vis. Usually, direct measurement of Vis cannot be considered in the same way as those obtained from measured particle size spectra, because of measurement issues. Using warm fog microphysical spectral measurements, Gultepe et al (2006) developed a parameterization that is based on the theory of extinction of visible light in a volume of fog droplets as

$$\beta_{ext} = \sum_{r1}^{r2} \pi Q_{eff}(r,\lambda) n(r) r^2 \Delta r \,, \qquad (65)$$

where β_{ext} is the extinction coefficient (cm^{-1}), Q_{eff} the extinction efficiency, r droplet radius (µm), λ the visible light wavelength (µm), n(r) the particle number density (cm^{-3} μm^{-1}), and r^2 the droplet surface area. Q_{eff} is usually assumed to be 2, because size parameters ($k=2\pi r/\lambda$) are within the regions where geometric optics apply. For sizes less than about 5 µm, Q_{eff} can be larger than 2, significantly affecting the extinction of visible light. Equation 5 can be used for calculating β_{ext} if the particle size spectrum is known for each time step, when NWP model simulations exist.

The extinction coefficient (Eq. 65) can be converted into Vis using the Koschmieder (1924) relationship as

$$Vis = \frac{-ln(C)}{\beta_{ext}} . \quad (76)$$

For the meteorological observed range (MOR), C is defined as the threshold value that best fits to conditions whereby the human eye can recognize a target during daytime and is taken as 0.05 (Gultepe et al 2014). Using Eq. 5 and Eq. 6, the Vis can be obtained as

$$Vis = \frac{-(\frac{4}{3}) ln(\varepsilon) \rho_w \sum_{r1}^{r2} n(r) r^3 \Delta r}{Q_{ext} LWC \sum_{r1}^{r2} n(r) r^2 \Delta r} . \quad (87)$$

Then, Eq. 67 can be simplified as

$$Vis = 5.216 \frac{\rho_w r_{eff}}{Q_{ext} LWC} , \quad (89)$$

where ρ_w is the liquid water density ≈1000 kg m^{-3}. Vis can be obtained from Eq. 89 if the effective radius (r_{eff}) and LWC are known. Mist conditions (defined as Vis>1 km and RH_w<100%) can also be important for visibility reduction due to swelled aerosols (Fig. 6). A lower limit for mist is usually defined as RH_w~80%. Haze is composed of dry aerosols where RHw is isually <70%. Lower limit of haze Vis can be down to a few km.

Formatted: Subscript

Since N_d is inversely related to particle size (e.g. r_{eff}), as r_{eff} decreases N_d usually increases. Gultepe and Milbrandt (2007) replaced Eq. 98 with the approximate form

$$Vis = \alpha \left[\frac{\rho_w}{Q_{eff} N_d LWC} \right]^{\gamma} , \quad (109)$$

where α and γ are regression constants, and N_d and LWC are obtained from fog DSD, respectively, as

$$N_d = \sum_{r1}^{r2} n(r) \Delta r \quad (101)$$

and

$$LWC = \sum_{r1}^{r2} (\frac{4}{3}) \pi \rho_w n(r) r^3 \Delta r . \quad (121)$$

Assuming that $Q_{eff,}$ and ρ_w are constants, Eq. 109 can be rewritten as

$$Vis = \alpha (N_d LWC)^{-\gamma}, \quad (123)$$

which can be converted to β_{ext} using Eq. 76. For Eq. 132, α and γ are provided in Table 34. In NWP models, Vis is usually diagnosed with post processed model outputs for LWC, which is typically a prognostic output variable. If a numerical forecast model can resolve microphysical processes at small time and space scales, Vis can also be predicted diagnostically. This parameterization does not need droplet spectra at each time step that increases calculation time significantly.

Vis parameterizations may not include effective size (or MVD) because N_d is a function of MVD as follows

$$N_d = \left(\frac{1}{k}\right)\frac{LWC}{MVD^3} \qquad (14~~3~~)$$

where $k=(4/3)\pi\rho_w$. Moreover, replacing N_d in Eq. 1~~2~~3 with Eq. 14~~3~~, Vis can be rewritten as follows

$$Vis = \alpha\left(\left(\frac{1}{k}\right)\frac{LWC}{MVD^{3/2}}\right)^{-2\gamma} . \qquad (1~~4~~5)$$

This suggests that knowing MVD and LWC, Vis can be obtained prognostically from a NWP model simulation without requirement of N_d. Therefore, the 3rd parameter from a DSD may not be required.

4 Results

4.1 The 8 September Case (Battery Site)

4.1.1 Vis-RH_w Parameterization

Vis-RH_w parameterizations are usually derived for fog coverage but not fog intensity, which are obtained based on observations of Vis and RH_w, as well as T_a-T_d differences. RH_w close to 100% indicates the existence of fog layers but does not indicate intensity because of measurement uncertainty in T and T_d measurements and RH_w (Gultepe et al 2019). In fact, RH_w is obtained as a function of T_a and T_d so it is redundant to use both T_a-T_d and RH_w in the same parameterization (Gultepe and Milbrandt 2010; Benjamin et al 2010; Smirnova et al. 2000). Figure 6 shows Vis versus RH_w for 3 sites located in Ferryland, including Battery, Blackhead, and the Downs, for 28 Sep 2018. In this figure, fog (Vis<1 km), mist (2>Vis>1 km), and haze layers (Vis>2 km & RH_w<80%) as well as rain data points are shown. Differences among RHw values are likely related to location and elevation differences. A best fit for the equation for Vis versus RH_w using 5% RH_w bins is also shown in the figure 6 and given in Table 3.~~.~~

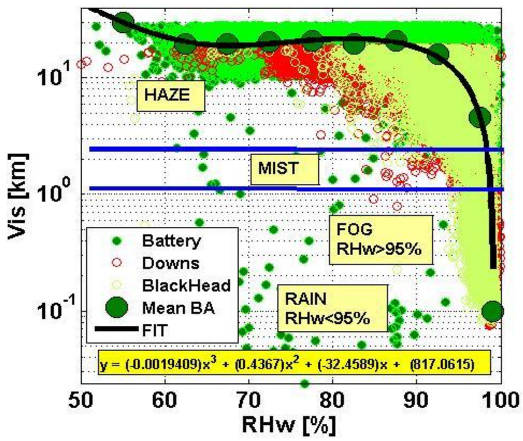

Fig. 6 Vis versus RH_w for NWS hydrometeor classification based on PWD instrument measurements at Battery, Blackhead, and Downs sites on 28 Sep 2018. The fit line is applied to bin averaged RH_w values at 5% intervals. The equation fitted is shown on the plot together with rain data points.

This figure suggests that Vis<1 km corresponds to RH_w>95%, which can be used as a criterion for detecting fog coverage but not intensity. Note that RH_w measurement accuracy is about 10% (Gultepe et al 2019). Haze and mist layers can occur when RH_w > 55% up to RH_w ~ 95% (Vis> 1 km). Rain with Vis <1 km occurs when RH_w < 95%. Evidently there is no clear distinction between mist and haze for Vis (>1 km). Another point is that Blackhead and The Downs had a larger RH_w compared to the Battery site, likely due to their higher elevations (30 m versus 2 m).

4.1.2 Time Series of Meteorological Parameters

Time series of Vis, PR, and precipitation types are shown in Fig. 7a based from PWD measurements at 1-min time resolution. Fog and mist are seen mainly in the early morning (segment 1; rectangular box) and later in the day (segment 2). Specifically, a drizzle and light rain event is clearly seen before segment 2, which likely played an important role for BL saturation. During fog events Vis was a few 100s of meters.

Fog formation and dissipation are likely related to the TKE magnitude and dissipation rate, which are related to the fluctuations of 3D wind components. The value for ε is calculated from Eq. 3 using 3D wind components and a 2D structure function (Eq.

4) and utilizing 1-min and 5-min running averages (Fig. 7b). The ε during fog is usually less than for fog free conditions (e.g. 0500 and 2000 UTC). The 3D wind components are shown in Fig. 7c. During fog events (see Vis time series in Fig. 7c), the magnitudes of 3D wind components are found to be significantly lower than for fog free conditions. The vertical air velocity (w_a) fluctuations were significantly smaller compared to u and v components for the entire day, indicating the importance of advection processes in the horizontal direction on the fog life cycle. Figure 7d shows 1-minute averaged local accelerations of u, v, and w_a, indicating that the turbulence intensity levels were almost 50% less compared to fog-free segments.

Results suggest that ε is about $3x10^{-4}$ m^2 s^{-3} in foggy segments compared to $>1x10^{-3}$ m^2 s^{-3} in fog-free conditions, which can be used as a criterion for fog formation and dissipation. These values are found to be comparable to those of The Downs site (Grachev et al. 2020) who showed that during foggy conditions ε_{dis} was between $1x10^{-3}$ m^2 s^{-3} and $1x10^{-4}$ m^2 s^{-3}. Some differences between their work and current work is that The Downs site at 30 m likely had stronger wind fluctuations compared to current one at sea level. Another reason may arise due to their use of TKE based on averages done over 15 mins.

4.1.3 Vis parameterization and microphysical parameters

To develop a Vis parameterization, fog microphysical parameters such as N_d, MVD, and LWC are needed because Vis is defined in terms of these parameters. Microphysical parameters are calculated from the FM120 measurements from the Battery site. Figure 8a shows a time series of N_d as a function of LWC, where N_d increases with increasing LWC. N_d time series as a function of log(Vis) is shown in Fig. 8b where log(Vis) ≤ 0 indicates fog conditions. Vis decreases with increasing N_d. These figures suggest that Vis is related to both N_d and LWC (Gultepe et al 2006). Figure 8c shows MVD versus N_d as a function of LWC (color bar) together with theoretical lines obtained from Eq. 13. The lines ranging from bottom to top in Fig. 8c represent values for LWC = 0.001:0.01:0.1 g m^{-3} with solid lines, and LWC = 0.1:0.05:0.3 g m^{-3} with dashed lines with theoretical lines calculated using Eq. 13 (c). Clearly MVD is a function of N_d, and decreases with increasing N_d while LWC increases. This suggests that Vis can be obtained as a function of either N_d and LWC or MVD and LWC. Figure 8d shows the fit equation for Vis = f(LWC, N_d) overlaid on observations, where mean values at dx intervals along x axis and percentile values are also shown. This equation is obtained from the measurements at Battery and represents local coastal fog conditions.

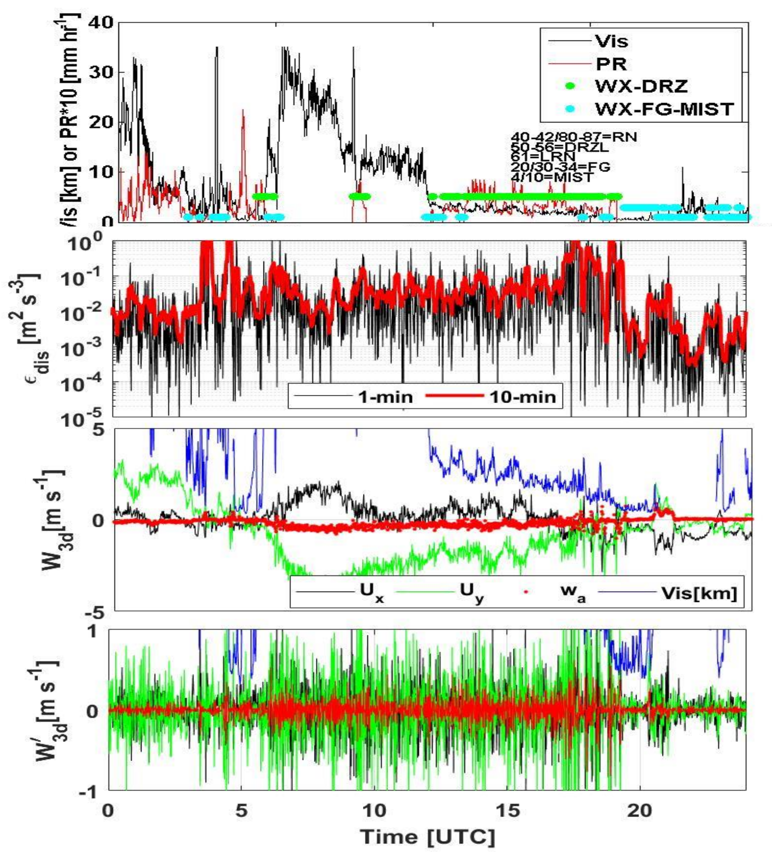

Fig. 7 Vis, PR, and NWS hydrometeor code time series on 28 Sep 2018 for Battery site (a) with fog regions shown with light blue data points, ε_{dis} (turbulence TKE dissipation rate) time series for 1-min and 5-min running averages are shown in (b), 1-min averaged 3D wind components of u_x, v_y, and w_a as well as Vis time series (purple line) are shown in (c) with fog regions indicated as blue colored horizontal bars, and (c), and acceleration terms du/dt (black line), dv/dt (green line), and dw/dt (red line) with dt=60 s and Vis time

series (blue line) are shown in (d). Note that during fog conditions these wind speed changes become comparable low versus fog free conditions.

4.2 The 29 September case (Battery site)

4.2.1 Time Series of Meteorological Parameters

Time series of Vis, PR, and precipitation types are shown in Fig. 9a, similar to the 28 Sep case, representing PWD measurements at 1-min sampling rate. Fog and mist are seen mainly between 0000 UTC and 1200 UTC early morning (segment 1) and mist and drizzle mainly later in the day (segment 2; 1300-0000 UTC). A drizzle event is seen during segment 2. During fog segment 1, Vis is a few hundred meters.

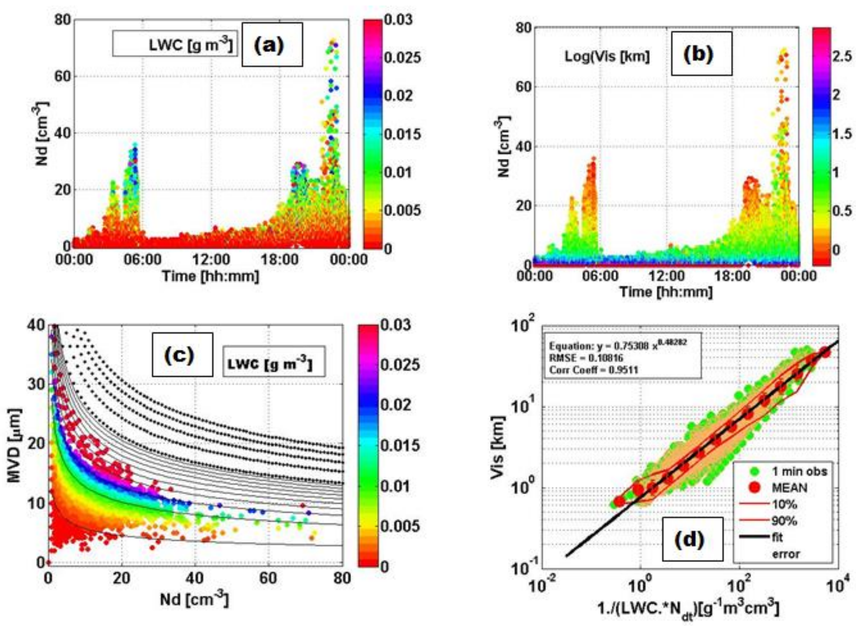

Fig. 8 Time series of N_d colored by LWC (a), N_d colored by log(Vis) (b), and MVD versus N_d with points colored by LWC (LWC=0.001:0.01:0.1 solid lines and LWC=0.1:0.05:0.3 dashed lines) (c) with theoretical lines calculated from Eq. 13. Vis parameterization as a function of fog index (FI along x axis) with statistical parameters and fit equation overlaid on observations are shown in (d) for 28 Sep 2018.

The calculation for ε is similar to the 28 Sep case, utilizing 1-min and 5-min running averages (Fig. 9b). The values for ε are found to fluctuate more during the foggy segment 1 (0000-1000 UTC), than segment 2 (1400-2300 UTC) fog and misty conditions. The values for ε change between $1x10^{-2}$ m^2 s^{-3} and $1x10^{-7}$ m^2 s^{-3} during the foggy segment 1, where u_y is highly variable between +1 and -1 m s^{-1} (Fig. 9c and 9d). Overall, ε_{dis} is less than 10^{-5} m^2 s^{-3} for both fog segments. Figure 9d shows 3D wind components and Vis, where stronger wind fluctuations likely play an important role, leading to increasing Vis values during segment 2 (light fog).

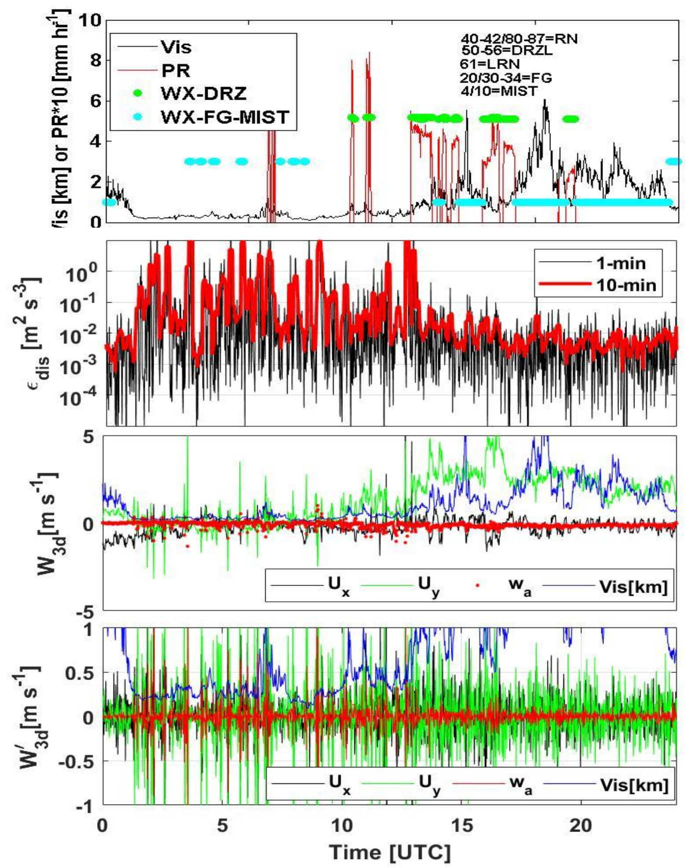

638

Fig. 9 Vis, PR, and NWS hydrometeor code time series on 29 Sep 2018 for Battery site (a) with fog regions shown with light blue data points, ε_{dis} (TKE dissipation rate) time series for _1 min and 5 min running averages are shown in (b), 1-min averaged 3D wind components of u, v, and w_a as well as Vis time series are shown in (c) with fog regions indicated as blue colored horizontal bars, and (c), and acceleration terms du/dt (black line), dv/dt (green line), and dw/dt (red line) with dt=60 s and Vis time series (blue line) are shown in (d). Note that during fog conditions these wind speed changes become comparable low versus fog free conditions.

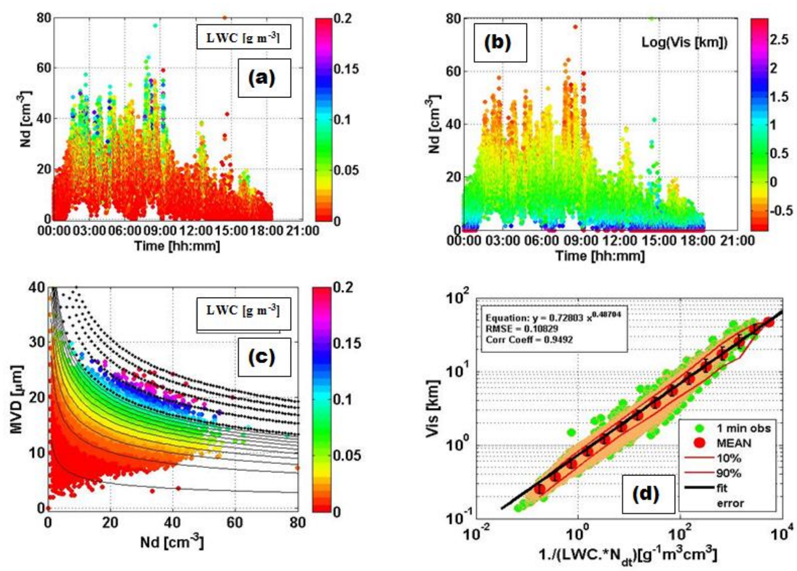

Fig. 10 Time series of microphysical parameters N_d versus LWC (a), N_d versus log(Vis) (b), and MVD versus N_d as a function of LWC (c) with theoretical lines calculated from Eq. 13. Vis parameterization as a function of fog index (FI along x axis) with statistical parameters and fit equation overly on observations are shown in (d) for 04 October 2018.

In summary, most of the ε data points are found below the dissipation rate of $3x10^{-5}$ m^2 s^{-3} during fog segments. The w_a fluctuations in segment 1 are smaller compared to drizzle and fog conditions seen in segment 2. Note that wetting of the sonic anemometer transmitter/receiver may occasionally cause large fluctuations of wind components during heavy fog conditions. Results suggest that, based on 1-min averages, minimum (max) ε is about $1x10^{-6}$ m^2 s^{-3} ($3x10^{-2}$ m^2 s^{-3}) in foggy segment 1, compared to $3x10^{-5}$ m^2 s^{-3} during mist and drizzle conditions (segment 2). Another point is that southerly wind fluctuations (wind coming from south) are likely responsible for warm and moist advection over the region, leading to fog formation similar to 28 Sep case.

4.2.2 Vis parameterization and microphysical parameters

Results and parameterizations for this case are obtained similar to that of 28 Sep case (Fig. 10). MVD and N_d are found to be comparatively larger on this day (Fig. 10a,b,c). For example, the maximum MVD reaches 40 µm compared to 30 µm on 28 Sep. The maximum N_d is about 60 cm^{-3} compared to a maximum for N_d of 70 cm^{-3} on 28 Sep. Finally, the Vis fit equation is shown in Fig. 10d. Overall, the slope of the best fit line is very similar to the 28 Sep case but with relatively lower values of observed Vis.

4.3 The 28 September Case (RV Sharp)

4.3.1 Time Series of Vis and RV Wind Components

Time series of *R/V Sharp*'s navigation parameters obtained from the VectorNav VN100 IMU and Trimble BX982 Dual GNSS receiver (Fernando et al 2020) are reported here at 1-min intervals (Fig. 11a). This figure shows the *R/V Sharp's* speed with respect to the ground (U_{RV}), true wind speed (U_{hT}), wind speed with respect to ground (U_{hR}) and smoothed values of U_{hR} over 10 mins intervals. During the fog event between 1000 UTC and 1600 UTC, the *R/V Sharp* was heading 250 deg (SW) until 1300 UTC, then changed to 50 deg NE with U_{RV} at about 5-8 m s^{-1}. Low Vis was observed between 1000 UTC and 1600 UTC, during which Vis improved from 1 km to 5 km after *R/V Sharp* changed direction. After 1600 UTC, Vis increased up to 15 km. Low Vis and haze conditions (Fig. 11b) before 1000 UTC likely played an important role later on for drizzle conditions after 1000 UTC. Thereafter, drizzle just before fog formation likely led to moistening of the BL and resulted in fog occurrence at about 1200 UTC.

Formatted: Left

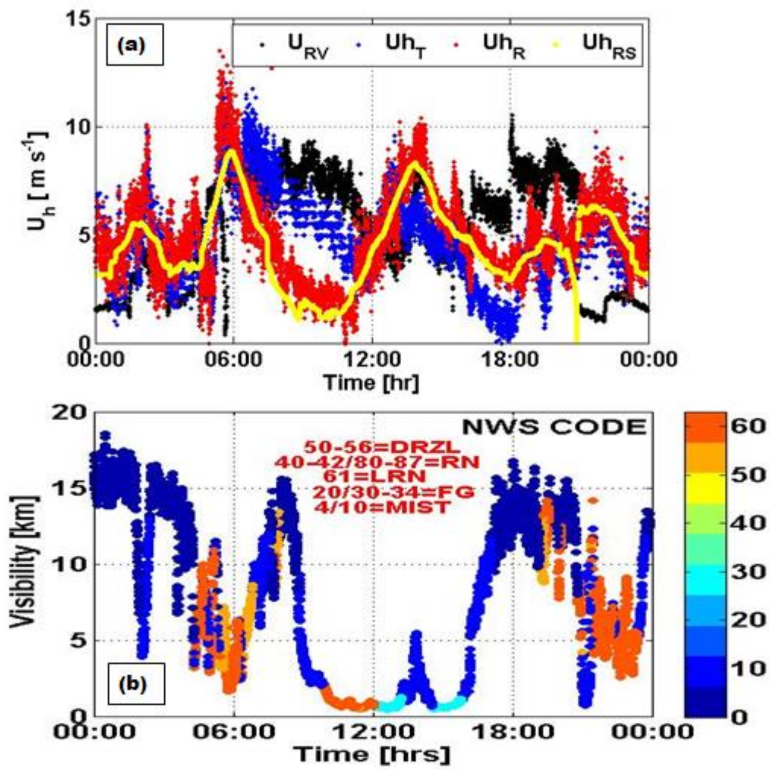

Fig. 11 Time series of U_{RV}, U_{hT}, U_{hR}, and U_{hRS} for 1 min and 10 min running averages are shown in (a) and Vis, PR, and NWS hydrometeor code time series on 28 Sep 2018 (b) with fog regions shown with light blue data points.

4.3.2Vis parameterization and microphysical parameters from the gondola

In this subsection, fog droplet spectral characteristics obtained from the CDP and BCP housed in the gondola (Fig. 2) are investigated. Both CDP and BCP plots were obtained similar to the Battery plots. Note that BCP (Fig. 12) measurement starts at 5 µm compared to CDP at 2 µm (Fig. 13) and had the capability for measurements up to 75 µm. Measurements of N_d, MVD, and LWC are less than 60 cm^{-3}, 40 µm, and 40 cm^{-3}, respectively. A parameterization is obtained with a power-law form similar to Eq. 12 and is shown in the figure. The best fit line indicates that increasing fog index (FI

=1/(LWC*N_d)) results in increasing Vis, which is found to be similar to the fit line obtained for the Battery site. FI increases with increasing values of either N_d or LWC. Note that N_d can be replaced with MVD using Eq. 14.

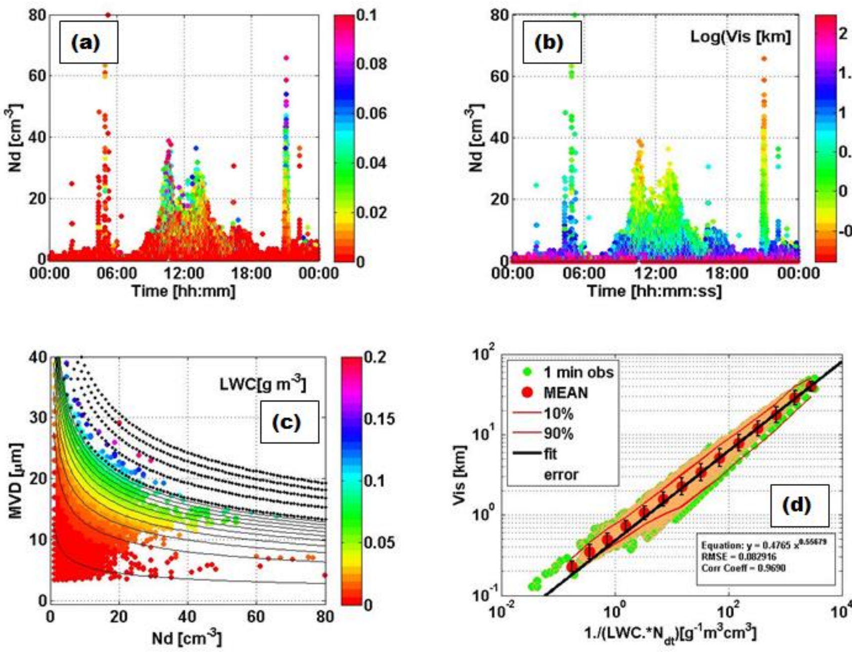

Fig. 12 Time series of microphysical parameters N_d versus LWC (a), N_d versus log(Vis) (b), and MVD versus N_d as a function of LWC (c) with theoretical lines calculated from Eq. 13. Vis parameterization as a function of fog index (FI along x axis) with statistical parameters and fit equation overly on observations are shown in (d) for RV CDP on 28 Sep 2018.

Fog-droplet spectral characteristics obtained from the BCP measurements are shown in Fig. 13. Note that because of missing the first 2 channels in BCP compared to CDP, N_d, LWC, and MVD cannot have the same values for both probes. N_d and LWC are based on BCP measurements and therefore, are expected to be less; but MVD is higher than CDP parameters. Results suggest that max values for N_d are about 15 cm^{-3}, for LWC about 0.07-0.08 g m^{-3}, and for MVD~60 μm.

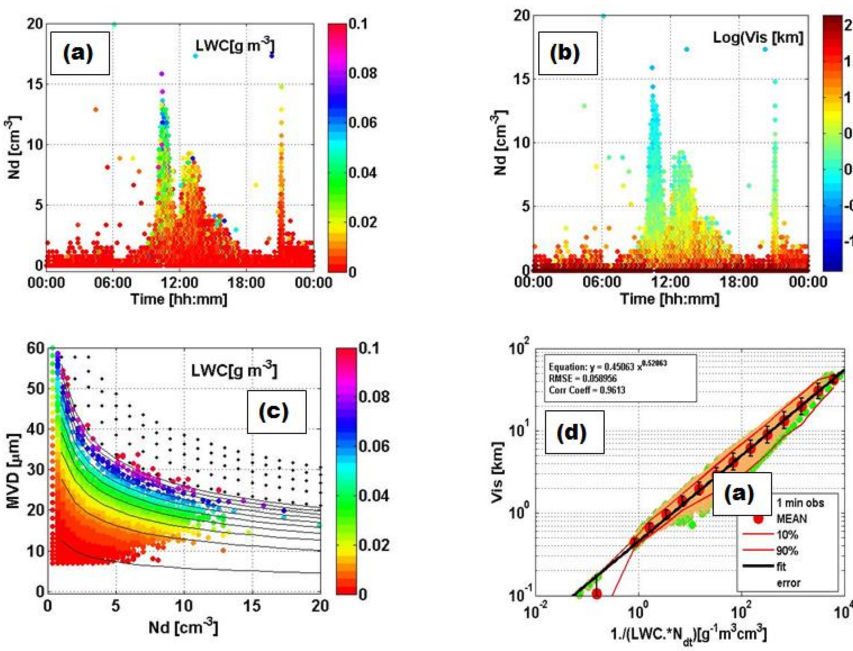

Fig. 13 Time series of microphysical parameters N_d versus LWC (a), N_d versus log(Vis) (b), and MVD versus N_d as a function of LWC (c) with theoretical lines calculated from Eq. 13. Vis parameterization as a function of fog index (FI along x axis) with statistical parameters and fit equation overly on observations are shown in (d) for RV BCP on 28 Sep 2018.

4.4 The 4 October Case (*RV Sharp*)

4.4.1 Time Series of Vis and RV Wind Components

Time series of *R/V Sharp's* navigation parameters are given in Fig. 14a. This figure also shows U_{RV}, U_{hT}, U_{hR}, and smoothed values of U_{hR} over 10-minute intervals. Fog occurred between 1900 and 2300 UTC. Before the fog event at 1900 UTC, the ship was headed 250 deg (SW), and U_{RV} changed from about 4 m s^{-1} to 8 m s^{-1}. U_{hR} was from north during the fog event (not shown). Low Vis (1 km) was observed between 1900 and 2300 UTC and Vis improved to 5 km at 2300 UTC. Before 1900 UTC, Vis increased to 15-20 km. Thereafter, the cloud base lowered to the surface and Vis decreased to <300 m. During low Vis conditions (Fig. 14b) near the end of fog event, drizzle was observed around 2300 UTC. After 1930 UTC, Vis improved significantly.

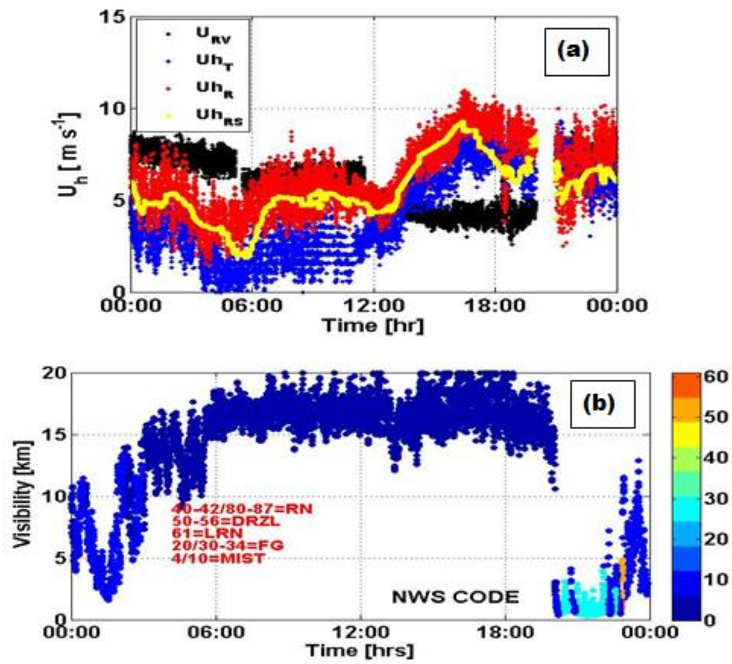

Fig. 14 Time series of U_{RV}, U_{hT}, U_{hR}, and U_{hRS} for 1 min and 10 min running averages are shown in (a) and Vis, PR, and NWS hydrometeor code time series on 28 Sep 2018 (b) with fog regions shown with light blue data points.

4.4.2 Vis Parameterization and Microphysical Parameters from the Gondola

Fog droplet spectral characteristics obtained from the CDP and BCP during the 29 Oct case are shown in Fig. 15 and Fig. 16, respectively. Note that max CDP N_d (Fig. 15a,b) is about 75 cm^{-3} and LWC reaches 0.4 g m^{-3}. Low Vis, representing fog conditions, is found between 2000 and 2200 UTC. MVD (Fig. 16c) ranged from a few µm up to 40 µm at low LWC and N_d but was at about 22 µm when N_d reached a maximum at 70 cm^{-3}. CDP measurements of MVD and LWC were less than 40 µm and 0.45 g m^{-3}, respectively. The parameterization obtained based on CDP measurements are shown in

Fig. 16d. Similar to previous cases, Vis also increases with increasing values of fog index (FI = 1/(LWC*N_d) but decreases with increasing LWC and N_d (with decreasing MVD). The best fit line indicates that increasing FI values result in similar increasing Vis conditions that represent the Battery site.

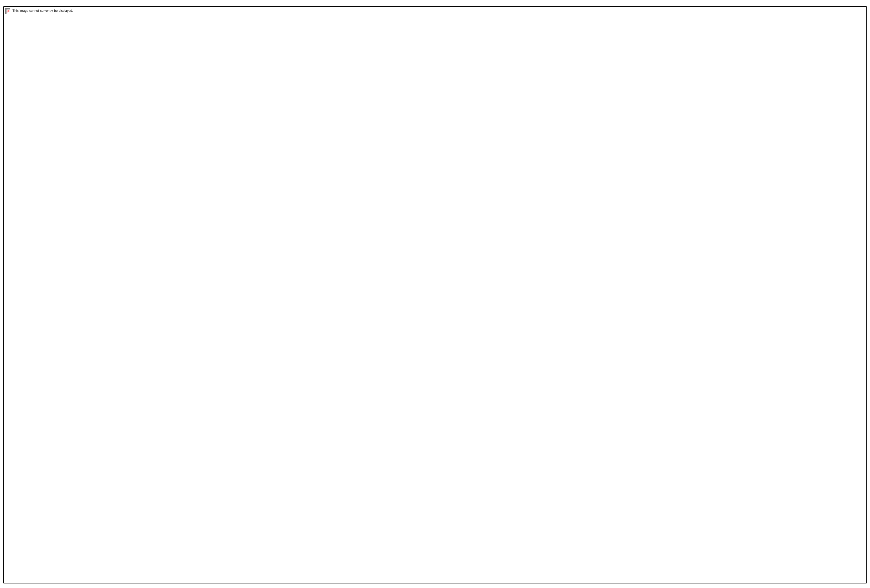

Fig. 15 Time series of microphysical parameters N_d versus LWC (a), N_d versus log(Vis) (b), and MVD versus N_d as a function of LWC (c) with theoretical lines calculated from Eq. 13. Vis parameterization as a function of fog index (FI along x axis) with statistical parameters and fit equation overly on observations are shown in (d) for RV CDP on 04 October 2018.

Fog droplet spectral characteristics based on BCP are shown in Fig. 16. Again, due to missing the first 2 channels of CDP in BCP measurements, CDP, N_d, LWC, and MVD cannot be directly compared to those of CDP measurements. As suggested previously, if there is no drizzle, N_d and LWC based on BCP measurements are expected to be less compared to CDP parameters; but MVD is expected to be higher because of larger droplets. Results suggest that max N_d was about 25 cm^{-3}, LWC about 0.4 g m^{-3}, and MVD~40 μm. The parameterization for this case based on BCP measurements is shown in Fig. 16d. Similar to previous cases, Vis increases with increasing FI.

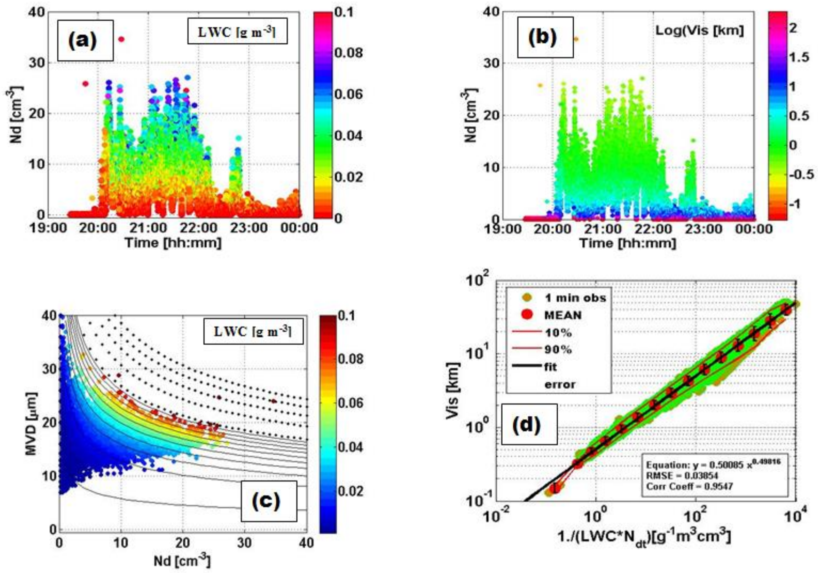

Fig. 16 Time series of microphysical parameters N_d versus LWC (a), N_d versus log(Vis) (b), and MVD versus N_d as a function of LWC (c) with theoretical lines calculated from Eq. 13. Vis parameterization as a function of fog index (FI along x axis) with statistical parameters and fit equation overly on observations are shown in (d) for RV BCP on 04 October 2018.

4.5 Summary of Vis Parameterizations

Vis parameterizations are obtained for each platform (*R/V Sharp* or Battery supersite) using FM100, CDP, and BCP probes and are summarized in Table ~~3~~4. The Vis-RH_w relationships are also provided to emphasize that they are used only as a threshold for fog formation (e.g. RH_w>95% in Fig. 6). Then, fog intensity (e.g. Vis) can be estimated based on model-predicted values for LWC and N_d (or MVD) (see Eq. 14). Note that the G2007 parameterization (Gultepe et al 2007) was obtained using FSSP measurements based on low-level flying aircraft observations over the Bay of Fundy, NS taken during the RACE (Regional Aerosol and Cloud Experiment) campaign. These parameterizations are discussed in the next section.

Table ~~3~~4 Summary of C-FOG Vis parameterizations and previous work. The FI (fog index) is defined as $1/(LWC \bullet N_{dt})$ with units of [$g^{-1}\ m^3\ cm^3$].

Case	Parameterization	FMD	Platform location
28 Sep - Battery	$Vis=0.7531(FI)^{0.4828}$	FM100	Ground-C-FOG
29 Sep - Battery	$Vis=0.7280(FI)^{0.4871}$	FM100	Ground-C-FOG
28 Sep -RV	$Vis=0.4765(FI)^{0.5568}$	CDP	Sharp RV-C-FOG
28 Sep -RV	$Vis=0.4506(FI)^{0.5206}$	BCP	Sharp RV-C-FOG
04 Oct -RV	$Vis=0.4012(FI)^{0.5455}$	CDP	Sharp RV-C-FOG
04 Oct -RV	$Vis=0.5009(FI)^{0.4982}$	BCP	Sharp RV-C-FOG
28 Sep - Battery	$Vis=-0.009RH^3+0.437RH^2 -2.459RH+817.062$	PWD	Ground-C-FOG
Gultepe et al 2007	$Vis=1.002(FI)^{0.6473}$	FSSP	Aircraft Obs. RACE

5 Discussion

5.1 Overview of Fog Forecasting

Fog prediction cannot be done accurately because of rapid changes in its intensity (Vis) over short time and space scales, as well as non-linear relationships between surface and atmospheric conditions. There are several methods for fog prediction. These methods include rule–based techniques (Toth et al 2007, Zhou and Du 2010), statistical methods (Claxton 2008, Miao et al 2012), numerical forecast models (Gultepe and Milbrandt 2010; Bott et al. 1990; Muller et al. 2007, 2010; Bott and Trautmann 2002; Clark et al. 2008; Shi et al. 2012) and integrated nowcasting methods (Golding, 1993; Golden, 1998; Wright and Thomas, 1998; Haiden et al 2014). If no persistence exists and turbulence becomes more dominant, prediction usually fails, unless very short-term data assimilation techniques are performed. More detailed information on fog modeling issues can be found in the works of Gultepe et al (2007a), Wilfried et al (2008), Croft et al (1997) and Fernando et al. (2020).

5.2 NWP and Microphysical Schemes

Prognostic fog forecasting is usually done using model-based prediction of LWC and N_d, and that uses detailed droplet nucleation processes described above. In general, a regional forecast model uses boundary conditions from a global model. As described in Section 1, assuming a gamma size distribution, visibility can be diagnosed from the size distribution parameters such as N_o (intercept parameter), μ (spectral shape parameter), and λ (slope parameter), or either N_{dt} or LWC or both (Gultepe and Milbrandt 2007b, Milbrandt and Yau 2005a,b). If both LWC and N_d are available as prognostic variables, Vis estimation can be obtained using NWP simulations.

Microphysical schemes are used to evaluate fog prediction conditions using NWP models. Cloud-droplet and fog-droplet size distributions are usually represented by a modified-gamma size distribution in NWP models. The parameters used in a modified gamma size distribution are the N_t (total droplet number concentration), and shape and slope parameters. N_t is obtained either from empirical relationships as a function of aerosol number concentrations (N_a) or from a prognostic equation for N_d with assumed size distribution parameters. The microphysical schemes (MPS) such as MY (Milbrandt and Yau 2005a,b), MG (Morrison and Gettelman 2008), and TO (Thompson et al. 2008, 2014) use modified-gamma size distributions and microphysical parameters based on DSD parameters.

The N_d can be obtained directly from N_a diagnostically, as stated, or based on S_w (supersaturation) which is function of vertical air velocity (w_a) and N_a as well as its composition (Twomey 1959; Chen 1994; Kohler 1934). The Kohler curve provides a general equilibrium relationship between an aqueous salt solution droplet size and water vapor. S_w can be calculated as a function of both w_a and N_d and that is directly related to size distribution and the composition and mixing state of aerosols. A similar relationship to Twomey (1959) is also suggested by Ghan et al. (1993, 1997) for large-scale cloud formation. Cohard et al. (1998) extended Twomey's power law expression by using a more realistic four parameter CCN activation spectrum with physiochemical properties of aerosols. The most important parameter to estimate N_d is S_w that is obtained using 3 methods (Schwenkel and Maronga 2019): 1) saturation adjustment scheme, 2) diagnostic scheme where S_w is diagnosed by the prognostic fields of T and q_v, and 3) a prognostic method (Clark 1973; Morrison and Grabowski 2007; Lebo et al. 2012). These methods are not discussed here, but are listed to emphasize the importance of w_a, CCN, and N_d on S_w.

In microphysical schemes, N_d is usually represented with a complete gamma size distribution function as

$$N_d(D) = N_o D^{\mu} e^{-\lambda D},$$ (1~~5~~6)

where D is the diameter, and N_o, μ, and λ_s should also be known to obtain an accurate droplet spectra. The μ parameter is obtained as a function of CCN (Wilkinson et al., 2013) or as $\mu = 1/\eta^2$ *-1* with η the dispersion of radius (sd/mean), which is given by Morrison and Gettelman (2008) as

$$\eta = 0.0005714 N_d + 0.2714,$$ (1~~6~~7)

where N_d can be obtained as a function of aerosol number concentration (N_a) (Jones et al. 1994; Martin et al. 1994; Gultepe and Isaac, 1999; Gultepe et al. 2015). But N_d versus N_a relationships are not unique, and their variability can be large. In Eq. 15, N_o and λ are usually obtained using a fixed μ and predicted value of total droplet number concentration (N_{dt}) and water vapor mixing ratio (q_w) as

$$\lambda_s = \left[\frac{\pi \rho_w N_{dt} \Gamma(\mu+4)}{6 q_w \Gamma(\mu+1)}\right]^{1/3}$$ (1~~7~~8)

and

$$N_{o=} \frac{N_{dt} \lambda^{\mu+1}}{\Gamma(\mu+1)}.$$ (1~~8~~9)

When models use a single-moment scheme, q_w (e.g. LWC) is predicted but N_{dt} and μ are fixed. In double-moment schemes, usually both q_w and N_{dt} are prognostic variables. N_d prediction is an important step in NWP models for accurate fog Vis estimation.

In the MPS, CCN concentration is assumed to be a function of S_w, and N_a for the ocean (N_{aO}) and land (N_{aL}) air masses set as fixed values. The values for CCN concentration as a function of supersaturation are also given in Fletcher (1966). The CCN parameterization, given as CCN=cS_w^k~~Sk~~ where c~1000 cm^{-3} and k~1 (a unitless constant), are for continental air masses and ~100 cm^{-3} and ~0.5 for maritime air masses (Feingold et al 1998). Sometimes, N_d is fixed as 100 cm^{-3} over ocean and 300 cm^{-3} over land (Wilkinson et al 2013). In reality, as stated in Cohard et al. (1998), the coefficients c and k change with high S_w. *They suggested that this happens especially in maritime environments*. Therefore, c and k should be matched locally to the activated CN. This

Formatted: Not Superscript/ Subscript suggests that parameterization of S_w and both c and k are critical to improve fog Vis predictions

5.3 Scale Issues

Fog usually happens over small areas and dissipates quickly; therefore, NWP models can have difficulty predicting short lived fog conditions. Although fog models can resolve the smaller scales, most of the physics developed for the NWP model cannot be used for high resolution fog models. Due to cloud coverage over the large scales (1-100 km), some dry air pockets result in lower values of RH_w, LWC, and N_d (Gultepe and Isaac, 1999; 2004) and these need to be extrapolated to fog occurrence scales (usually less than 1 km) (Wilkinson et al 2013). The latter study clearly recognizes the issues for better fog prediction on various grid areas. This suggests that further improvement of fog microphysical parameterizations is required for better fog prediction.

5.4 Variability in Vis

Visibility calculation based on observations and NWP model outputs may include large uncertainties due to fog microphysical and BL processes. Variability in Vis based on measurements of PWD located at Battery, Downs, Blackhead, and Judges Hill sites for 28-29 Sep is shown in Fig. 17. Figure 17a shows mean Vis from all these sites with a standard deviation. Overall, Vis at Judges Hill had the lowest values compared to the other stations, likely due to its elevation of 129 m (Fig. 17b). The second lowest Vis values are found at The Downs site, at 32 m above sea level. Blackhead and Battery Vis follow, with the next highest values. During dense fog conditions, Vis from Blackhead was much higher than others, likely due to the distance between the Blackhead and Ferryland sites. Vis, representing a scale of about 1.5 km, ranged from 0.2 km up to 1 km for any given time (Fig. 17); therefore, NWPs should be capable of simulating fog conditions at 1 min time intervals and 100 m spatial scales.

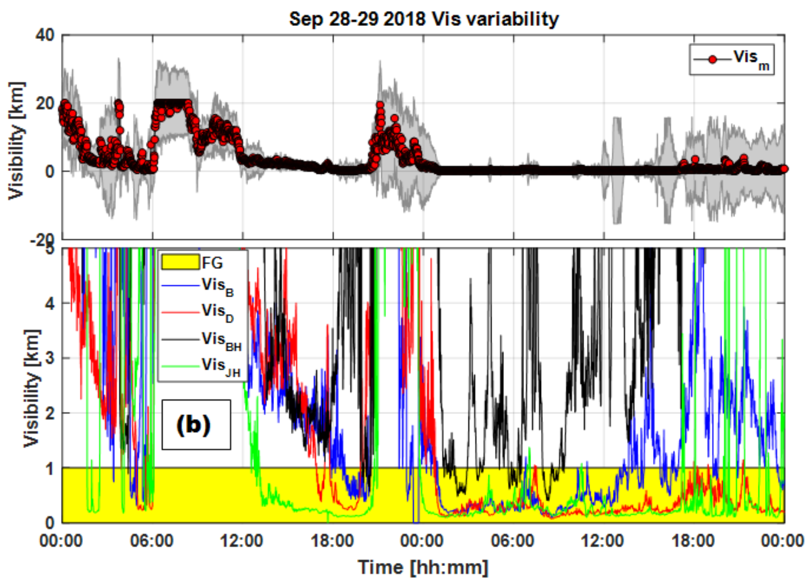

Fig. 17 Time series of mean– (red filled circles) and sd (gray colored regions) of Vis based on measurements of PWDs (indicated in (b)) are shown in (a). Time series of Vis representing Battery (Vis_B), Downs (Vis_D), Blackhead (Vis_{BH}), and Jack Hill (Vis_{JH}) for 28-29 Sep 2018 are shown in (b). Fog regions are shown for Vis<1 km (yellow colored area).

5.5 Variability in sonic anemometer wind components

The 3-D wind component time series of mean and sd obtained from the (20Hz) measurements of sonic anemometers located at 1, 2, 5, 8, and 15 m levels of the Battery supersite tower are shown in Fig. 18a for 28-29 Sep cases. Figure 18b shows 3D wind components and Vis from each of the 5 levels. The U_{3d} values (3-D wind speed) between 0600-1200 UTC indicate some noise in the data and should be ignored because of heavy condensation on the prongs of the sonic anemometers. The largest U_{3d} fluctuations are seen at 5, 8, and 15 m levels but these were reduced to lower values during fog events on May 28 (Fig. 18b). Vertical air velocities (w_a) in Fig. 18c are obtained at the same levels as in Fig. 18b. Figure 18c shows the mean and standard deviation of w_a obtained from measurements, representing all levels from 1 m up to 15 m. Clearly, w_a fluctuations were higher in the fog-free layers compared to foggy layers, indicating greater turbulent heat, moisture and momentum fluxes in the vertical direction. Note that large fluctuations of

w_a at 15 m from 0600 to 1200 UTC in Fig. 18d were likely noise, as noted previously. The w_a fluctuations within the fog layers were found generally between +0.3 and -0.3 m s^{-1}, but were more than -0.7 m s^{-1} and +0.7 m s^{-1} in fog-free layers. These suggest that without estimating 3D wind fluctuations accurately, NWP models cannot properly handle the fog life cycle.

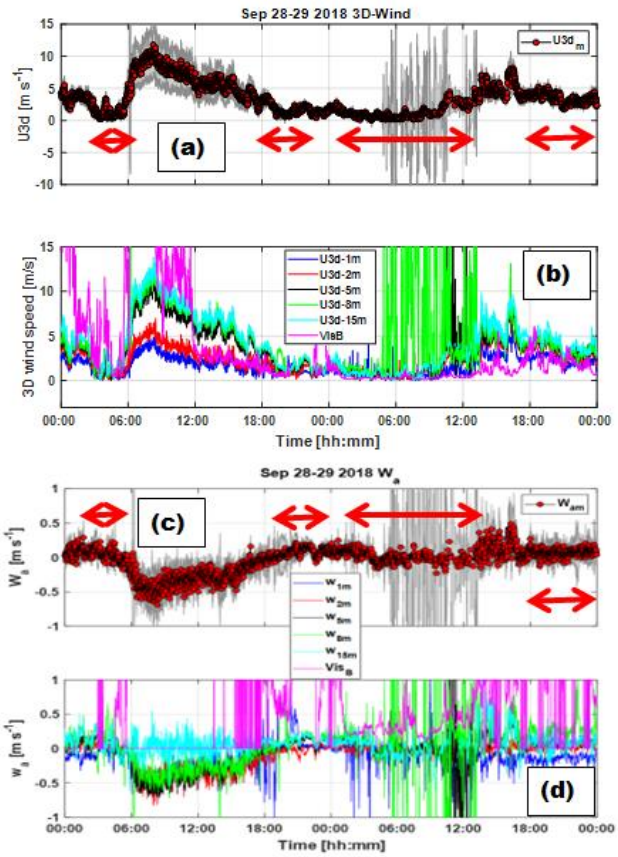

Fig. 18 Wind components obtained from the sonic anemometers located at 1, 2, 5, 8, and 15 meters levels of a tower and Vis at 2 m (purple line) are shown in (a) for mean and sd of U_{3d} (3D wind component) and in (b) for U_{3d} for each level, representing 28-29 Sep cases at the Battery supersite. Mean (red filled circles) and sd (gray lines) of vertical air velocity (w_a) are shown in (c) and w_a measurements at each level are shown in (d). Fog layers indicated by red double arrow are obtained from PWD Vis shown in (d) and previous plots.

5.5 N_d Uncertainty and Droplet Spectra

Droplet spectra from CDP, BCP, and FM120 probes include uncertainties related to the calculations of TAS, turbulence, wind speed and ship direction. The aspirator used in FM100 pulls in air at about 5 m s^{-1} but winds coming directly into the inlet can increase (or decrease) the aspirator wind speed. Usually, using a higher TAS compared to a fixed TAS at 5 m s^{-1} set up in FM120 results in a significant decrease (~50-100%) in N_d. For ship measurements, these errors can be much larger. For example, a ship heading north (0 degrees) at 8 m s^{-1} plus a wind from NE can result in

$$TAS = U_{RV} + U_h cos\theta. \quad (20~~19~~)$$

Therefore, the error in TAS estimation, applying a derivative of TAS with respect to time, can be written as

$$\varepsilon_{TAS} = \frac{dTAS}{dt} = \frac{dU_{RV}}{dt} + U_h \frac{dcos\theta}{dt} + cos\theta \frac{dU_h}{dt}. \quad (21~~0~~)$$

The l.h.s of Eq. 20, ε_{TAS} represents an error in TAS per unit time [(m s^{-1})/s]. Assuming that error in the first term of the r.h.s of Eq. 20 is approximately 1 m s^{-1} per unit time (e.g., dt=1 s) at U_{RV}=8 m s^{-1}, and U_h has an error of 10% say at 0.5 m s^{-1} and wind directional error is about 10 degrees (second term on the rhs), then using U_h=10 m s^{-1}, ε_{TAS}=1 m s^{-1}+ 10 m s^{-1}* (cos30-cos40) +cos(30)*0.5 m s^{-1}=1.0+1.0+0.43=2.43 m s^{-1}. Absolute error in TAS~18 m s^{-1} can then be calculated at about 15%. This means that N_d uncertainty is also about 15%, but likely increases with decreasing TAS. Following works can be suggested for further evaluation of errors related to TAS calculations; Moffat (1982) and Kline and McClintock (1953).

Figure 19 shows fog droplet spectra obtained from the CDP and BCP probes for Sep 28 (a and b) and Oct 04 (c and d) cases. The mean (black line) and standard deviation (red line) of each bin during fog events of Sep 28 and Oct 4 are shown. Each colored line represents 1 s spectra. Clearly, Sep 28 droplet spectrum is much different from the Oct 04 droplet spectra, based on both probes. Multi-modes in DSD indicate the various fog regimes that were likely related to droplet fall velocities (V_f) and w_a. For both cases, DSD did not indicate drizzle droplet sizes > 50 μm. MVD for the Oct 04 was much larger than for the Sep 28 case. Note that the mean DSD can shift upward if a lower threshold of N_d is chosen to have a higher value (e.g. 1 # cm^{-3} instead of 0.1 # $cm^{-3)}$. In BCP measurements, having a large value for N_d at about 25 μm, may indicate some cooling processes leading to increasing values for N_d.

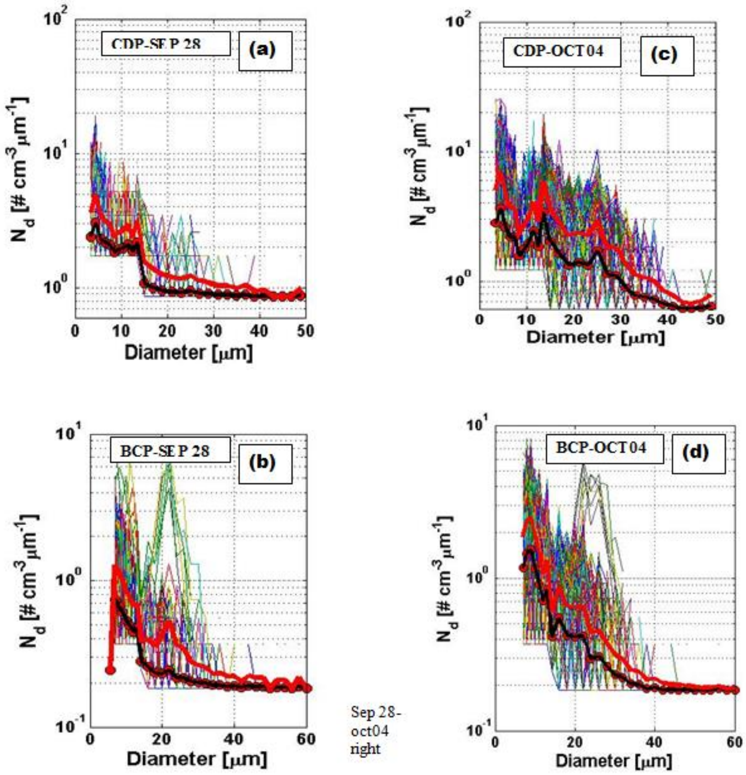

Fig. 19 F~~shows f~~og droplet spectra obtained from CDP and BCP probes for 28 Sep (a and b) and Oct 04 (c and d) cases. The mean (black line) and sd (red line) values of each bin during time periods representing fog events of 28 Sep and 4 Oct 2018 are also shown on the plots. Each line with a color represents 1 s spectra.

Sea spray particles can also affect N_d spectra (at 10m) significantly because of breaking waves, especially at small size ranges because of their low settling rates. In the marine environment, droplets can be generated by wave breaking processes, which can then be counted as fog droplets. Entrainment of air at breaking wave crests leads to the formation of a large number of bubbles, which emerge at the ocean surface because of their positive buoyancy and then burst into droplets at the water surface (Troitskaya et al 2018). The spray production due to the bursting of bubbles with sizes smaller than <10 µm has been studied by Blanchard (1963) and Spiel (1995, 1997, 1998). All of these studies suggest that bursting bubbles are the main source of the ocean spray process, generating droplets with radii less than 50 µm (Wu, 1981).

5.6 Impact of TKE Dissipation Rate on Vis

Fog occurs usually at the end of a dynamically unstable environment along coastlines and marine environments and is augmented sometimes by thermal inversions, keeping moisture trapped below a stable layer. Thereafter, when the mature fog stage has developed under dynamically stable conditions, fog dissipates as a result of droplet growth, increasing turbulence, entrainment, and solar heating. All these factors play an important role for fog dissipation without considering direct impact of a larger scale event such as pressure systems and associated fronts systems. In this work, calculated dissipation rates suggest that higher ε values result in improved Vis conditions. Accuracy of ε will not be discussed here, except in its usage in a fog prediction scheme. TKE dissipation rate is calculated in NWP models using TKE based on various turbulence prediction schemes (Mellor and Yamada 1982; Castelli et al 2005; Duynkerke 1988); therefore, it can be used to improve fog prediction.

Table 5. Mean and std of TKE dissipation rate calculated using Eq. 3 and Eq. 26,, representing 1 hr time segments based on a 10-min filtering method for Sep 28 and Sep 29 2018 cases. Sep 29 case did not have wind measurements during heavy fog conditions.

Formatted: Font: 10 pt

Formatted: Font: 10 pt

Formatted: Font: 10 pt

Method	*Sep 28 Mean ε_{dis} [$m^2 s^{-3}$]*	*Sep 28 Std ε_{dis} [$m^2 s^{-3}$]*	*Sep 29 Mean ε_{dis} [$m^2 s^{-3}$]*	*Sep 29 Std ε_{dis} [$m^2 s^{-3}$]*
Using Eq. 3 Foggy	1.23×10^{-2}	1.73×10^{-2}	1.65×10^{-2}	1.19×10^{-2}
Using Eq. 26 Foggy	8.73×10^{-2}	24.94×10^{-2}	7.53×10^{-2}	9.21×10^{-2}
Using Eq. 3 Clear	7.76×10^{-2}	10.3×10^{-2}	-	-
Using Eq. 26 Clear	20.00×10^{-2}	25.59×10^{-2}	-	-

Table 5 is prepared using Eq. 3 and Eq. 26 for mean and std of ε_{dis}I during foggy and fog free conditions, representing means of 1 hr time intervals. It shows that for both Sep 28 and 29, foggy conditions had much smaller ε_{dis} than fog free conditions (excluding Sep 29 case). For fog free conditions, Sep 29 had larger values of ε_{dis} that likely was contributed by wetting of the 3D sonic anemometer optics. It is shown based on Table 5 that fog occurs usually when ε<1x10^{-25} m^2 s^{-3} and dissipates for ε>1x10^{-24} m^2 s^{-3} .(see figures for time series of ε). Between these two limits, intermediate fog intensity can likely occur. A conversion equation between ε and TKE (Scully et al 2011) can be obtained using,

$$L = C_\mu^3 \frac{TKE^{3/2}}{\varepsilon}, \qquad (22)$$

where L and C_μ are turbulent length scale (kz=0.41*2) where k is the Von Karman constant and z is the height (m), and the nondimensional stability function, respectively, that is assumed as a constant (0.447). Then, Eq. 25 becomes approximately as

$$TKE = 0.876\sqrt[3]{\varepsilon^2}. \qquad (23)$$

Note that ε and TKE are function of scales that need to be further evaluated and developed to improve NWP models based fog Vis predictions.

Based on ε time series (Figs. 7 and 9) and equations given in Table 34, we can suggest the following parameterizations for fog (Vis<1 km & RHw>95%), mist (Vis>1 km & RH_w><8095%), and light fog (Vis>1 km & RH_w>95%) conditions, respectively, as

$$RH_w > 95\% \ \& \ \varepsilon < 10^{-25} m^2 s^{-3} \ \& \ Vis = 0.412(LWC \cdot N_d)^{-0.5455} \qquad (214)$$

$$80\% < RH_w < 95\% \ \& \ \varepsilon <> 10^{-42} m^2 s^{-3} \ \& \ Vis = -0.0094RH_w^3 + 0.437RH_w^2 - 32.459RH_w + 817.062 \qquad (252)$$

and

Formatted: Highlight

Formatted: Highlight

Formatted: Highlight

Formatted: Highlight

Formatted: Highlight

Formatted: Highlight

$$RH_w > 95\% \;\&\; 10^{-4} < \varepsilon <> 10^{-52} m^2 s^{-3} \;\&\; Vis = 1.002(LWCN_d)^{-0.6473}. \qquad (236)$$

The thresholds for TKE corresponding ε thresholds is estimated as <4.06x10^{-2} m^{2} s^{-2}, >1.88x10^{-2} m^{2} s^{-2}. and between them for Eqs. 24, 25, and 26, respectively. These values are calculated using Eq. 23. Note that these criteria need to be further checked and developed to improve NWP model based fog Vis predictions.

Formatted: Right: 0.47", Space After: 12 pt

Formatted: Superscript

Formatted: Superscript

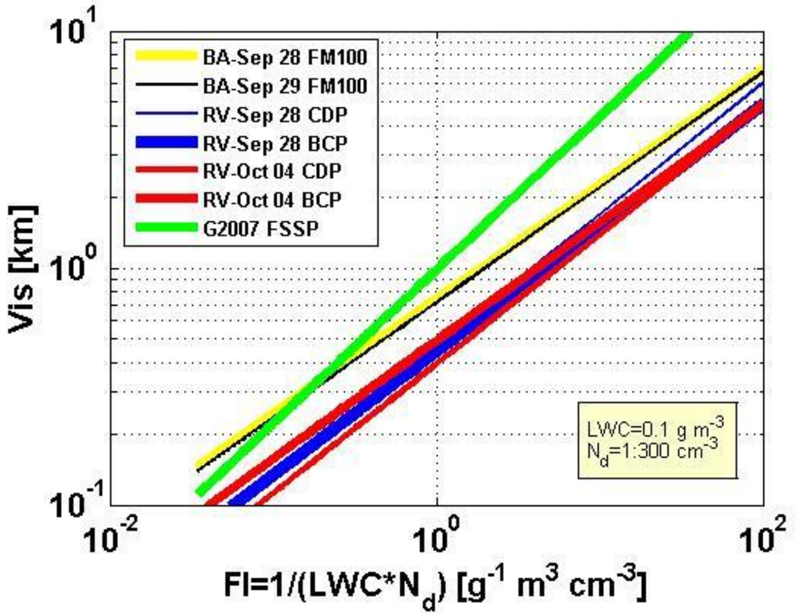

Fig. 20 Vis parameterizations obtained for all the cases based on Table ~~3~~4. LWC was fixed at 0.1 g m^{-3} while N_d changed from 1 to 300 cm^{-3}. RV represents research vessel, BA Battery, G2007 Gultepe et al (2007) and FI fog index. FM100, CDP, BCP, and FSSP probes are used for droplet spectral measurements.

6 Conclusions

In this paper, Vis associated with fog environmental parameters such as RH_w, 3D wind components, and microphysical parameters, including LWC, N_d, and MVD were studied for four cases. Results representing two IOPs from the Battery supersite and two IOPs from the *R/V Sharp* are used in Vis parameterization development and to verify the previous parameterizations. Based on the results of this work, the following points can be drawn:

1. Synoptic weather conditions and ocean-atmosphere interactions are the larger-scale factors that affect coastal fog microphysics and visibility. The cold ocean surface off the coast of Ferryland was usually a major reason for fog formation observed there.
2. The main synoptic weather systems that affected fog were usually related to a high-pressure system located to the NE, a low-pressure system along W-NW, and a chain of tropical cyclonic motions. This may not be valid early in the fog season and usually can be valid during the Fall transition period~~.~~
3. Vis is found to be less than 1 km when RH_w is greater than 95%, and this suggests that the T_a-T_d difference is an important variable indicating fog regions, but not intensity.
4. By decreasing dynamic activity, indicated by smaller 3D wind fluctuations and lifting, the eddy dissipation rate decreases during mature fog conditions that can be used for a threshold for prediction of mature fog conditions. Wind components; u, v, and w_a are relatively smaller in fog-developed regions than in fog-free regions.
5. The w_a fluctuations were 0.1 m s^{-1} during mature fog conditions compared to >0.3 m s^{-1} for fog-free regions. Note that these values can be much larger at the time scale of 16Hz or 32Hz.
6. The TKE dissipation rate was usually <10^{-5} m^2 s^{-3} during mature fog events compared to >10^{-4} m^2 s^{-3} for fog–free regions and can be used for fog predictions criteria based on NWP models.

7. Vis parameterizations that we constructed suggest that the slopes of the Vis versus fog index (FI) relationships are consistent with each other; but found to be comparably smaller in magnitude. This can be related to the nature of the measurement platform, fog season, as well as cloud versus fog measurements.
8. Vis is found to be function of LWC and N_d and this can be replaced with LWC and MVD without involvement of a 3rd parameter; this can be more generally applicable for NWP models.
9. Vis < 1km observations showed a large variability, covering few km^2 (1.5 km^2) up to 20 km^2, and the difference was very high between a station at height 129 m (Judges' Hill) compared to one at the sea level, 2 m, (Battery station) although the horizontal separation distance was only about 1.0 km.
10. BCP droplet number concentration is found to be at least half of the CDP N_d and this is likely due to BCP's higher threshold of 5 μm; there were no droplets larger than 50 μm.
11. There were double and triple peaks for fog DSDs and this can affect the NWP's fog prediction algorithms and needs to be further researched.

Based on these points, it is suggested that Vis parameterizations can be obtained using both dynamical and microphysical parameters, but fog droplet spectra representation for various fog conditions need to be further investigated. Specifically, the turbulence impact on droplet spectra and the nucleation processes are very critical for the fog life cycle in low vertical air velocity situations. Moreover, this is the most important parameter affecting the auto-conversion of fog droplets to drizzle formation.

Acknowledgments: This research was funded by the Office of Naval Research Award # N00014-18-1-2472 entitled: Toward Improving Coastal Fog Prediction (C-FOG).

~~References~~

Nomenclature

BCP: Backscattering Cloud Probe	RF: radiative fluxes
C: A constant ~0.18 in Eq. 3	SA: Sample Area

Formatted: Don't add space between paragraphs of the same style, Line spacing: single

Formatted: Font: 10 pt

Formatted Table

Formatted: Font: 10 pt

C: Visibility threshold constant as 0.05	SV: sampling volume
CN: Condensation nuclei	T_a: Air temperature
CCN: Cloud Condensation Nuclei	T_d: Td: dew point temperature
CDP: Cloud Droplet Probe	TKE: Turbulent Kinetic Energy
D_s: The structure function	u, v, w_a: Measured wind components along x,y, z
DSD: Droplet Size Distribution	u',v', w': Wind fluctuations
FI: Fog Index	U_{ha}: The apparent wind speed
FSSP: Forward Spectral Scattering Probe	U_{dx} and U_{dy}: wind speed along x and y axis at dt t
FM100: DMT fog measuring device (FMD)	U_{RV}: *RV Sharp's* speed with respect to the ground
IR and SW: Infrared and shortwave rad.fluxes	U_{hT} : True wind speed over 10 mins intervals
k: The Von Karman constant as 0.41	U_{hR}: Wind speed with respect to ground
L: Turbulent length scale	U_{3D}: 3D wind component
L: The turbulent length scale	Vis: Visibility
LES: large eddy simulation	V_f: Droplet fall velocity
LWC: liquid water content	V_d: Doppler velocity
MVD: Mean Volume Diameter	Vis_B: Vis at Battery site
n(r): Droplet number spectra	Vis_D: Vis at Downs site
N_a: Aerosol number concentration	Vis_{BH}: Vis at Blackhead site
N_{aO}: Aerosol number conc. over ocean	Vis_{JH}: Vis at Jack Hill site
N_{aL}: Aerosol number concentration over land	Z_e: Radar reflectivity factor
N_c: Droplet counts	z: The height (m)
N_d: Droplet number concentration	α and γ: empirical constants in Eq. 13
N_{dt}: total droplet number concentration	μ: spectral shape parameter
N_o: intercept parameter	λ: slope parameter
NWP: Numerical Weather Prediction	β_{ext}: Extinction coefficient
PR: Precipitation Rate	β: Lidar backscatter coefficient
Q_{eff}: Extinction efficiency	η: the dispersion of radius (sd/mean),
r: droplet radius	ρ_w: water density
r_{eff}: Effective radius	*θ*: Angle between the ship heading and U_{ha}
Δr: The horizontal distance in Eq. 3.	ε: Eddy dissipation rate
Δt: Time interval	ε_{TAS}: Error in TAS
RH_w: relative humidity with respect water	

References

Abdul-Razzak, H., and S. Ghan (2000) A parameterization of aerosol activation: 2. Multiple aerosol type, *J. Geophys. Res*., 105, 6837–6844.

Benjamin, S.G., B.D. Jamison, W.R. Moninger, S.R. Sahm, B.E. Schwartz, and T.W. Schlatter (2010) Relative Short-Range Forecast Impact from Aircraft, Profiler, Radiosonde, VAD, GPS-PW, METAR, and Mesonet Observations via the RUC Hourly Assimilation Cycle. *Mon. Wea. Rev.*, 138, 1319–1343, https://doi.org/10.1175/2009MWR3097.1

Blanchard, D. C. (1963) The electrification of the atmosphere by particles from bubbles in the sea. *Prog. Oceanogr.*, 1, 73–202, https://doi.org/10.1016/0079-6611(63)90004-1

Bergot, T., D. Carrer, J. Noilhan, and P. Bougeault (2005) Improved Site-Specific Numerical Prediction of Fog and Low Clouds: A Feasibility Study. *Wea. Forecasting*, 20, 627–646, https://doi.org/10.1175/WAF873.1

Beswick, K., D. Baumgardner, M. Gallagher, A. Volz-Thomas, P. Nedelec4, K.-Y. Wang, and S. Lance (2014) The backscatter cloud probe – a compact low-profile autonomous optical spectrometer *Atmos. Meas. Tech*., 7, 1443–1457. www.atmos-meas-tech.net/7/1443/2014/doi:10.5194/amt-7-1443-2014

Bott A., U. Sievers, and W. Zdunkowski (1990) A Radiation Fog Model with a Detailed Treatment of the Interaction between Radiative Transfer and Fog Microphysics. *J. Atmos. Sci.*, 47, 2153–2166.

Bott A, and T. Trautmann (2002) PAFOG – A new efficient forecast model of radiation fog and low-level stratiform clouds. *Atmos. Res*. 64, 191–203.

Bott A, and T. Trautmann (2002) PAFOG – A new efficient forecast model of radiation fog and low-level stratiform clouds. *Atmos. Res*. 64, 191–203.

Burrows, W. R. and G. Toth (2011) Automated fog and stratus forecasts from the Canadian RDPS operational NWP model. *Extended Abstracts, 24th Conference on Weather and Forecasting*, 23-27 January, 2011, Seattle, WA, USA, 33pp, Amer. Meteor. Soc. DOI: 10.13140/2.1.4852.0648.

Castelli, S.T., E. Ferrero, D. Anfossi and R. Ohba (2005) Turbulence Closure Models and their Application in RAMS *Environmental Fluid Mechanics*, 5, 169–192

Wainwright, C., and D. Richter (2020) Investigating the sensitivity of marine fog to physical and microphysical processes using large-eddy simulation. *BLM*, submitted.

Chen, J. P. (1994) Theory of Deliquescence and Modified Kohler Curves, J. Atmos. Sci., 51, 3505-3516.

Clark, T. L. (1973) Numerical modeling of the dynamics and microphysics of warm cumulus convection, J. Atmos. Sci., 30, 857–878.

Claxton, B.M. (2008) using a neural network to benchmark a diagnostic parameterization: The Met Office's visibility scheme. *Q. J. R. Meteorol. Soc.*, 134, 1527-1537

Cohard, JM, Jean-Pierre Pinty, and Carole Bedos (1998) Extending Twomey's Analytical Estimate of Nucleated Cloud Droplet Concentrations from CCN Spectra. *J. Atmos. Sci.*, 55, 3348–3357.

Croft, P.J., Pfost, R.L., Medlin, J.M., and Johnson, G.A. (1997) Fog forecasting for the southern region: A conceptual model approach. *Weather Forecast. 12*, 545–556.

Dimitrova, R., • Ashish Sharma • Harindra J. S. Fernando • Ismail Gultepe • Ventsislav Danchovski • Sandeep Wagh • Stef Bardoel • Sen Wang (2020) WRF model simulations for coastal fog prediction. *BLM*, submitted.

Dorman, C.E., Hoch, S.W., Gultepe, I., Fernando, H.J.S., Krishnamurthy, R. (2020) Large scale synoptic weather systems and fog during the C-FOG field experiment. *BLM*, submitted.

Duynkerke, P.G.: 1988, Application of the E-ε turbulence closure model to the neutral and stable atmospheric boundary layer, *J. Atmos. Sci.* **45**, 865–880

Fernando, H.J.S., I. Gultepe, C. Dorman, E. Pardyjak, Q. Wang, S. Hoch, D. Richter, E. Creegan, S. Gaberšek, T. Bullock, C. Hocut, R. Chang, D. Alappattu, R. Dimitrova, D. Flagg, A. Grachev, R. Krishnamurthy, D.J. Singh, I. Lozovatsky, B. Nagare, A. Sharma, S. Wagh, C. Wainwright, M. Wroblewski, R. Yamaguchi, S. Bardoel, R.S. Coppersmith, N. Chisholm, E. Gonzales, N. Gunawardena, O. Hyde, T. Morrison, A. Olson, A. Perelet, W. Perrie, S. Wang, B. Wauer (2020) C-FOG: Life of Coastal Fog, *Bull of AMS*, accepted.

Fletcher, N.H. (1966) *The physics of rainclouds*. Cambridge University Press, 390 pp.

Feingold, G., S. Yang, R. M. Hardesty, and W. R. Cotton (1998) Feasibility of Retrieving Cloud Condensation Nucleus Properties from Doppler Cloud Radar, Microwave Radiometer, and Lidar. *J. Atmos. Oceanic Technol*., 15, 1188–1195.

Ghan, S. J., G. Guzman, and H. Abdul-Razzak (1998) Competition between sea salt and sulfate particles as cloud condensation nuclei, *J. Atmos. Sci*., 55, 3340– 3347.

Ghan, S. J., N. S. Laulainen, R. C. Easter, R. Wagener, S. Nemesure, E. G. Chapman, Y. Zhang, and L. R. Leung (2001) Evaluation of aerosol direct radiative forcing in MIRAGE, *J. Geophys. Res*., 106, 5295–5316.

Ghan, S. J., C. C. Chuang, and J. E. Penner (1993) A Parameterization of Cloud Droplet Nucleation, Part I: Single Aerosol Type. *Atmos. Res*. 30:197-221.

Ghan, S. J., Leung, L. R., Easter, R. C., and Abdul-Razzak, H. (1997) Prediction of cloud droplet number in a general circulation model, *J. Geophys. Res*., 102, 777–794.

Golding B. W. (1998) Nimrod: A system for generating automated very short range forecasts. *Meteorol. Appl*. 5, 1–16.

Golding, B. W. (1993) A study of the influence of terrain on fog development. *Mon. Weather Rev.*, 121, 2529-2541.

Grachev A.A., Krishnamurthy R., Fernando H.J.S., Fairall C.W., Bardoel S.L., Wang S. (2020) Atmospheric turbulence measurements in coastal zone with and without fog. *Boundary-Layer Meteorol.*, current issue (submitted).

Gultepe, I., Pardyjak, S. W. Hoch, H.J.S Fernando, C. Dorman, D.D. Flagg, R. Krishnamurthy, Q. Wang, S. Gaberšek, E. Creegan, N. Scantland, S. Desjardins, A. Heidinger, M. Pavolonis, A.J. Heymsfield (2020) Coastal Fog Microphysics Using In-Situ Observations and GOES-R Retrievals. *BLM*, Submitted.

Gultepe, I., and Milbrandt, J. (2007a) Microphysical observations and mesoscale model simulation of a warm fog case during FRAM project. *Pure Appl. Geophys.* 2007, *164*, 1161–1178.

Gultepe, I., M. D. Müller, and Z. Boybeyi (2006) A new warm fog parameterization scheme for numerical weather prediction models. *J. Appl. Meteor*., 45, 1469-1480.

Gultepe, I., and Starr, D. O'C. (1995) Dynamical structure and turbulence in cirrus clouds: Aircraft observations during FIRE. *J. Atmos. Sci*., 52, 4659-4182.

Gultepe I, and G.A. Isaac (1996) The relationship between cloud droplet and aerosol number concentrations for climate models. *Inter. J. of Clim*. 16, 941-946.

Gultepe, I., Isaac, G. A., Leaitch, W. R., and Banic, C. M. (1996) Parameterization of marine stratus microphysics based on in-situ observations: Implications for GCMs. *J. Climate*, 9, 345-357.

Gultepe, I., and G. A. Isaac (1999) Scale effects on averaging of cloud droplet and aerosol number concentrations: observations and models. *J. Climate*, 12, 1268-1279.

Gultepe, I., R. Tardif, S.C. Michaelides, J. Cermak, A. Bott, J. Bendix, M. Müller, M. Pagowski, B. Hansen, G. Ellrod, W. Jacobs, G. Toth, S.G. Cober (2007c) Fog research: a review of past achievements and future perspectives. *J. of Pure and Applied Geophy.*, Special issue on fog, edited by I. Gultepe. 164, 1121-1159.

Gultepe, I., M. Pagowski, and J. Reid (2007b) Using surface data to validate a satellite based fog detection scheme. *J. of Weather and Forecasting*, 22, 444-456.

~~Gultepe, I., and J. Milbrand (2007a) Microphysical observations and mesoscale model simulation of a warm fog case during FRAM project. *J. of Pure and Applied Geophy*. 164, 1161-1178.~~

Gultepe, I., G. Pearson J. A. Milbrandt, B. Hansen, S. Platnick, P. Taylor, M. Gordon, J. P. Oakley, and S.G. Cober (2009) The fog remote sensing and modeling (FRAM) field project. *Bull. Of Amer. Meteor. Soc*., 90, 341-359.

Gultepe, I., and J. A. Milbrandt (2010) Probabilistic Parameterizations of Visibility Using Observations of Rain Precipitation Rate, Relative Humidity, and Visibility. *J. Appl. Meteor. Climatology*. 49, 36–46.

Gultepe, I., T. Kuhn, M. Pavolonis, C. Calvert, J. Gurka, G.A. Isaac, A. J. Heymsfield, P.S.K. Liu, B. Zhou, R. Ware, B. Ferrier, J. Milbrandt, B. Hansen, and B. Bernstein (2014) Ice fog in Arctic during FRAM-IF project: Aviation and nowcasting applications. *Bulletin of Amer. Met. Soc.*, 95, 211–226.

Gultepe, I., B. Zhou, J. Milbrandt, A. Bott, Y. Li, A. J. Heymsfield, B. Ferrier, R. Ware, M. Pavolonis, T. Kuhn, J. Gurka, P. Liu, and J. Cermak (2015) A review on Ice Fog: Observations and Modeling. *Atmospheric Research*. DOI: 10.1016/j.atmosres. 2014.04.014.

Gultepe, I. (2019) Low level ice clouds-ice fog. *Encylopedia of Water: Science, Technology, and Society*, edited by Patricia A. Maurice. ISBN: 9781119300755 John Wilesy & Sons Inc., DOI: 10.1002/9781119300762.wsts0140. 19 pp.

Gultepe, I., Pardyjak, E., Hoch, S.W., Fernando, H.J.S., Dorman, C., Flagg, D.D., Krishnamurthy, R., Wang, Q., Gaberšek, S., Creegan, E., Scantland, N., Desjardins, S., Heidinger, A., Pavolonis, M., Heymsfield, A.J., Coastal Fog Microphysics Using In-Situ Observations and GOES-R Retrievals, *Boundary Layer Meteorology*, accepted.

Haeffelin, M., T. Bergot, T. Elias, R. Tardif, D. Carrer, P. Chazette, M. Colomb, P. Drobinski, E. Dupont, J. Dupont, L. Gomes, L. Musson-Genon, C. Pietras, A. Plana-Fattori, A. Protat, J. Rangognio, J. Raut, S. Rémy, D. Richard, J. Sciare, and X. Zhang (2010) Parisfog. *Bull. Amer. Meteor. Soc.*, 91, 767–783, https://doi.org/10.1175/2009BAMS2671.1

Haiden, T., A. Kann, and G. Pistotnik (2014) Nowcastiong with INCA during SNOW-V10. J. *Pure and App. Geophy*. 171, No: 5-6, 231-242.

Isaac, G.A., T. Bullock, J. Beale, and S. Beale (2020) Characterizing and Predicting Marine Fog Offshore Newfoundland and Labrador. *Wea. Forecasting*, **35**, 347–365, https://doi.org/10.1175/WAF-D-19-0085.1

Jones, A., DL Roberts, and A. Slingo (1994) A climate model study of indirect radiative forcing by anthropogenic sulfate aerosols. *Nature*, 370, 450-453.

Kline, S. J., and F. A. McClintock (1953) Analysis of uncertainty in single-sample experiments. *Mechanical Engineering* 75, 3-9.

Koschmieder, H. (1924) Theorie der horizontalen sichewite, *Beitr. Phys. Atmos*., 12, 33-53.

Formatted: Font: (Default) Times New Roman

Formatted: Font: (Default) Times New Roman, Italic

Formatted: Font: (Default) Times New Roman

Köhler, H. (1936) The nucleus in and the growth of hygroscopic droplets. *Trans. Faraday Soc.*, 32, 1152–1161, https://doi.org/10.1039/TF9363201152.

Kunkel, B.A. 1984 Parameterization of droplet terminal velocity and extinction coefficient in fog models. *J. Clim. Appl. Meteorol.* 1984, *23*, 34–41.

Lebo, Z. J., Morrison, H., and Seinfeld, J. H. (2012) Are simulated aerosol induced effects on deep convective clouds strongly dependent on saturation adjustment?, *Atmos. Chem. Phys*., 12, 9941–9964, https://doi.org/10.5194/acp-12-9941-2012.

LPM (2011) *Laser Precipitation Monitor*. 5.4110.xx.x00, V2.5x STDNWS. Adolf Thies GmbH&Co. KG. Document # 000904. 66 pp.

Martin, G. M., D. W. Johnson, and A. Spice (1994) The measurement and parameterization of effective radius of droplets in warm stratocumulus clouds. *J. Atmos. Sci*., 51, 1823–1842.

Mellor, G., and T. Yamada (1982) Development of a turbulence closure model for geophysical fluid problems. *Rev. Geophys. Space Phys*., 26, 851–875.

Miao, Y., R. Potts, X. Huang, G. Elliott, and R. Rivett (2012) A Fuzzy Logic Fog Forecasting Model for Perth Airport *J. Pure and App. Geophy.* 169, No: 5-6 , 1107-1119.

Milbrandt, J.A. and M.K. Yau (2005a) A Multimoment Bulk Microphysics Parameterization. Part I: Analysis of the Role of the Spectral Shape Parameter. *J. Atmos. Sci*., 62, 3051–3064, https://doi.org/10.1175/JAS3534.1

Milbrandt, J.A. and M.K. Yau (2005b) A Multimoment Bulk Microphysics Parameterization. Part II: A Proposed Three-Moment Closure and Scheme Description. *J. Atmos. Sci*., 62, 3065–3081, https://doi.org/10.1175/JAS3535.1

Moffat, R. J. (1982) Contributions to the theory of single-sample uncertainty analysis. 250-258 pp.

Morrison, H. and Grabowski, W. W. (2007) Comparison of bulk and bin warm-rain microphysics models using a kinematic framework, *J. Atmos. Sci.*, 64, 2839–2861.

Morrison, H., and A. Gettelman (2008) A New Two-Moment Bulk Stratiform Cloud Microphysics Scheme in the Community Atmosphere Model, Version 3 (CAM3). Part I: Description and Numerical Tests. *J. Climate*, 21, 3642–3659.

Muller M. D., M. Masbou, and A. Bott (2010) Three-dimensional fog forecasting in complex terrain. *Quart. J. Roy. Meteor. Soc.*, 136, 2189-2202.

Muller, M. D., C. Schmutz, and E. Parlow (2007) A one dimensional ensemble forecast and assimilation system for fog prediction. *J. Pure Appl. Geophys*., 164, 1241–1264.

Niu, S.J., Lu, C.S., Zhao, L.J., Lu, J.J., and Yang, J. (2010) Analysis of the microphysical structure of heavy fog using a droplet spectrometer: a case study, *Adv. Atmos. Sci.* 27(6), 1259-1275, doi:10.1007/s00376-010-8192-6.

Paluch, I.R. and D.G. Baumgardner (1989) Entrainment and Fine-Scale Mixing in a Continental Convective Cloud. *J. Atmos. Sci*., 46, 261–278, https://doi.org/10.1175/1520-0469(1989)046<0261:EAFSMI>2.0.CO;2

Panofsky, H. A., and J. A. Dutton (1984) *The atmosphere Turbulence*. John Wiley and Sons, 397 pp.

Perelet, A., I. Gultepe, S. W. Hoch, and E. Pardyjak (2020) Response of infrared and microwave scintillometer to hydrometeors. *BLM*. Submitted.

Pezzoli, A., Moncalero, M., Boscolo, A., Cristofori, E., Giacometto, F., Gastaldi, S., Vercelli, G. (2010) The meteo-hydrological analysis and the sport performance: which are the connections? The case of the XXI Winter Olympic Games, Vancouver 2010. *Journal of Sports Medicine and Physical Fitness*, **50**:19-20.

Price, J.D., S. Lane, I.A. Boutle, D.K. Smith, T. Bergot, C. Lac, L. Duconge, J. McGregor, A. Kerr-Munslow, M. Pickering, and R. Clark (2018) LANFEX: A Field and Modeling Study to Improve Our Understanding and Forecasting of Radiation Fog. *Bull. Amer. Meteor. Soc.*, 99, 2061–2077, https://doi.org/10.1175/BAMS-D-16-0299.1

Price, J. D. (2019) On the formation and development of radiation: An observational study. Bound. Layer Meteor., 172, 167–197.

Pu, Z., Chachere, C., Hoch, S., Pardyjak, E., & Gultepe, I. (2016). Numerical prediction of cold season fog events over complex terrain: The performance of the WRF model during MATERHORN-Fog and early evaluation. *Pure and Applied Geophysics*. https://doi.org/10.1007/s00024-016-1375-z.

Dimitrova, D., Sharma, A., Fernando, H.J.S., Gultepe, I., Danchovski, V., Wagh, S., Bardoel, S., and Wang, S. WRF model simulations for coastal fog prediction, Submitted to *Boundary Layer Meteorology*. Accepted.

Formatted: Font: (Default) Times New Roman, 10 pt

Formatted: Font: Not Italic

Formatted: Font: Italic

Formatted: Font: Italic

Schemenauer, R.S., I. Gultepe, Witiw, M. (2016) Fog Studies. *Meteorological Technology International*. April Issue, 52-54.

Schwenkel, J., and B. Maronga (2019) Large-eddy simulation of radiation fog with comprehensive two-moment bulk microphysics: impact of different aerosol activation and condensation parameterizations *Atmos. Chem. Phys*., 19, 7165–7181, 2019. https://doi.org/10.5194/acp-19-7165-2019

Scully, M. E., W.R. Geyer, J. H. Trowbridge (2011) The Influence of Stratification and Nonlocal Turbulent Production on Estuarine Turbulence: An Assessment of Turbulence Closure with Field Observations. *J. of Phys. Ocean*., 41, 166-185. DOI: 10.1175/2010JPO4470.1

Shi, C., L. Wang, H. Zhang, X. Deng, Y. Li, and M. Qiu (2012) Fog Simulations Based on Multi-Model System: A Feasibility Study. *Pure Appl. Geophys*. 169, 941–960.

Singh, D.K., Sebastian W. Hoch, Ismail Gultepe, and Eric R. Pardyjak (2020) A case study of the life cycle of a stratus-lowering coastal fog event in Newfoundland, CA. *Boundary-Layer Meteorology*, Submitted.

Smirnova, T.G., S.G. Benjamin, J.M. Brown (2000) Case study verification of RUC/MAPS fog and visibility forecasts. Preprints, *9th Conf. on ARAM, AMS*, Orlando, FL, 31-36.

Spiegel, J. K., Zieger, P., Bukowiecki, N., Hammer, E., Weingartner, E., and Eugster, W. (2012) Evaluating the capabilities and uncertainties of droplet measurements for the fog droplet spectrometer (FM-100), *Atmos. Meas. Tech*., 5, 2237–2260, https://doi.org/10.5194/amt-5-2237-2012.

Spiel, D. E. (1995) On the births of jet drops from bubbles bursting on water surfaces. *J. Geophys. Res*., 100, 4995–5006, https://doi.org/10.1029/94JC03055.

Spiel, D. E. (1997) More on the births of jet drops from bubbles bursting on seawater surfaces. *J. Geophys. Res.*, 102, 5815–5821, https://doi.org/10.1029/96JC03582.

Spiel, D. E. (1998) On the births of film drops from bubbles bursting on seawater surfaces. *J. Geophys. Res.*, 103, 24 907–24 918, https://doi.org/10.1029/98JC02233.

Stoelinga, T. G. and T. T. Warner (1999) Non-hydrostatic, mesobeta-scale model simulations of cloud ceiling and visibility for an east coast winter precipitation event. *J. Appl. Meteor*., 38, 385-404.

Storelvmo, T., J. E. Kristjansson, Steven J. Ghan, Alf Kirkevag, Ø. Seland, and Trond Iversen (2006) Predicting cloud droplet number concentration in Community Atmosphere Model (CAM)-Oslo, *JGR*, 111, D24208, doi:10.1029/2005JD006300

Thompson, G., and T. Eidhammer (2014) A study of aerosol impacts on clouds and precipitation development in a large winter cyclone. *J. Atmos. Sci.*, 71, 3636–3658, doi:10.1175/ JAS-D-13-0305.1.

Thompson G., P. R. Field, R. M. Rasmussen, and W. D. Hall (2008) Explicit forecasts of winter precipitation using an improved bulk microphysics scheme. Part II: Implementation of a new snow parameterization. *Mon. Wea. Rev.*, 136, 5095–5115, doi:10.1175/2008MWR2387.1.

Torregrosa, A., T. A. O'Brien, and I.C. Faloona (2014), Coastal fog, climate change, and the environment. *Eos*, 95 (50), 473; DOI: 10.1002/2014EO500001.

Toth, G., I. Gultepe, J. Milbrandt, B. Hansen, G. Pearson, C. Fogarty, and W. Burrows (2011) *The Environment Canada Handbook on Fog and Fog Forecasting. Environment Canada.* Tech. Manual. ISBN # 978-1-100-52518-1. Available from Environment Canada, Toronto, Canada. 93 pp.

Troitskaya, Y., A. Kandaurov, O. Ermakova, D. Kozlov, and D. Sergeev, and S, Zilitinkevich (2018) The ''Bag Breakup'' Spume Droplet Generation Mechanism at High Winds. Part I: Spray Generation Function. *J. of Physical Ocean*., 48, 2167-2188.

Twomey, S. (1959) The nuclei of natural cloud formation. Part II: The supersaturation in natural clouds and the variation of cloud droplet concentration. *Geophys. Pure Appl.*, 43, 243–249.

Twomey, S. (1974) Pollution and planetary albedo, *Atmos. Environ*., 8, 1251–1256.

Twomey, S. (1991) Aerosols, Clouds and Radiation, *Atmos Environ*., 25, 2435–2442.

Wagh, S., R. Krishnamurthy , C. Wainwright, S. Wang and H. J. S. Fernando, and I. Gultepe (2020) Microphysics of Marine Fog during Stratus cloud lowering. *BLM*, submitted.

Wang, S., Li Yi, S. Zhang , X. Shi, and X. Chen (2020) The Microphysical Properties of a Sea-Fog Event along the West Coast of the Yellow Sea in Spring, *MDPI Atmosphere*, *11*, 413; doi:10.3390/atmos11040413

Formatted: Underline

Formatted: Underline

Formatted: Underline

Formatted: Font: (Default) Times New Roman, 10 pt

Formatted: Font: (Default) Times New Roman, 10 pt, Italic

Formatted: Font: (Default) Times New Roman, 10 pt

Wang, Q., et al. (2020) Coastal fog microphysics and dynamic at Downs Supersite during C-FOG, *BLM*, submitted.

Wilfried, J., V. Nietosvaara, A. Bott, J. Bendix, J. Cermak, M. Silas, I. Gultepe (2008) *Short range forecasting methods of fog visibility and low clouds.* COST Action 722, Earth System Science and Environmental Management Final report on COST-722 Action. ISBN # 978-92-898-0038-9Available from COST Office, Avenue Louise 149, B-1050 Brussel, Belgium. 489 pp.

Wilkinson JM, A. N.F. Porson, F. J. Bornemann, M. Weeks, P.R. Field, and A. P. Lock (2013) Improved microphysical parametrization of drizzle and fog for operational forecasting using the Met Office Unified Model, *Q. J. Roy. Meteorol. Soc*., 139, 488-500.

Wright B. J., and Thomas N. (1998) An objective visibility analysis and very short- range forecasting system. *Meteorol. Appl*. 5. 157–181.

Wu, J. (1981) Evidence of sea spray produced by bursting bubbles. *Science,* 212, 324–326, https://doi.org/10.1126/science.212.4492.324.

Yang, D., H. Ritchie, S. Desjardins, G. Pearson, A. MacAfee, and I. Gultepe (2009) High Resolution GEM-LAM application in marine fog prediction: Evaluation and diagnosis. *Weather and Forecasting*. 25, 727-748.

Zhou, B. and J. Du (2010) Fog prediction from a multi-model mesoscale ensemble prediction system. *Wea. Forecasting*, 25, 303-322.

Zhou, B. and B. S. Ferrier (2008) Asymptotic analysis of equilibrium radiation fog. *J. App. Met. And Clim.*, 47, 1704-1722. https://doi.org/10.1175/2007JAMC1685.1.

Formatted: Font: Italic